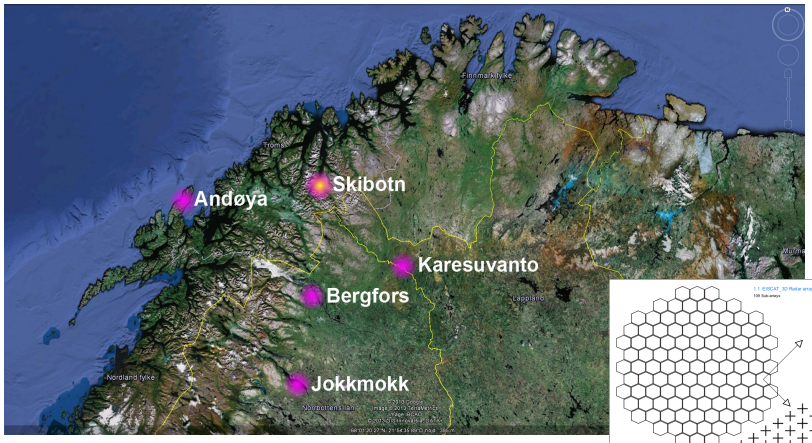


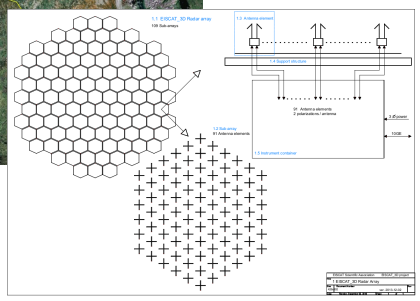

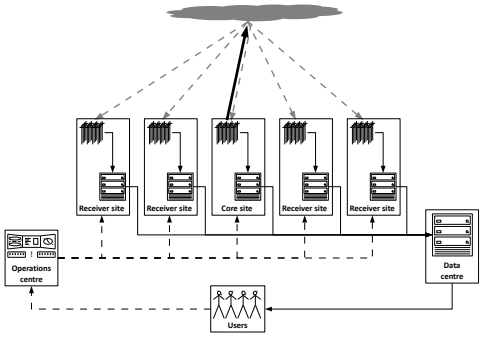


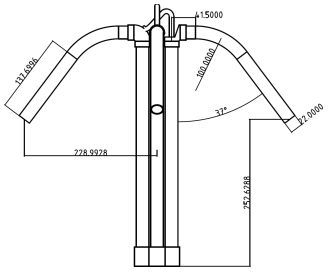


# EISCAT

## EUROPEAN INCOHERENT SCATTER SCIENTIFIC ASSOCIATION

## ANNUAL REPORT 2013 – 2014

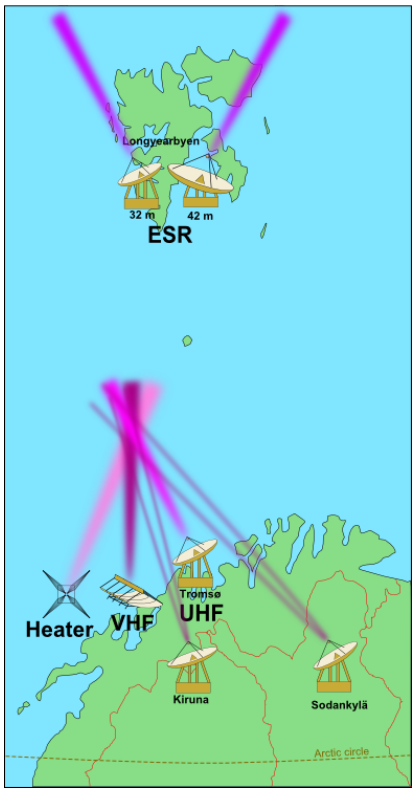


# EISCAT Radar Systems

| Location | Tromsø | | Kiruna | Sodankylä | Longyearbyen | |
|---|---|---|---|---|---|---|
| Geographic coordinates | 69°35′N 19°14′E | | 67°52′N 20°26′E | 67°22′N 26°38′E | 78°9′N 16°1′E | |
| Geomagnetic inclination | 77°30′N | | 76°48′N | 76°43′N | 82°6′N | |
| Invariant latitude | 66°12′N | | 64°27′N | 63°34′N | 75°18′N | |
| Band | UHF | VHF | VHF | VHF | UHF | |
| Frequency (MHz) | 929 | 224 | 224 | 224 | 500 | |
| Maximum bandwidth (MHz) | 8 | 3 | 8 | 8 | 10 | |
| Transmitter | 2 klystrons | 1 klystron | - | - | 16 klystrons | |
| Channels | 6 | 6 | 6 | 6 | 12 | |
| Peak Power (MW) | 2.0 | 1.6 | - | - | 1.0 | |
| Average power (MW) | 0.25 | 0.20 | - | - | 0.25 | |
| Pulse duration (ms) | 0.001–2.0 | 0.001–2.0 | - | - | 0.0005–2.0 | |
| Phase coding | binary | binary | binary | binary | binary | |
| Minimum interpulse (ms) | 1.0 | 1.0 | - | - | 0.1 | |
| Digital processing | 14 bit ADC on IF, 32 bit complex autocorrelation functions, parallel channels | | | | | |
| Antenna | parabolic dish 32 m steerable | parabolic cylinder 120 m × 40 m steerable | parabolic dish 32 m steerable | parabolic dish 32 m steerable | Antenna 1 parabolic dish 32 m steerable | Antenna 2 parabolic dish 42 m fixed |
| Feed system | Cassegrain | line feed 128 crossed dipoles | crossed dipole | crossed dipole | Cassegrain | Cassegrain |
| System temperature (K) | 90 | 250 | 100 | 100 | 80 | 65 |
| Gain (dBi) | 48.1 | 46 | 48.1 | 48.1 | 42.5 | 44.8 |
| Polarisation | circular | circular | any | any | circular | circular |

# EISCAT Heating Facility (Tromsø)

Frequency range: 4.0 MHz to 8.0 MHz, Maximum transmitter power: 12×0.1 MW, Antennas: Array 1 (5.5 MHz to 8.0 MHz) 30 dBi, Array 2 (4.0 MHz to 5.5 MHz) 24 dBi, Array 3 (5.5 MHz to 8.0 MHz) 24 dBi.
Additionally, a Dynasonde is operated at the heating facility.

---

**Cover pictures:**

EISCAT_3D system overview,
Images from EISCAT_3D Preparatory Phase Deliverables 2.4, 8.4, and 14.2.

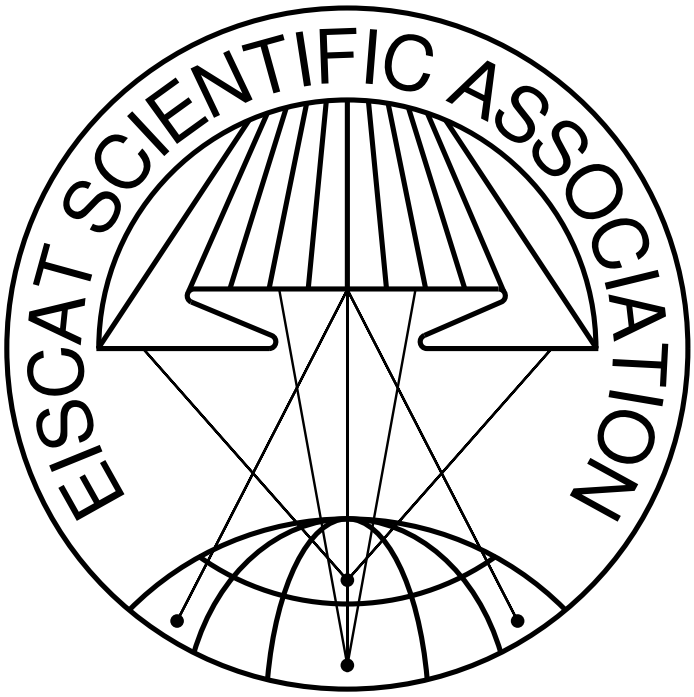


# EISCAT Scientific Association
# 2013 – 2014

*EISCAT, the European Incoherent Scatter Scientific Association, is established to conduct research on the lower, middle and upper atmosphere and the ionosphere using the incoherent scatter radar technique. This technique is the most powerful ground-based tool for these research applications. EISCAT is also being used as a coherent scatter radar for studying instabilities in the ionosphere, investigating the structure and dynamics of the middle atmosphere, studying meteors and as a diagnostic instrument in ionospheric modification experiments with the heating facility.*

*There are fourteen incoherent scatter radars in the world, and EISCAT operates three of the highest-standard facilities. The EISCAT sites are located north of the Arctic Circle in Scandinavia. They consist of two independent radar systems on the mainland, together with a radar constructed on the island of Spitzbergen in the Svalbard archipelago — the EISCAT Svalbard Radar (see sketch and operating parameters on the inside of the front cover).*

*The EISCAT VHF radar operates in the 224 MHz band with a peak transmitter power of 1.6 MW, using a 120 m × 40 m parabolic cylinder antenna which is subdivided into four sectors. This antenna can be steered mechanically in the meridional plane from vertical to 60° north of the zenith; limited east-west steering is also possible using alternative phasing cables. Receiving sites are also located in Kiruna (Sweden) and Sodankylä (Finland), allowing for tri-static radar measurements.*

*The monostatic EISCAT UHF radar in Tromsø operates in the 931 MHz band with a peak transmitter power of 2.0 MW, and employs fully steerable 32 m parabolic dish antennas.*

*The EISCAT Svalbard radar (ESR), located near Longyearbyen, operates in the 500 MHz band with a peak transmitter power of 1.0 MW, and employs a fully steerable parabolic dish antenna of 32 m diameter and a fixed antenna, aligned with the local magnetic field, with a 42 m diameter. The high latitude location of this facility is particularly aimed at studies of the cusp and the polar cap region.*

*The basic data measured with the incoherent scatter radar technique are profiles of electron density, electron and ion temperatures and bulk ion velocity. Subsequent processing allows derivation of a wealth of further parameters, describing the ionosphere and neutral atmosphere. A selection of well-designed radar pulse schemes are available to adapt the data-taking routines to many particular phenomena, occurring at altitudes from about 50 km to above 2000 km. Depending on geophysical conditions, a best time resolution of less than one second and an altitude resolution of a few hundred meters can be achieved.*

*Operations of 3000 h to 4000 h each year are distributed between Common Programmes (CP) and Special Programmes (SP). At present, six well-defined Common Programmes are run regularly, for between one and three days, typically about once per month, to provide a data base for long term synoptic studies. A large number of Special Programmes, defined individually by Associate scientists, are run to support national and international studies of both local and global geophysical phenomena.*

*Further details of the EISCAT system and its operation can be found in various EISCAT reports, including illustrated brochures, which can be obtained from EISCAT Headquarters in Kiruna, Sweden.*

*The investments and operational costs of EISCAT are shared between:*

*China Research Institute of Radiowave Propagation, Peoples Republic of China*
*National Institute of Polar Research, Japan*
*Natural Environment Research Council, United Kingdom*
*Norges forskningsråd, Norway*
*Solar-Terrestrial Environment Laboratory, Nagoya University, Japan*
*Suomen Akatemia, Finland*
*Vetenskapsrådet, Sweden*

# Contents

# Director's page

I became director the EISCAT Scientific Association in January of 2013, at a time when the association was (and remains) in the process of planning for a number of truly revolutionary and exciting developments. Chief among those developments is, of course, the EISCAT_3D project but that is hardly the only area of exciting scientific and technical advancement. The world is experiencing a constant march of technology in areas very much relevant to EISCAT's scientific goals; radio frequency techniques, at least at lower power levels, are easier to implement and more affordable than ever and the availability of low cost but incredibly powerful computing technologies opens a wide variety of scientific opportunities that have simply not been possible in years past. What does remain a challenge is making intelligent use of available technologies with a view toward long-term utility and maintenance. In many ways, the tradeoff is one of purchasing nearly-capable subsystems that are largely closed vs. using precious staff hours to build special purpose electronics that will do the full job and be maintainable over the long run through ownership of the designs.

The European Commission-funded EISCAT_3D FP7 Preparatory Phase project continued through 2013 and came to completion in 2014. A number of important decisions were made with respect to the final design and capabilities of the system, including decisions concerning the antenna elements and configuration, site locations, frequencies, transmitter power, and signal flow. The science case for EISCAT_3D completed its third iteration with performance and sensitivity goals sufficient to enable ground-breaking science. The project also supported ultimately successful proposal efforts in Finland, Norway and Sweden. In response to feedback from Vetenskapsrådet in Sweden, a staged approach to implementing EISCAT_3D was developed. This approach split the implementation into four stages with defined capabilities after each stage. It focused most fundraising efforts on the first stage.

The ESR 32-m antenna suffered a major failure of one of its gearboxes in January 2012. Repairing this gearbox required extraordinary efforts under difficult conditions but, with help from auto workshops in Longyearbyen, the system was finally brought to full operation near the end of 2013. Additionally, ten new klystrons were purchased and delivered during 2014 as part of a final build by the tube manufacturers prior to shutting down their product line. This should ensure that the ESR transmitters can be maintained for the foreseeable future.

Work also continued toward the addition of a third antenna in Svalbard. This antenna was the subject of a technical study, frequency allocation requests, and addition to the regional plan (Delplan) for Longyearbyen. An extraordinary council meeting was held in the spring of 2013 to discuss whether the project should proceed to an implementation. Unfortunately, for a number of reasons that included both financial constraints and manpower issues, the project was ultimately cancelled.

On the mainland, EISCAT completed a retrofit of the receive-only antennas in Kiruna and Sodankylä for use on the VHF transmitter frequency in Ramfjordmoen. This change was driven by increasingly problematic interference issues at UHF frequencies, especially in Finland. EISCAT also initiated actions toward extending transmit licenses for both UHF and VHF frequencies in Norway. Competition for the UHF band, in particular, has become more intense and the EISCAT frequencies were put up to bid and leased by cellular telephone concerns in Norway. EISCAT has secured the right to secondary usage of the bands, as long as the primary owners do not see interference with their operations.

Overall, the future for EISCAT looks very promising. Once the EISCAT_3D implementation is under way, the prospects will be especially bright.

*Dr. Craig Heinselman*
*Director*
*EISCAT Scientific Association*

# EISCAT_3D

During 2014 the EISCAT_3D Preparatory Phase project was finished. The final report from that project is available at the EISCAT_3D website[1]. Here follows a summary of the EISCAT_3D Preparatory Phase.


## Project context and objectives

EISCAT_3D will be an international research infrastructure that is using radar observations and the incoherent scatter technique for studies of the atmosphere and near-Earth space environment above the Fenno-Scandinavian Arctic as well as for support of the solar system and radio astronomy sciences. The radar system is designed to investigate how the Earth's atmosphere is coupled to space but it will also be suitable for a wide range of other scientific targets. It will be operated by EISCAT Scientific Association and hence be an integral part of an organisation that has successfully operated incoherent scatter radars for more than thirty years.

The EISCAT_3D system will consist of five phased-array antenna fields located in the northernmost areas of Finland, Norway and Sweden, each with around 10 000 crossed dipole antenna elements. One of these sites (the core site) will transmit radio waves at 233 MHz, and all five sites will have sensitive receivers to measure the returned radio signals. Digital control of the transmission and low-level digitisation of the received signal will permit instantaneous electronic steering of the transmitted beam and measurements using multiple simultaneous beams. The central antenna array at each site will be surrounded by smaller outlying arrays which will facilitate aperture synthesis imaging to acquire sub-beam transverse spatial resolution. The central array of each site will be of a size of about 70 m from side to side, and the sites will be located from 90 km to 250 km from the core site in order to be able to maximise the coverage by the system.

[1] www.eiscat3d.se/content/eiscat3d2-final-report

EISCAT_3D will measure the spectra of radiowaves that are back-scattered from free electrons, whose motions are controlled by inherent ion-acoustic and electron plasma waves in the ionosphere. The measured spectra reveal high-resolution information on the ionospheric plasma parameters, but can also be used for obtaining atmospheric data and observations of meteors and space debris orbits. In both active and passive mode, the receivers will provide high-quality scientific and monitoring data from the ionosphere as well as from space within its designed frequency spectrum. The research will both be organised through common observation modes and through requests from individual groups.

EISCAT_3D is designed to use several different measurement techniques which, although they have individually been used elsewhere, have never been combined together in a single radar system. The design of EISCAT_3D allows large numbers of antennas to be combined together to make either a single radar beam, or a number of simultaneous beams, via beam-forming. While traditional radar systems with a single slow-moving antenna, and thus a single beam, can only show us what is happening along a single line in the upper atmosphere, volumetric imaging allows us to see geophysical events in their full spatial context, and to distinguish between processes which vary spatially and those which vary over time.

Since EISCAT_3D is very flexible compared to traditional ionospheric radars, it will allow several new operating modes, including the capabilities to determine vector velocities of moving ob-

jects and to respond intelligently to changing conditions, for instance by changing the parameters of a scanning experiment. EISCAT_3D will also allow remote continuous operations, limited only by power consumption and data storage. This is important for monitoring the state of the atmosphere, especially as a function of solar variability, as well as capturing events that appear suddenly and are hard to predict. Radio astronomy observations will be performed when the transmitters are inactive.

The Preparatory Phase, running from October 2010 to September 2014, aimed to ensure that the project will reach a sufficient level of maturity so that the implementation of EISCAT_3D can begin after its conclusion.

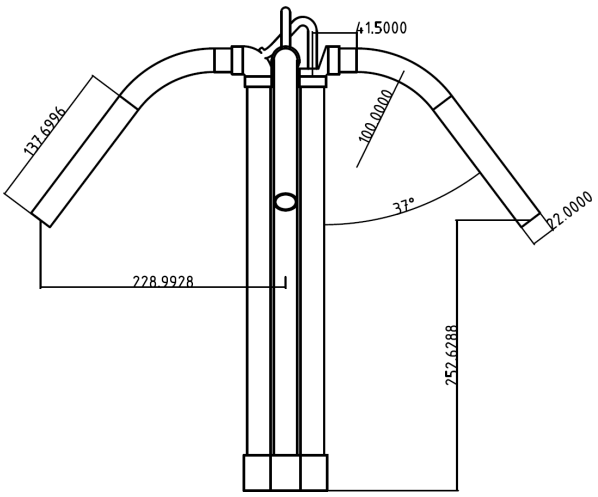


Updated EISCAT_3D antenna design. (From Deliverable 8.5 of the EISCAT_3D Preparatory Phase project)

## Description of work and main results

The EISCAT_3D Preparatory Phase was concerned with forming a consortium, procuring the financing, selecting the sites, preparing for the data handling, considering the scientific requirements and planning the construction and operation of the system. The present EISCAT Scientific Association, which will be the basis for the future EISCAT_3D consortium, is funded by research councils and funding bodies in six countries. EISCAT revised its membership policy in May 2013 in order to make it more attractive to new members, and is now open also for institutional members with a smaller financial commitment. Procedures are also implemented within the research infrastructure to safeguard good scientific practice and to ensure the commitment to excellent research. EISCAT has made progress in the work to revise its data policy to prepare for the new system.

To procure the finances, major investments will be needed from several countries. The current estimate of the investment required for EISCAT_3D is 128 M€ over 8 years. This estimate is based on figures given by individual manufacturers, and reductions may still be possible on individual parts, depending on the exact specification as well as bidding from several competitors. Proposals for funding EISCAT_3D have been submitted in Norway and Sweden, and the process is well under way in Finland, Japan and the United Kingdom.

A number of sites for the EISCAT_3D arrays were surveyed, and a list of preferred sites was finalised. In the first stage of the construction of the EISCAT_3D system, the core site and two receiver sites will be built. Areas near Bergfors in Sweden and Karesuvanto in Finland were identified as suitable for the first receiver sites. For the later stages of the construction, areas near Andøya (Norway) and Jokkmokk (Sweden) were identified as locations for receiver sites.

The scientific requirements have a major influence on the system design and for this a Science Case has been continuously revised in collaboration with the present EISCAT user community and with prospective future users. Communication with the scientific user community was facilitated through outreach activities, conference presentations and a series of dedicated meetings organised by the project. The website for EISCAT_3D is online since March 2009 and is regularly maintained and updated.

The planning of the construction and operation of the new system requires a detailed instrument design. The project made use of innovative theoretical studies in signal processing, radar coding, data handling and data analysis, that was summarised in a handbook of measurement principles. The EISCAT_3D will carry out signal processing using software-defined radio receiver systems. The design of the hardware elements needed for the final system and the work on the technical integration of these subsystems were the focus of several of the Work Packages in the project.

A radar system of the complexity of EISCAT_3D requires specialised software both for the system control and for the signal processing and beamforming. The EISCAT system control software

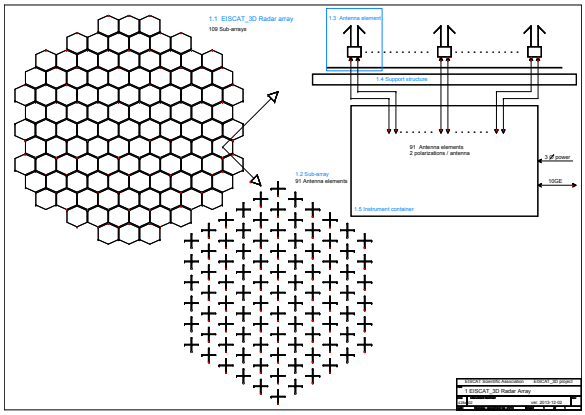


Layout for the central portion of an EISCAT_3D radar array. It contains 109 subarrays with 91 antenna elements each, and thus 9919 antenna elements in total. (From Deliverable 14.2 of the EISCAT_3D Preparatory Phase project)

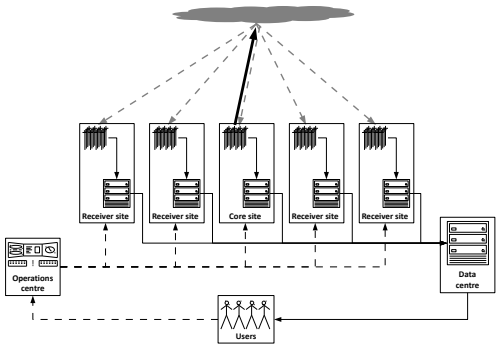


An overview of the EISCAT_3D system. (From Deliverable 14.2 of the EISCAT_3D Preparatory Phase project)

EROS was updated to be able to be used in the context of EISCAT_3D. A parallelised tool for signal processing and data analysis, RLIPS, to be used in the EISCAT_3D radar system was developed, and signal processing and beam-forming software were prepared and tested.

Some of the e-infrastructure needs of EISCAT_3D, such as the network connections between the sites and the computing and data storage near the instruments, require local solutions. Hence a plan was developed with e-infrastructure providers in the host countries for their future involvement in the planning.

# Final results and potential impacts

The overall theme of EISCAT_3D is to explore the multiple facets of the question how the Earth's atmosphere is coupled to space. The EISCAT_3D science encompasses climate change, space weather, space debris and near-Earth object studies. The technical challenges to handle large data volumes will employ tools from the newly emerging field of e-science and spur collaboration with local computing centres. EISCAT_3D will provide an unprecedented resource for observations of the near-Earth space. It will provide long-term time-series data of the ionospheric conditions enabling studies of variations on a time-scale over several solar cycles.

When in operation, EISCAT_3D will be at a central position in the international, and trans-regional, space cluster of Northernmost Scandinavia, which includes large space research centres in Kiruna (Sweden), Sodankylä (Finland) and Tromsø (Norway), two rocket launch facilities in Andøya (Norway) and Esrange (Sweden), and several other instruments and instrument networks for geospace observation such as magnetometers and auroral cameras.

The scientific data from EISCAT_3D will be an invaluable asset for models and near real-time forecasts of space weather effects on modern technology, including power grids and other important infrastructures. EISCAT_3D can also contribute to the Space Situational Awareness (SSA) programme by tracking known space debris and assisting communication and navigation services like the Galileo navigation satellites. Discussions have just been initiated between EISCAT, agencies and institutes in the Nordic countries and the European Space Agency (ESA) on the prospect of including EISCAT_3D in ESA's SSA programme. EISCAT will continue to be an active participant in global observation campaigns and international and European research projects. From its foundation EISCAT has been a purely scientific organisation. The radar technologies to be used with EISCAT_3D allow the detection and tracking of small objects in space. The new Bluebook has stipulations that ensures that the EISCAT facilities will be used strictly for scientific and civilian purposes.

The construction of EISCAT_3D requires close interaction with industry in order to ensure the production of components of the high quality and the large numbers needed. This includes the manufacturing of the antenna elements and the corres-

The participants at the 6th EISCAT_3D User Meeting in Uppsala, Sweden, 12–14 May 2014.

ponding electronics. Engineering solutions could be a development driver for large scale distributed systems in harsh environments.

EISCAT and its users are working together with industry to develop technology and applications for EISCAT_3D. Enterprises, both regional and national, within the EISCAT member countries are expected to respond to invitations to tender for e.g. radio and the digital signal processing instruments, antenna front end and timing systems, and other advanced subsystems.

The timing of EISCAT_3D is ideal. It is now feasible to construct and operate the system and to handle the data volume that the system will provide; this was not the case a few years ago. An increasingly technology-dependent society needs to understand the ionospheric processes caused by space weather in order to minimise their effects on sensitive systems. EISCAT_3D will offer state-of-the-art instruments to the scientific community for dedicated observation campaigns to study processes important for the understanding of our environment and climate, such as the energy coupling between the upper and lower atmosphere, the linkages between the different layers of the upper atmosphere and to interplanetary space, small-scale structures and phenomena as well as micro-meteoroids that enter the atmosphere and participate in atmospheric processes.

# Scientific highlights 2013 – 2014

## The ionosphere

### Seasonal variation and solar activity dependence of the quiet-time ionospheric trough

Ishida et al. (2014) have conducted a statistical analysis of the ionospheric F region trough, focusing on its seasonal variation and solar activity dependence under geomagnetically quiet and moderate conditions, using plasma parameter data obtained via Common Program 3 observations performed by the European Incoherent Scatter (EISCAT) radar between 1982 and 2011. It was confirmed that there is a major difference in frictional heating between the high- and low-latitude sides of the EISCAT field of view (FOV) at about 73°0′N to 60°5′N (geomagnetic latitude) at an altitude of 325 km, which is associated with trough formation (Figure 1). The statistical results show that the high-latitude and mid-latitude troughs occur on the high- and low-latitude sides of the FOV, respectively. Seasonal variations indicate that dissociative recombination accompanied by frictional heating is a main cause of trough formation in sunlit regions. During summer, therefore, the occurrence rate is maintained at 80 % to 90 % in the postmidnight high-latitude region owing to frictional heating by eastward return flow. Solar activity dependence on trough formation indicates that field-aligned currents modulate the occurrence rate of the trough during the winter and equinox seasons. In addition, the trough becomes deeper via dissociative recombination caused by an increased ion temperature with $F10.7$, at least in the equinox and summer seasons but not in winter.

T. Ishida, et al., "Seasonal variation and solar activity dependence of the quiet-time ionospheric trough", Journal of Geophysical Research, 119, doi:10.1002/2014JA019996, 2014.

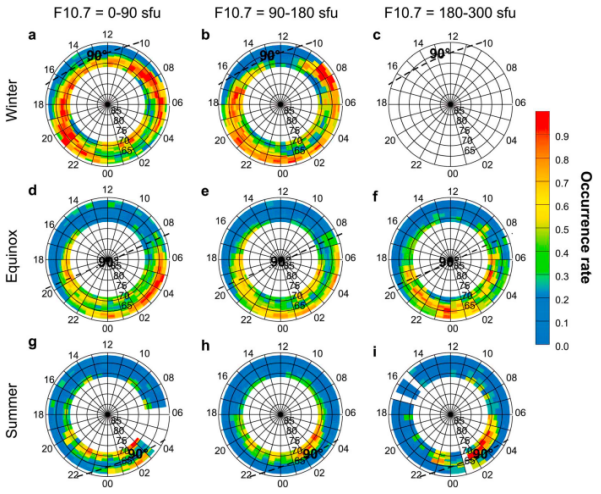


Figure 1: The occurrence rate of the trough divided into three seasons and three solar activities. The black dashed line in each polar plot indicates the average solar terminator, where the solar zenith angle equals 90°.

### Observations of polar cap flow channel and plasma sheet flow bursts during substorm expansion

Pitkänen et al. (2013) present the first simultaneous observations of an enhanced polar cap flow impinging on the nightside polar cap boundary (PCB), two flow bursts in the plasma sheet and a conjugate ionospheric flow burst within the auroral oval (Figure 2). The ionospheric measurements on 3 September 2006 were made by the EISCAT radars and the magnetospheric measurements by the four Cluster spacecraft. In the end of a substorm growth phase, EISCAT measured a channel of enhanced equatorward plasma flow within the polar cap, which was about 1° wide in latitude and drifted slowly equatorward. During the substorm expansion phase, the PCB started to contract poleward. The interaction between the equatorward drifting polar cap flow channel and the poleward contracting PCB took 2 min to 3 min. During this time, the F-region electron temperature was elevated at the PCB, which is inter-

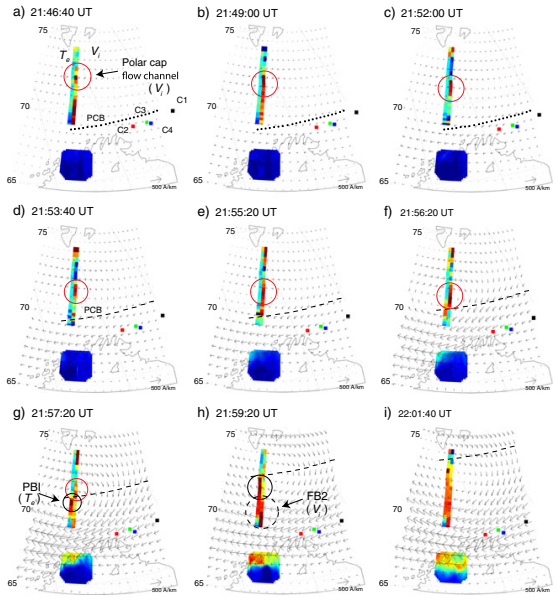


Figure 2: (a–i) Ground-based data during the substorm on 3 September 2006. Coloured bars along the VHF radar beam are $T_e$ (left) and $V_i$ (right) measurements. The octagon displays the IRIS riometer data (arbitrary scale), and black arrows are the equivalent current vectors. The red circle indicates the channel of enhanced ionospheric plasma flow. The black dotted and dashed lines mark the polar cap boundary. The black solid and dashed circles indicate the PBI and the ionospheric counterpart flows of FB2, respectively. The Cluster footpoints are marked by colour squares (black, red, green and blue for Cluster 1, 2, 3, and 4, respectively).

preted as a possible signature of an auroral poleward boundary intensification (PBI). After that, enhanced equatorward flows were measured inside the auroral oval by EISCAT. During this period, the Cluster satellites measured two fast earthward flow bursts in the plasma sheet, which were associated with depolarisation of the magnetic field, depletions in plasma density, and return flows. It is suggested that the second flow burst in the plasma sheet represents the same flow burst that is seen in the ionosphere by EISCAT and propose that the plasma sheet flow bursts were triggered by the enhanced flow structure on open polar cap field lines.

T. Pitkänen, A. T. Aikio, and L. Juusola, "Observations of polar cap flow channel and plasma sheet flow bursts during substorm expansion", Journal of Geophysical Research A, 118, 774–784, 2013.

## Strong E region ionisation caused by the 1767 trail during the 2002 Leonids

Intensive E region ionisation extending up to 140 km altitude and lasting for several hours was observed with the European Incoherent Scatter (EISCAT) UHF radar during the 2002 Leonids meteor shower maximum. The level of global geomagnetic disturbance as well as the local geomagnetic and auroral activity in northern Scandinavia were low during the event. Thus, the ionization cannot be explained by intensive precipitation. The layer was 30 km to 40 km thick, so it cannot be classified as a sporadic E layer which are typically just a few kilometers wide. Incoherent scatter radars have not to date reported any notable meteor shower-related increases in the average background ionization. The 2002 Leonids storm flux, however, was so high that it might have been able to induce such an event. The Chemical Ablation Model is used to estimate deposition rates of individual meteors. The resulting electron production, arising from hyperthermal collisions of ablated atoms with atmospheric molecules, is related to the predicted Leonid flux values and observed ionization on 19 November 2002, see also Figure 3. The EISCAT Svalbard Radar (ESR) located at some 1000 km north of the UHF site did not observe any excess ionization during the same period. The high-latitude electrodynamic conditions recorded by the SuperDARN radar network show that the ESR was within a strongly drifting convection cell continuously fed by fresh plasma while the UHF radar was outside the polar convection region maintaining the ionization.

A. K. Pellinen-Wannberg, et al., "Strong E region ionization caused by the 1767 trail during the 2002 Leonids", Journal of Geophysical Research Space Physics, 119, 7880–7888, doi:10.1002/2014JA020290, 2014.

## Steep plasma depletion in dayside polar cap during a CME-driven magnetic storm

A series of steep plasma depletions was observed in the dayside polar cap during an interval of highly enhanced electron density on 14 October 2000 through EISCAT Svalbard Radar (ESR) field-aligned measurements and northward-directed low-elevation measurements (Figure 4). Each depletion started with a steep dropoff to as low as $10^{11}\,\mathrm{m}^{-3}$ from the enhanced level of about $3 \times 10^{12}\,\mathrm{m}^{-3}$ at F2 region altitudes, and it continued for 10 min to 15 min before returning to the en-

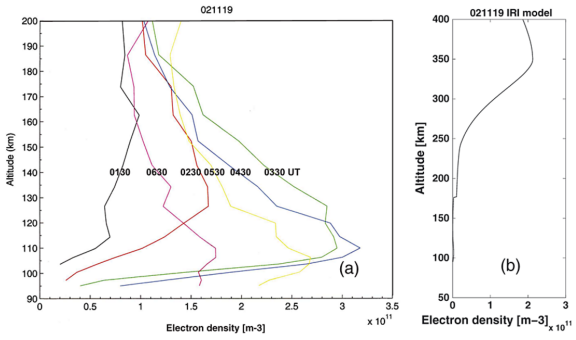


Figure 3: (a) One minute integrated electron density profiles at a set of half hours (1.30, 2.30, 3.30, 4.30, 5.30 and 6.30UT) from EISCAT UHF data. (b) The IRI model electron density profile over Tromsø for the same night.

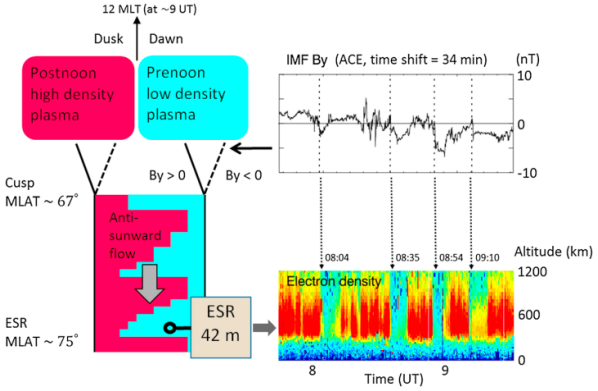


Figure 4: Simplified representation of the process of the ESR electron density variation event observed on 14 October 2000. Two sources of plasmas are depicted at the upper left corner. The reddish color and bluish color represent high-density plasma and low-density plasma respectively. Solid lines and dotted lines represent the shifted convection throat for different IMF $B_y$ conditions, i.e., solid lines for $B_y > 0$ and dotted lines for $B_y < 0$. The undulating boundary between the high-density plasma and low-density plasma in the antisunward flow, which is caused by the IMF $B_y$ change (upper right), is responsible for the ESR density variation (lower right).

hanced level. These depletions moved poleward at a speed consistent with the observed ion drift velocity. DMSP spacecraft observations over an extended period of time which includes the interval of these events indicate that a region of high ion densities extended into the polar cap from the equatorward side of the cusp, i.e., a tongue of ionization existed, and that the ion densities were very low on its prenoon side. Solar wind observations show that a sharp change from IMF $B_y > 0$ to $B_y < 0$ is associated with each appearance of the ESR electron density dropoff. From this unprecedented clear correlation a specific scenario is presented: the series of plasma density depletions observed using the ESR is a result of the poleward drift of the undulating boundary of the tongue of ionization; this undulation is created in the cusp roughly 20 min before the ESR observation by the azimuthal intrusion, in response to the rapid prenoon shift of the footprint of the reconnection line, of the low-density plasmas originating in the morning sector.

J. Sakai, et al., "Steep plasma depletion in dayside polar cap during a CME-driven magnetic storm", Journal of Geophysical Research, 118, doi:10.1029/2012JA018138, 2013.

## Solar wind effect on Joule heating in the high-latitude ionosphere

The effect of solar wind on several electrodynamic parameters, measured simultaneously by the EISCAT radars in Tromsø and on Svalbard, has been evaluated statistically. The main emphasis is on Joule heating rate $Q_J$, which has been estimated by taking into account the neutral wind. In addition, a generally used proxy $Q_E$, which is the Pedersen conductance times the electric field squared, has been calculated. The most important findings are:

1. The decrease in Joule heating in the afternoon-evening sector due to winds requires southward interplanetary magnetic field (IMF) conditions and a sufficiently high solar wind electric field. The increase in the morning sector takes place for all IMF directions within a region where the upper E neutral wind has a large equatorward component and the F region plasma flow is directed eastward.

2. At ESR, an afternoon hot spot of Joule heating centred typically at 14 to 15 magnetic local time (MLT) is observed during all IMF conditions. Enhanced Pedersen conductances within the hot spot region are observed only for the IMF $B_z+/B_y-$ conditions, and the corresponding convection electric field values within the hot spot are smaller than during the other IMF conditions. Hence, the hot spot represents a region of persistent magnetospheric electromagnetic energy input, and the median value is about 3 mW/m$^2$.

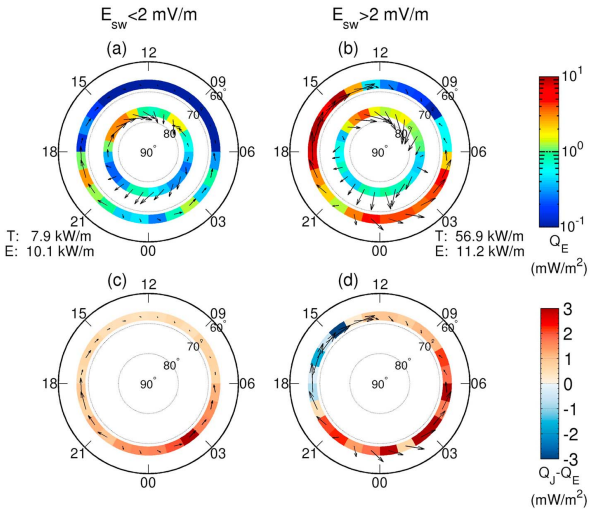


Figure 5: Effect of the solar wind electric field $E_{\mathrm{sw}}$ during IMF $B_z-/B_y+$. (a and b) Joule heating rate $Q_{\mathrm{E}}$ and plasma drift velocities at Tromsø and at ESR. (c and d) Difference $Q_{\mathrm{J}} - Q_{\mathrm{E}}$ and plasma drift velocities at Tromsø. (a) and (c) show results for low-level solar wind electric field $E_{\mathrm{sw}} \leq 2$ mV/m, and (b) and (d) show results for high-level $E_{\mathrm{sw}} > 2$ mV/m. The MLT-integrated $Q_{\mathrm{E}}$ at Tromsø (T) and at ESR (E) are shown in the bottom corner of (a) and (b).

3. For the southward IMF conditions, the MLT-integrated $Q_{\mathrm{E}}$ for $B_y-$ is twice the value for $B_y+$ at TRO. This can plausibly be explained by the higher average solar wind electric field values for $B_y-$.

See Figure 5.

L. Cai, A. T. Aikio, and T. Nygrén, "Solar wind effect on Joule heating in the high-latitude ionosphere", Journal of Geophysical Research Space Physics, 119, doi:10.1002/2014JA020269, 2014.

## Comparison of temporal fluctuations in TEC estimates

A comparison was made between Total Electron Content estimates from EISCAT and GPS measurements using EISCAT data from along the same line of sight of a given GPS satellite observed from Tromsø (Figure 6). The temporal fluctuations in the TEC between the two techniques was compared, which indicated a contribution from structures at E and F region altitudes. This was attributed to the presence of ionisation enhancements possible caused by particle precipitation and it was suggested that EISCAT_3D will have great potential for resolving questions over the cause of TEC variability for Space Weather applications.

B. Forte, et al., "Comparison of temporal fluctuations in the total electron content estimates from EISCAT and GPS along the same line of sight", Annales Geophysicae, 31, doi:10.5194/angeo-31-745-2013, 2013.

## IMF effect on the polar cap contraction and expansion during a period of substorms

The polar cap boundary (PCB) location and motion in the nightside ionosphere has been studied by using measurements from the EISCAT radars and the MIRACLE magnetometers during a period of four substorms on 18 February 2004. The OMNI database has been used for observations of the solar wind and the Geotail satellite for magnetospheric measurements. In addition, the event was modelled by the GUMICS-4 MHD simulation. The simulation of the PCB location was in a rather good agreement with the experimental estimates at the EISCAT longitude (Figure 7). During the first three substorm expansion phases, neither the local observations nor the global simulation showed any poleward motions of the PCB, even though the electrojets intensified. Rapid poleward motions of the PCB took place only in the early recovery phases of the substorms. Hence, in these cases the nightside reconnection rate was locally higher in the recovery phase than in the expansion phase.

In addition, Aikio et al. (2013) suggest that the IMF $B_z$ component correlated with the nightside tail inclination angle and the PCB location with about a 17 min delay from the bow shock. By taking the delay into account, the IMF northward turnings were associated with depolarisations of the magnetotail and poleward motions of the PCB in the recovery phase. The mechanism behind this effect should be studied further.

A. T. Aikio, et al., "IMF effect on the polar cap contraction and expansion during a period of substorms", Annales Geophysicae, 31, 1021–1034, 2013.

## Enhanced plasma-line spectral measurements in the E-region of the polar ionosphere

Strong radar back-scatter from Langmuir-waves, (plasma-lines), are only observed when there is

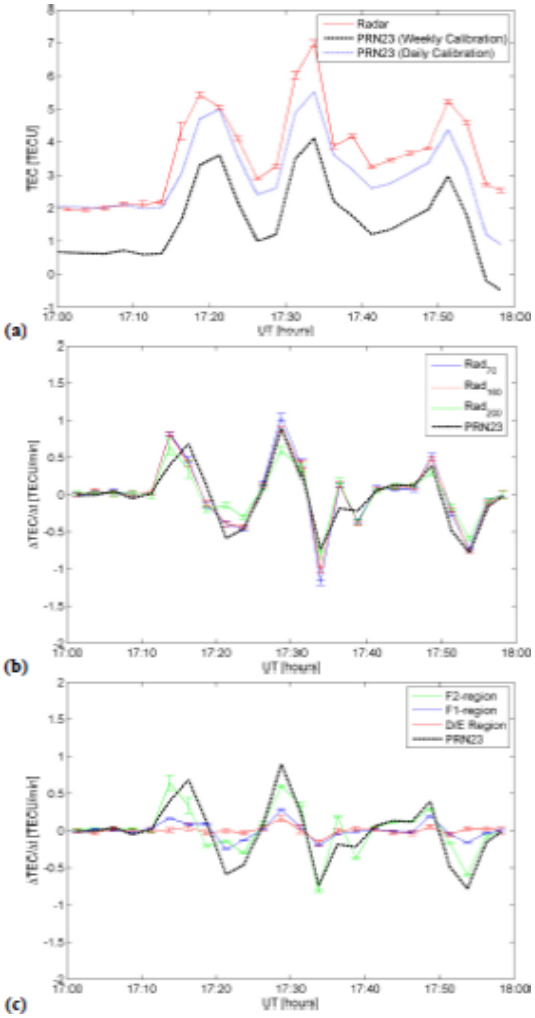


Figure 6: Comparison of slant TEC and its temporal fluctuations between radar and GPS for the measurements from Tromsø on 12 December 2011. (a) Slant TEC as obtained from EISCAT (Tromsø, 12 December 2011) electron density profiles integrated between 70 km altitude and 500 km range in comparison with estimates of the GPS TEC along the same line of sight. (b) Temporal fluctuations in slant TEC along the EISCAT (Tromsø, 12 December 2011) line of sight as integrated from altitudes 70 km (blue), 150 km (red), 200 km (green) upwards until range 500 km. Temporal fluctuations in slant TEC from PRN23 (dashed black) along the same direction are shown as well. The temporal fluctuations are calculated over an interval of approximately 150 s. (c) Contributions to temporal fluctuations in TEC from different ionospheric layers (i.e. D/E, F1 and F2 nominally) in comparison with the overall GPS TEC fluctuations (Tromsø, 12 December 2011). The temporal fluctuations are calculated over an interval of approximately 150 s.

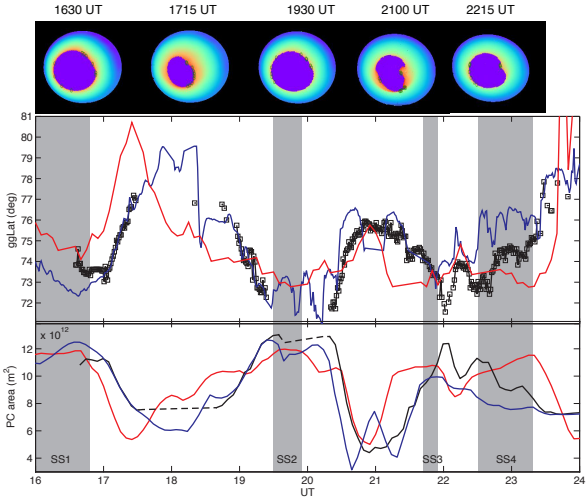


Figure 7: Top panel: Selected plots of the Northern Hemisphere from the GUMICS simulation with violet colour showing the polar cap (12:00 MLT is up and 06:00 MLT to the right). Middle panel: PCB from EISCAT (black line and squares), PCB from the GUMICS simulation (red) and the MCRB (blue). Bottom panel: Polar cap area from the GUMICS simulation (red) and estimates of the polar cap area from EISCAT (black) and MIRACLE (blue). Grey areas denote expansion phases of substorms.

sufficient flux of electrons with suitably high energies, at energies of 5 eV to 100 eV. Such electron-fluxes are at hand during day-time when the ionosphere is sun-lit, and solar EUV causes ionisation and production of photo-electrons, but in dark conditions it only occurs when there is auroral precipitation causing the production of secondary electrons. Traditionally measurements of plasma-lines have been made in rather narrow frequency windows and there only analysed as power integrated over all ranges. With improved data-taking capabilities the EISCAT radars now have the capacity to resolve the plasma-line spectra with 3 km altitude resolution in three wide frequency bands.

We have made observations of strong plasma-line back-scatter during an auroral event, showing enhanced plasma-line power from the E-region peak up to the lower parts of the F-region, and occasionally the strong back-scatter extends even lower/higher (Figure 8). Observations of plasma-line profiles promise significant improvements in the accuracy of electron density estimates compared to ion-line power-based estimates, further it also opens a window to measure field-aligned currents, ion composition and possibly heat-flows. More interestingly we see indications that the

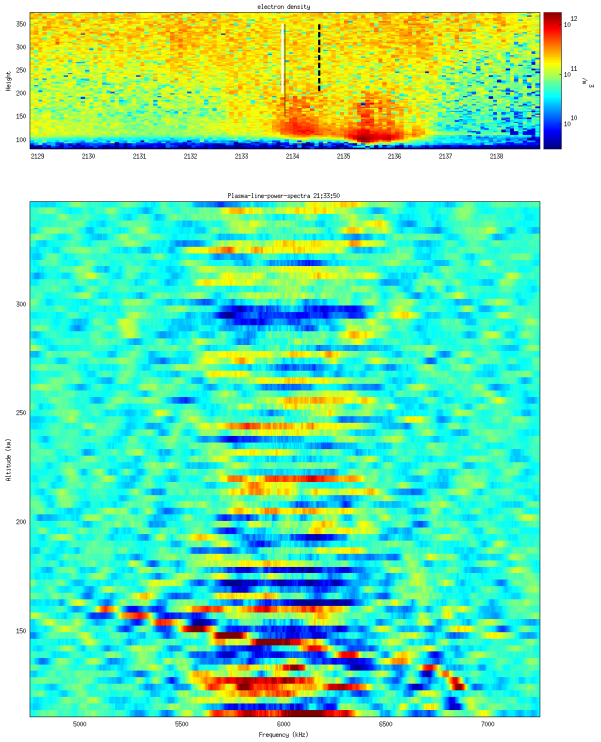


Figure 8: The top panel shows electron density measurements covering the altitude range from about 80 km to 380 km. The bottom panel contains an altitude spectrogram taken at 21:33:50 near the beginning of a precipitation induced electron density enhancement as seen in the top panel.

plasma-line power is significantly larger at altitudes where the plasma-line frequency is just above a multiple of the electron gyro-frequency.

## Two-dimensional direct imaging of structuring of polar cap patches

A highly sensitive all-sky electron multiplier charge-coupled device airglow imager has been operative in Longyearbyen, Norway (78.1° N, 15.5° E), since October 2011. The imager obtains the 630.0 nm all-sky images with an exposure time of 4 s, which is about 10 times shorter than the conventional cooled CCD airglow imagers. This new equipment allows imaging of the ongoing structuring of polar cap patches in 2-D fashion. A case is reported in which faint undulations appeared along the trailing edge of patches propagating in the central polar cap (Figure 9). The separation between the fingers in the undulations was about 50 km to 100 km and the e-folding time of their growth was about 5 min. It is suggested that the gradient-drift instability (GDI) is one of the possible generation mechanisms of the undulating structures. The reasons for this interpretation are:

1. The asymmetry in the preference of structuring between the leading and trailing edges is qualitatively consistent with the GDI mechanism.

2. The linear growth rate of GDI calculated by using electron density estimates from simultaneous European Incoherent Scatter Svalbard radar observations is roughly consistent with the observed growth time of the fingers.

Such "unstable polar cap patches" could be important sources of seed irregularities, which would eventually be broken down to smaller-scale density perturbations affecting the transionospheric satellite communications in the central polar cap.

K. Hosokawa, et al., "Two-dimensional direct imaging of structuring of polar cap patches", Journal of Geophysical Research, 118, doi:10.1002/jgra.50577, 2013.

## ULF wave modulation of the ionospheric parameters: Radar and magnetometer observations

The global Pc5 pulsations at the recovery phase of strong magnetic storm on 31 October 2003 are examined using the IMAGE magnetometer and tri-static EISCAT mainland radar data (Figure 10). This radar facility gives possibility to determine the vertical profile of basic ionospheric parameters and their variations with time cadence 30 s. The comparison of magnetometer data from Tromsø with the ionospheric parameters shows a significant modulation by Pc5 pulsations of the electron density in the E layer, height-integrated ionospheric conductances, and ion temperature in the F layer. This modulation has been observed in the absence of quasi-periodic electron precipitation as evidenced by riometer data. The mechanisms underlying the modulation effects, probably, comprise the Joule ion heating by ULF wave electric field, and feeding/depleting the ionospheric electron content by the wave field-aligned current. The impact of ULF waves on the ionosphere results in a non-linear distortion of ULF wave form, as revealed by the phase portrait method.

V. Pilipenko V., et al., "ULF wave modulation of the ionospheric parameters", Journal of Atmospheric and Solar-Terrestrial Physics, 108, 68–76., doi:10.1016/j.jastp.2013.12.015, 2014.

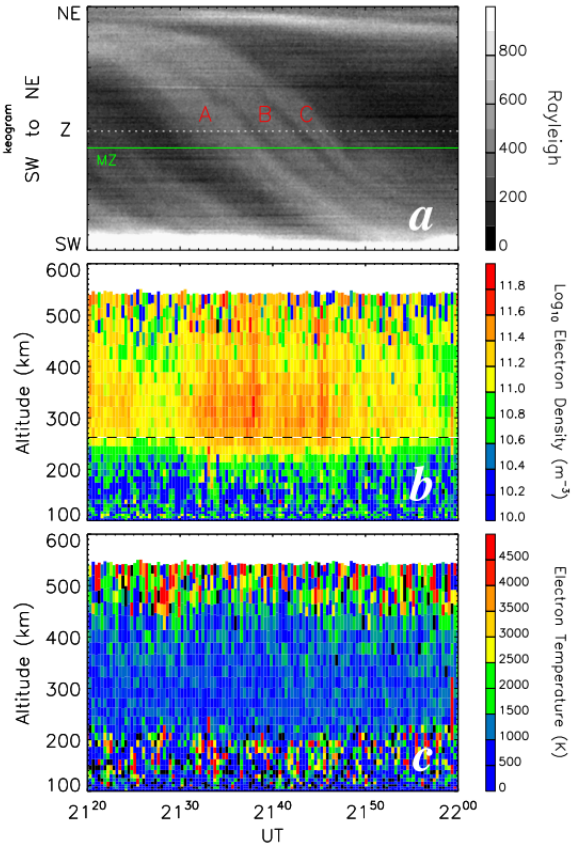


Figure 9: (a) Keogram reproduced from 630.0 nm all-sky images along the SW-NE cross section during a 40 min interval from 2120 to 2200 UT. (b) Altitude-time-intensity plot of the electron density obtained by the 42 m antenna of ESR. (c) Altitude-time-intensity plot of the electron temperature obtained by the 42 m antenna of ESR.

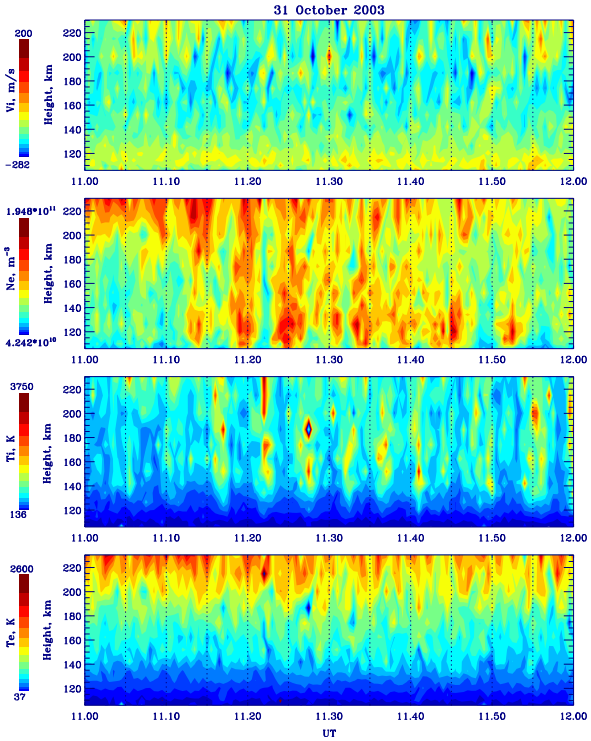


Figure 10: The quasi-3D altitude-time variations of the ionospheric parameters: plasma velocity $V_i$, electron density $N_e$, ion temperature $T_i$, and electron temperature $T_e$.

## Upper atmosphere cooling over the past 33 years

Theoretical models and observations have suggested that the increasing greenhouse gas concentration in the troposphere causes the upper atmosphere to cool and contract. However, our understanding of the long-term trends in the upper atmosphere is still quite incomplete, due to a limited amount of available and well-calibrated data. The European Incoherent Scatter (EISCAT) radar has gathered data in the polar ionosphere above Tromsø for over 33 years. Using this long-term data set, Ogawa et al. (2014) have estimated the first significant trends of ion temperature at altitudes between 200 km and 450 km (Figure 11). The estimated trends indicate a cooling of 10 K/decade to 15 K/decade near the F region peak (220 km to 380 km altitude), whereas above 400 km the trend is nearly zero or even warming. The height profiles of the observed trends are close to those predicted by recent atmospheric general circulation models. These results are the first quantitative confirmation of the simulations and of the qualitative expectations.

Y. Ogawa, et al., "Upper atmosphere cooling over the past 33 years", Geophysical Research Letters, 41, doi:10.1002/2014GL060591, 2014.

## Isolated nighttime substorms and morning geomagnetic Pc5 pulsations from ground-based and satellite (THEMIS) observations

The analysis results of a complex of phenomena that were developing in the evening and morning magnetospheric and ionospheric sectors during two events (January 18 and February 19, 2008) are presented (Figure 12). The analysis is based on the observation data in the magnetotail from the THEMIS satellites and ground-based observations in the morning (MIRACLE network) and nighttime (THEMIS ground-based network) sec-

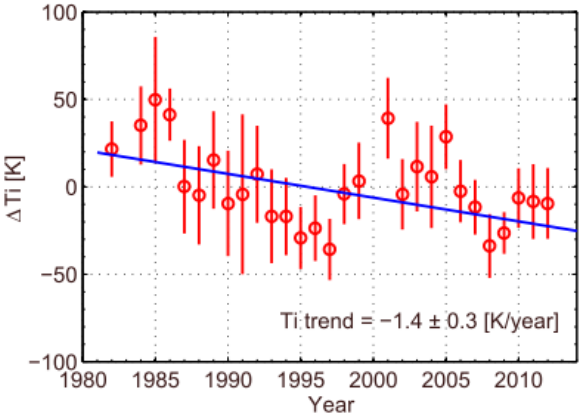


Figure 11: The residual ion temperature at 310 km to 340 km altitude after removal of the solar effects (in red) and a linear fit to it (in blue).

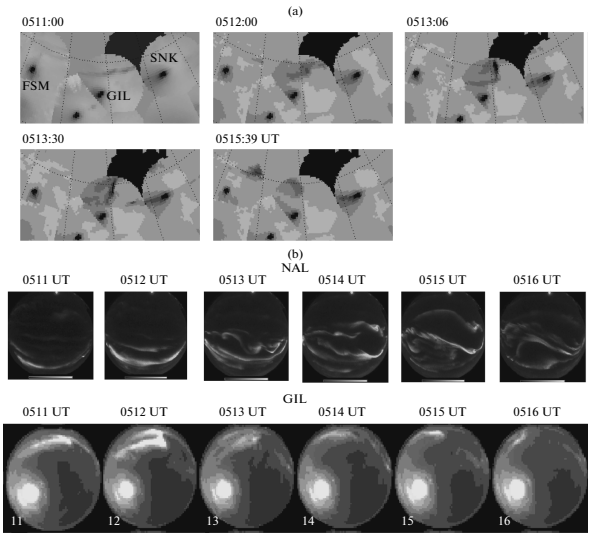


Figure 12: (a) Maps of the dynamics of auroras in the night sector; (b) comparison of simultaneous ASC frames in the morning (NAL observatory) and evening (GIL observatory) sectors.

tors. The events with moderate substorms in the nighttime sector were preceded by strong geomagnetic Pc5 pulsations in the morning sector, the regime of which changed during the development of auroral disturbances. The substorms were accompanied by dipolisations in the magnetotail at distances of about 10 $R_e$ and unexpected jump-like fluxes of electrons with energies around 200 keV. The fluxes appeared within several minutes after a breakup at three central THEMIS satellites simultaneously spaced up to 10 $R_e$. According with the ASC data at the NAL observatory (3 frames/min) and with the THEMIS network of ASC data, onset of auroral activations in the night and morning sectors occurred simultaneously. Probable reasons for the sudden suppression or intensification of Pc5 pulsations are discussed.

K. Kauristie, et al., "Isolated Nighttime Substorms and Morning geomagnetic Pc5 Pulsations from Ground-Based and Satellite (THEMIS) observations", Geomagnetism and Aeronomy, 53, 5, 613–625, 2013.

# The mesosphere and the lower thermosphere

## First modulation of high-frequency polar mesospheric summer echoes by radio heating of the ionosphere

The first high-frequency (HF, 8 MHz) observations were presented of the modulation of polar mesospheric summer echoes (PMSE) by artificial radio heating of the ionosphere. They were compared to observations at 224 MHz and model predictions (Figure 13), and it was shown that model results are in qualitative and partial quantitative agreement with the observations, supporting the prediction that with certain ranges of ice particle radii and concentration, PMSE at HF radar wavelengths can be enhanced by heating due to the dominance of dust charging over plasma diffusion.

A. Senior, et al., "First modulation of high-frequency polar mesospheric summer echoes by radio heating of the ionosphere", Geophysical Research Letters, 41, doi:10.1002/2014GL060703, 2014.

## EISCAT and ESRAD radars observations of polar mesosphere winter echoes during solar proton events on 11–12 November 2004

Remarkable and strong radar echoes from the Earth's mesosphere, the upper boundary of the middle atmosphere, are detected at polar regions, in the months near both summer and winter solstice. These are called Polar Mesospheric Summer and Winter Echoes, PMSE and PMWE. In so-called solar proton events (SPE) the density in the D-region is enhanced, and so these are good opportunities to study particularly PMWE with radars. PMWE were detected by two radars, ESRAD at 52 MHz located near Kiruna, Sweden, and EISCAT at 224 MHz located near Tromsø, Norway, during the strong SPE on 11–12 November 2004. PMWE maximum volume reflectivity was estimated to be

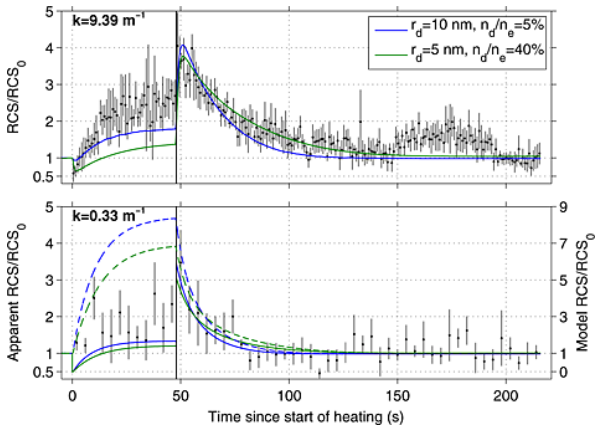


Figure 13: Median change in RCS (radar cross sections per unit volume) over a heating cycle during subinterval a for the (top) VHF and (bottom) HF radars. The vertical line at 48 s after start of heating indicates when heating ceased. The time resolution is 0.96 s for the VHF and 4 s for the HF radar. The backscattering irregularity wave number $k$ is marked in each frame. The error bars show the standard error of the median RCS. In both frames, the solid blue and green lines correspond to modeled RCS variations for dust parameters of $r_d$=10 nm, $n_d/n_e$=5 % and $r_d$=5 nm, $n_d/n_e$=40 %, respectively. In the bottom panel, the dashed blue and green lines show the modeled RCS variations without corrections for observational effects; refer to the right-hand scale for these lines.

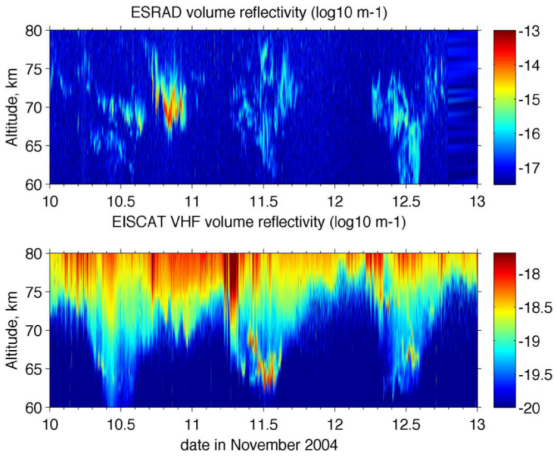


Figure 14: Time–altitude maps of ESRAD (upper panel) and EISCAT VHF volume reflectivities during the SPE on 10–12 November 2004.

$3 \times 10^{-15}$ m$^{-1}$ for ESRAD and $2 \times 10^{-18}$ m$^{-1}$ for EISCAT, see Figure 14. It was found that the shape of the echo power spectrum is close to Gaussian inside the PMWE layers, and outside of them it is close to Lorentzian, similar as the standard incoherent scatter (IS) ion line . The EISCAT PMWE spectral width is about 5 m s$^{-1}$ to 7 m s$^{-1}$ at 64 km to 67 km height and 7 m s$^{-1}$ to 10 m s$^{-1}$ at 68 km to 70 km. At the lower altitudes the PMWE spectral widths are close to those for the IS ion line derived from the EISCAT data outside the layers. At the higher altitudes the PMWE spectra are broader by 2 m s$^{-1}$ to 4 m s$^{-1}$ than those for the ion line. The ESRAD PMWE spectral widths at 67 km to 72 km altitude are 3 m s$^{-1}$ to 5 m s$^{-1}$, that is, 2 m s$^{-1}$ to 4 m s$^{-1}$ larger than ion line spectral widths modelled for the ESRAD radar. The PMWE spectral widths for both EISCAT and ESRAD showed no dependence on the echo strength. It was found that all these facts cannot be explained by a turbulent origin of the echoes. It is suggested that evanescent perturbations in the electron gas generated by incident infrasound waves may explain the observed PMWE spectral widths. However, a complete theory of radar scatter from this kind of disturbance needs to be developed before a full conclusion can be made.

E. Belova, S. Kirkwood, and T. Sergienko, "EISCAT and ESRAD radars observations of polar mesosphere winter echoes during solar proton events on 11–12 November 2004, Annales Geophysicae, 31, 1177–1190, doi:10.5194/angeo-31-1177-2013, 2013.

## Variations of the neutral temperature and sodium density between 80 km and 107 km above Tromsø during the winter of 2010 – 2011 by a new solid state sodium LIDAR

A new solid-state sodium lidar installed at Ramfjordmoen, Tromsø (69.6° N, 19.2° E), started observations of neutral temperature together with sodium density in the mesosphere-lower thermosphere (MLT) region on 1 October 2010. The new lidar provided temperature data with a time resolution of 10 min and with good quality between 80 km and 105 km from October 2010 to March 2011. Nozawa et al. (2014) aim at introducing the new lidar with its observational results obtained over the first 6 months of observations. They succeeded in obtaining neutral temperature and sodium density data of about 255.5 h in total. In order to evaluate our observations, they compared:

1. The sodium density with that published in the literature.

2. The average temperature and column sodium density data with those obtained with Arctic Lidar Observatory for Middle Atmosphere Research Weber sodium lidar

3. The neutral temperature data with those obtained by Sounding of the Atmosphere with Broadband Emission Radiometry/Thermosphere Ionosphere Mesosphere Energetics and Dynamics satellite.

For the night of 5 October 2010, they succeeded in conducting simultaneous observations of the new lidar and the European Incoherent Scatter UHF radar with the tristatic Common Program 1 (CP-1) mode (Figure 15). Comparisons of neutral and ion temperatures showed a good agreement at 104 km between 0050 UT and 0230 UT on 6 October 2010 when the electric field strength was smaller, while significant deviations (up to 25 K) are found at 107 km. Contributions of Joule heating and electron-ion heat exchange were evaluated, but derived values seem to be underestimated.

S. Nozawa, et al., "Variations of the neutral temperature and sodium density between 80 and 107 km above Tromsø during the winter of 2010–2011 by a new solid-state sodium lidar", Journal of Geophysical Research, 119, doi:10.1002/2013JA019520, 2014.

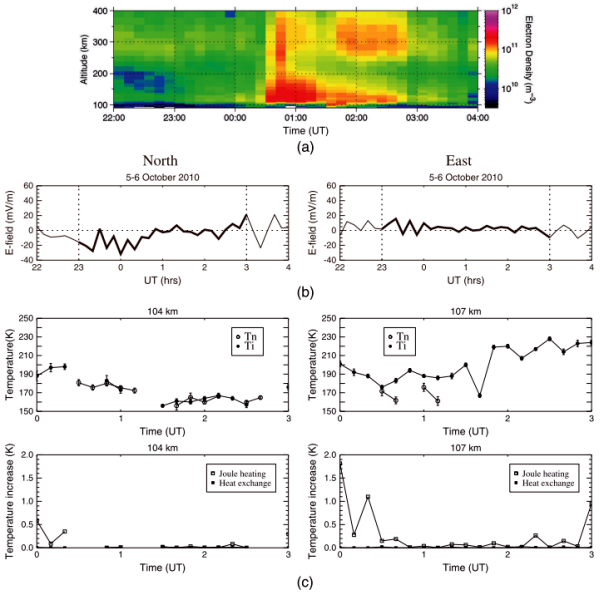


Figure 15: (a) Temporal and altitude variations of the electron density observed with the EISCAT UHF radar at Tromsø are shown from 2200 UT on 5 October to 0400 UT on 6 October 2010. (b) Temporal variations of the electric field of the (left) northward and (right) eastward components observed with the EISCAT UHF radar at Tromsø are shown from 2200 UT on 5 October to 0400 UT on 6 October 2010. Thicker lines denote the electric field values during the simultaneous observations with the sodium lidar. (c) Comparison of neutral (open circle: lidar) and ion (solid circle: EISCAT) temperatures (top left) at 104 km and (top right) at 107 km are shown from 0000 UT to 0300 UT on 6 October 2010. Vertical line associated with each symbol denotes its error value. Calculated temperature increase due to Joule heat (open square) and electron-ion heat exchange (solid square) derived by EISCAT data (bottom left) at 104 km and (bottom right) at 107 km are shown.

# The aurora

## Height-dependent ionospheric variations in the vicinity of nightside poleward expanding aurora after substorm onset

High-latitude ionospheric variations at times near auroral substorms exhibit large temporal variations in both vertical and horizontal extents. Statistical analysis was made of data from the European Incoherent Scatter UHF radar at Tromsø, Norway, and International Monitor for Auroral Geomagnetic Effects magnetometer for finding common features in electron density, ion and electron temperatures and relating these to currents and associated heating (Figure 16). Oyama etal. (2014) particularly focused on the height dependencies. Results show clear evidences of large electric field with corresponding frictional heating and Pedersen currents located just outside the front of the poleward expanding aurora, which typically appeared at the eastside of westward traveling surge. At the beginning of the substorm recovery phase, the ionospheric density had a large peak in the E region and a smaller peak in the F region. This structure was named as C form in this paper based on its shape in the altitude-time plot. The lower altitude density maximum is associated with hard auroral electron precipitation probably during pulsating aurora. The upper F region density maximum was attributed to local ionization by lower energy particle precipitation and/or long-lived plasma that is convected horizontally into the overhead measurement volume from the dayside hemisphere.

S. Oyama, et al., "Height-dependent ionospheric variations in the vicinity of nightside poleward expanding aurora after substorm onset", Journal of Geophysical Research, 119, doi:10.1002/2013JA019704, 2014.

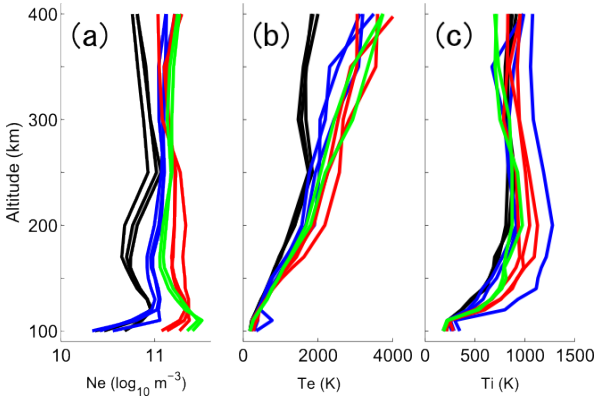


Figure 16: Height profile of (a) electron density, (b) electron temperature, and (c) ion temperature from the superposed epoch analysis of the EISCAT data. Time intervals are grouped by four colors (black: $60 < dt < 30$ min, blue: $30 < dt < 0$ min, red: $0 < dt < +30$ min, and green: $+30 < dt < +60$ min.

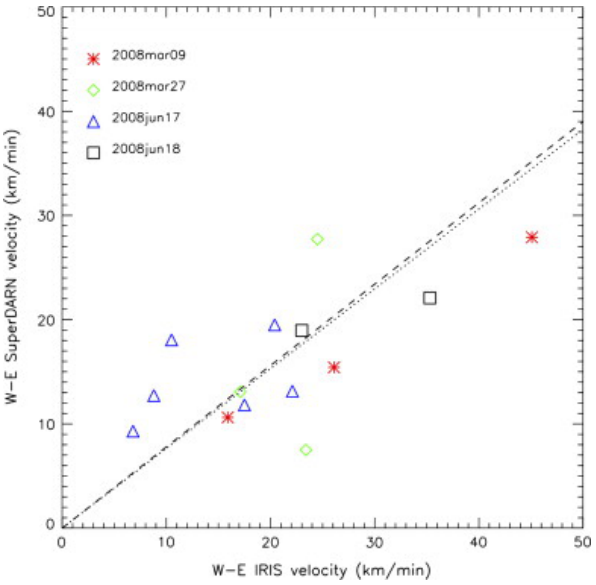


Figure 17: (a) Keogram reproduced from 630.0 nm all-sky images along the SW-NE cross section during a 40 min interval from 2120 to 2200 UT. (b) Altitude-time-intensity plot of the electron density obtained by the 42 m antenna of ESR. (c) Altitude-time-intensity plot of the electron temperature obtained by the 42 m antenna of ESR.

## Properties of auroral radio absorption patches observed in the morning sector

The properties and behaviour of fine structured auroral radio absorption in the morning sector were determined using EISCAT measurements to provide estimates of the energy spectrum of the incoming electrons. It was shown that the observed motion of the absorption was not consistent with the gradient-curvature drift associated with the observed energies, rather the motion was in line with F-region drifts determined from coherent scatter radars suggesting that the cause of the precipitation lies in moving structures within the magnetosphere (Figure 17).

M. J. Birch, J. K. Hargreaves, and B. J. I. Bromage, "Properties of auroral radio absorption patches observed in the morning sector using imaging riometer and incoherent-scatter radar", Journal of Atmospheric and Solar-Terrestrial Physics, 105, doi:0.1016/j.jastp.2012.12.004, 2013.

## On the relation of Langmuir turbulence radar signatures to auroral conditions

Schlatter et al. (2014) present a statistical study of anomalous radar echoes observed in the auroral ionosphere thought to be signatures of Langmuir turbulence (LT). Data obtained with the European Incoherent Scatter Svalbard radar during the international polar year (IPY) were searched for these anomalous echoes in the auroral F region. In incoherent scatter radar experiments LT may in certain circumstances be observed as enhanced backscattered radar power at the ion line frequencies, plasma line frequencies, and at zero Doppler shift, see Figure 18. The power enhancement at zero Doppler shift could arise due to Bragg scattering from non-propagating density fluctuations caused by strong LT. In the IPY data set, around 0.02 % of the data comply with the search criteria for altitudes above 190 km based on the ion line spectrum including enhancement at zero Doppler shift. The occurrence frequency of the identified events peaks in the pre-midnight sector and increases with local geomagnetic disturbance. Enhanced backscattered power is observed with limited altitude extent (below 20 km in 70 % of the events), and the altitude distribution of identified radar signatures in the ion line channel has a peak at about 220 km. Enhancement of the plasma line is observed with the ion line enhancements in more than 60 % of the events. Two classes of enhanced plasma lines occur. In the first class, plasma lines are limited in frequency and altitude and occur at altitudes of ion line enhancements. In the second class, the plasma lines are spread in frequency and range and are observed at lower altitudes than the first class (at about 170 km) with frequencies close to 3 MHz. Available optical data

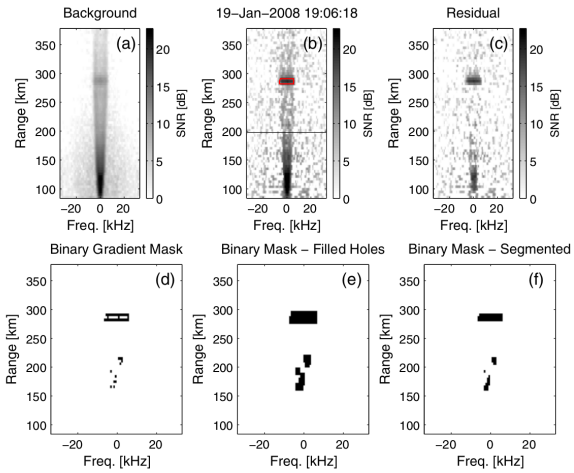


Figure 18: Example of a positive detection observed on 19 January 2008 at 19:06:18 UT. (a) Background power spectral density, (b) ion line power spectral density to be searched, (c) residual of panels (a) and (b), (d) binary gradient mask, (e) extended binary mask with filled holes, and (f) segmented mask. In panel (b) the identified echo is highlighted in red. The horizontal black line corresponds to the cutoff range of the search.

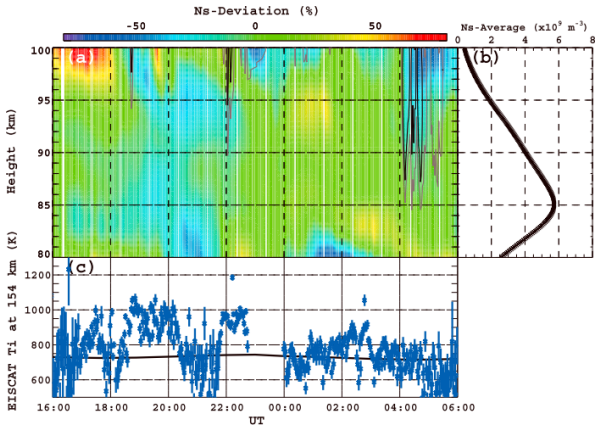


Figure 19: Deviation from averaged sodium number density at each height ($\mathrm{Ns}-\mathrm{Deviation}$), (b) the averaged sodium number density ($\mathrm{Ns}-\mathrm{Average}$), and (c) the ion temperature (blue) at 154 km and the neutral temperature (black thick line) from the NRLMSISE-00 model. Black and gray lines overlaid on the $\mathrm{Ns}-\mathrm{Deviation}$ indicate the electron densities of $3 \times 10^{11}$ m$^{-3}$ and $2 \times 10^{11}$ m$^{-3}$, respectively.

available indicate that the identified events to occur during auroral breakup with high-energy electron precipitation.

N. M. Schlatter, N. Ivchenko, and I. Häggström, "On the relation of Langmuir turbulence radar signatures to auroral conditions", Journal of Geophysical Research Space Physics, 119, 8499–8511, doi:10.1002/2013JA019457, 2014.

## Decrease in sodium density observed during auroral particle precipitation over Tromsø

Using a simultaneous and common-volume observation by a European incoherent scatter (EISCAT) VHF radar and a sodium lidar at Tromsø, Norway (69.6° N, 19.2° E), the effect of pure particle precipitation, excluding that of the electric field, on sodium density variations has been determined for the first time. The observation on 24–-25 January 2012 (Figure 19) showed that sodium atom density decreased when there was no ion temperature enhancement (indicating a weak electric field) and the electron density increased (indicating strong particle precipitation). From the results, it was concluded that auroral particle precipitation induced sodium atom density decrease in this event. Furthermore, a discussion is provided regarding the time response of the decrease in sodium density.

T. T. Tsuda, et al., "Decrease in sodium density observed during auroral particle precipitation over Tromsø, Norway", Geophysical Research Letters, 40, doi:10.1002/grl.50897, 2013.

## Height-dependent energy exchange rates in the high-latitude E-region ionosphere

The statistical properties of the altitude profiles of the different energy transfer rates in the auroral ionosphere are studied by using EISCAT radar measurements in Tromsø. During active conditions, winds reduce the height-integrated Joule heating rates in the evening but enhance them in the morning. Cai et al. (2013) show that the reduction in the evening takes place close to and above the peak altitude of Joule heating, so that the Joule heating peak descends from the Pedersen conductivity maximum at 120 km down to about 115 km. Values close to the peak are reduced also in the morning, but the positive effect by winds above the peak makes the net effect positive. The altitude range where the electromagnetic energy of magnetospheric origin is converted to the mechanical energy of the neutrals is only 20 km to 35 km wide in the E region and shows a clear magnetic local time variation. Model calculations are used

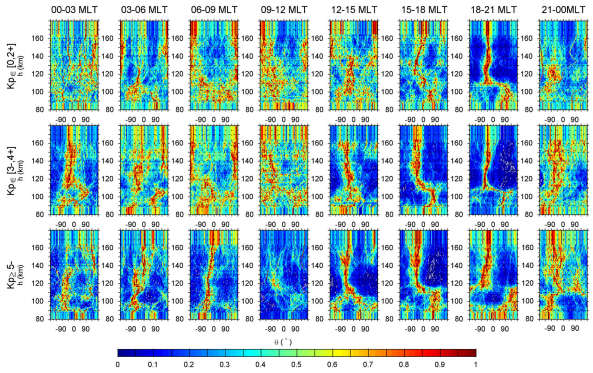


Figure 20: The angle $\theta$ between the wind velocity $\vec{u}_\perp$ and the electric field $\vec{E}$ are shown by a normalised number of samples as a function of the geomagnetic activity (rows) and MLT sectors (columns). The value $-90°$ corresponds to the $\vec{E} \times \vec{B}$ direction.

to study the effect of the angle between the wind and electric field directions (Figure 20) on the energy transfer rates and to explain the observed features.

L. Cai, A. T. Aikio, and T. Nygrén, "Altitude profiles of energy exchange rates in the high-latiude ionosphere", Journal of Geophysical Research A, in press, 2013.

## Enhanced EISCAT UHF backscatter during high-energy auroral electron precipitation

Natural enhancements in the backscattered power of incoherent scatter radars up to five orders of magnitudes above the thermal backscatter are sometimes observed at high latitudes. Recently observations of enhancements in the backscattered power including a feature at zero Doppler shift have been reported. These enhancements are limited in altitude to tens of kilometers. The zero Doppler shift feature has been interpreted as a signature of electron density cavitation. Enhanced plasma lines during these observations have also been reported. Schlatter et al. (2013) report on the first EISCAT UHF observations of enhanced backscattered radar power including a zero Doppler shift feature. The enhancements originated from two distinct and intermittent layers at about 200 km altitude. The altitude extent of the enhancements, observed during auroral high-energy electron precipitation, was <2 km. See also Figure21.

N. M. Schlatter, et al., "Enhanced EISCAT UHF backscatter during high-energy auroral electron precipitation", Annales Geophysicae, 31, 1681-1687, doi:10.5194/angeo-31-1681-2013, 2013.

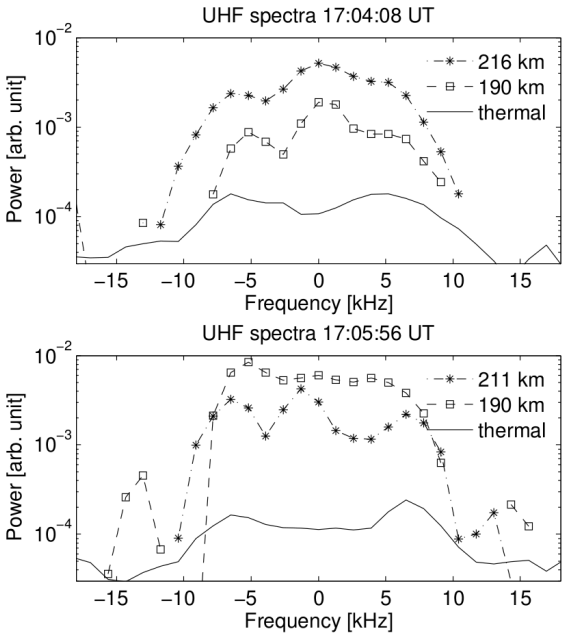


Figure 21: Radar ion line spectra at 17:04:08 and 17:05:56 UT for the upper (dot-dashed line, asterisks) and lower (dashed line, squares) enhancements with 4 s integration time. The two solid lines show thermal spectra with integration time of 20 s from the altitude region in between the two layers of enhanced backscattered power.

# Studies using the Heating facility

## Observation of VHF incoherent scatter spectra disturbed by HF heating

An ionospheric heating experiments carried out on 13 September 2010 at EISCAT in Tromsø, Norway. During the experiment, it was found that the altitude of the enhanced spectral lines descends in the altitude throughout the heater-on period, for which one possible mechanism being response is given. Namely, due to ionospheric heating, the electrons near the interaction region diffuse, resulting in two electron density peaks on both sides of this region, the below one of which form a new the ordinary reflection height.

Cheng Musong, Xu Bin, Wu Zhensen, Li Haiying, Wang Zhange, Xu Zhengwen, Wu Jun and Wu Jian, "Observation of VHF incoherent scatter spectra disturbed by HF heating", Journal of Atmospheric and Solar-Terrestrial Physics 105–106, 245–252, 2013.

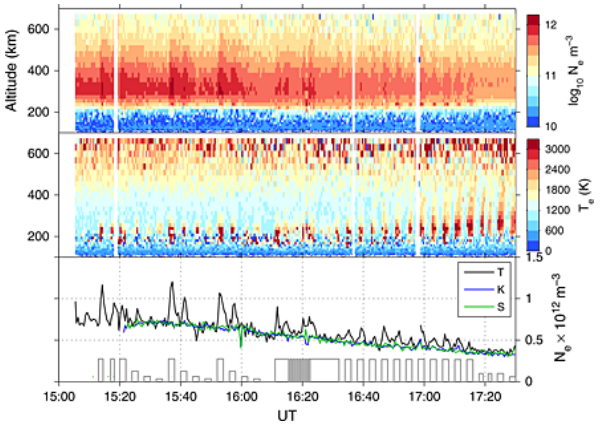


Figure 22: (top) Time series of electron density profiles from the UHF radar on 11 November 2001. (middle) The corresponding time series of electron temperature profiles. (bottom) Time series of electron density at an altitude of 302 km from Tromsø (black), at 291 km from Kiruna (blue) and at 300 km from Sodankylä (green). The grey bars indicate the relative pump power.

## Radio-induced incoherent scatter ion line enhancements

An investigation was performed of recently reported large electron density enhancements measured during high power radio wave injection experiments at EISCAT. The apparent enhancements extend over a wide altitude range, including the topside ionosphere. Observational evidence are presented showing that the apparent density enhancements seem to exhibit aspect-sensitive backscattering and are not associated with corresponding changes in the frequency of the incoherent scatter plasma line (Figure 22). From this it is concluded that the enhancement in the power in the ion-line is not actually a result of an enhancement in the plasma density but is rather due to some other mechanism that preferentially scatters the radar wave back along the magnetic field line. A physical mechanism to explain this has not yet been described.

A. Senior, et al., "Radio-induced incoherent scatter ion line enhancements with wide altitude extents in the high-latitude ionosphere", Geophysical Research Letters, 40, doi:10.1002/grl.50272, 2013.

## A large increase of electron density in ionospheric heating experiment

During a high latitude ionospheric heating experiment carried out with the EISCAT heater in November 2011 in Norway. An obviously increased electron density was observed by UHF radar, which is up to 269.3 % around the reflection height and about 30 % to 50 % at the altitude range of 300 km to 500 km. To the authors' knowledge, the large increase of electron density in such a large range of space is extremely rare and may be caused by suprathermal electrons.

Cheng MuSong, Xu Bin, Wu ZhenSen, et al., "A large increase of electron density in ionospheric heating experiment", Chinese Journal Geophysics 57(11), 3633–3641, doi:10.6038/cjg20141117, 2014.

## Observations of HF-induced instability in the auroral E region

Enhancements were observed in backscattered radar power during an ionospheric heating experiment from two distinct altitude regions in the auroral E region above Tromsø. For the experiment the EISCAT Tromsø heater was operated with O mode and X mode alternated at 4.04 MHz, close to the third electron gyroharmonic. Ion-line data recorded with the EISCAT UHF radar reveal different temporal evolutions as well as different ion-line characteristics for the enhancements from the two altitude regions. The upper layer is dominated by a strong central feature, whereas the lower layer has three peaks corresponding to the central feature and the two ion lines. The altitude region of the two closely spaced (altitude separation around 5 km) but distinct enhancements is close to the critical altitude for the heater wave. Figure 23 shows an example.

N. M. Schlatter, et al., "Observations of HF-induced instability in the auroral E region", Annales Geophysicae, 31, 1103-1108, doi:10.5194/angeo-31-1103-2013, 2013.

## High latitude artificial periodic irregularity observations with the upgraded EISCAT heating facility

Vierinen et al. (2013) present a recently developed ionospheric modification experiment that produces artificial periodic irregularities in the ionosphere and uses them to make observations of the spatio-temporal behaviour of the irregularities. In addition, the method can be used to measure Faraday rotation and vertical velocities. They also introduce a novel experiment that allows monitoring the formation of the irregularities during heating, in addition to observing their

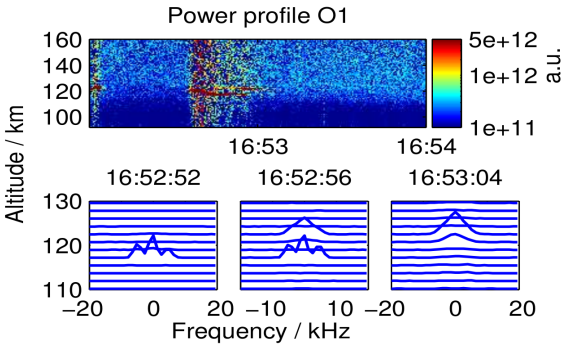


Figure 23: The top panel shows the radar power profile observed during O-mode heating cycle O1 (16:52–16:54 UT) with enhancements in back scattered power from two distinguished altitude layers. At times of enhanced backscatter self-clutter caused by the radar program can be seen at altitudes up to 180 km. In the bottom panel ion-line spectra are shown measured at 16:52:52, 16:52:56 and 16:53:04 UT with 4 s integration. The spectra are normalized to an arbitrary value and the baseline of each spectrum corresponds to altitude.

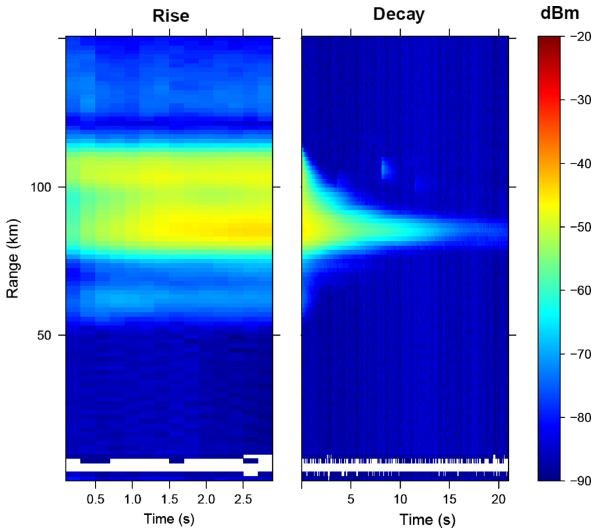


Figure 24: The rise and decay of the API echoes on the 12th of December 2011. All probing pulses are X-mode. The power is averaged over 20 min (9:30–9:50 UTC). The averaged decay plot also contains weak signatures of several meteor trail echoes.

decay after heating. The first measurements indicate, contrary to existing theory, that the amplitude of the radar echoes from the periodic irregularities grows faster than they decay (Figure 24). The focus is on the API effects in the D and E region of the ionosphere.

J. Vierinen, A. Kero, and M. T. Rietveld, "High latitude artificial periodic irregularity observations with the upgraded EISCAT heating facility", Journal of Atmospheric and Solar-Terrestrial Physics, 105, 253–261, doi:10.1016/j.jastp.2013.08.012, 2013.

# Observation techniques

## TID characterised using joint effort of incoherent scatter radar and GPS

Travelling Ionospheric Disturbances (TIDs), which are caused by Atmospheric Gravity Waves (AGWs), are detected and characterised by a joint analysis of the results of two measurement techniques: incoherent scatter radar and multiple-receiver GPS measurements (Figure 25). The strengths of both techniques are combined, in order to obtain semi-automatic tools for TID detection. The radar provides a good vertical range and resolution and the GPS measurements provide a good horizontal range and resolution, while both have a good temporal resolution. Using the combination of the methods, the following parameters of the TID can be determined: the time of day when the TID occurs at one location, the period length (or frequency), the vertical phase velocity, the amplitude spectral density, the vertical wave-length, the azimuth angle of horizontal orientation, the horizontal wavelength, and the horizontal phase velocity. This technique will allow a systematic characterisation of AGW-TIDs, which can be useful, among other things, for statistical analyses.

M. Van de Kamp, D. Pokhotelov, and K. Kauristie, "TID characterised using joint effort of incoherent scatter radar and GPS", Annales Geophysicae, 32, 1511–1532, doi:10.5194/angeo-32-1511-2014, 2014.

## Radar baud length optimisation of spatially incoherent time-independent targets

While it may be a general belief that the optimal baud length for radar measurements of range extended targets should be close to the desired resolution, this is only an approximate truth for weak targets and not true at all for strong targets. Lehtinen and Damtie (2013) use full measurement error estimates with proper correlations and find numerically the baud length which optimises the posteriori variance of an extended target (Figure 26). While the pulse is assumed to be a simple

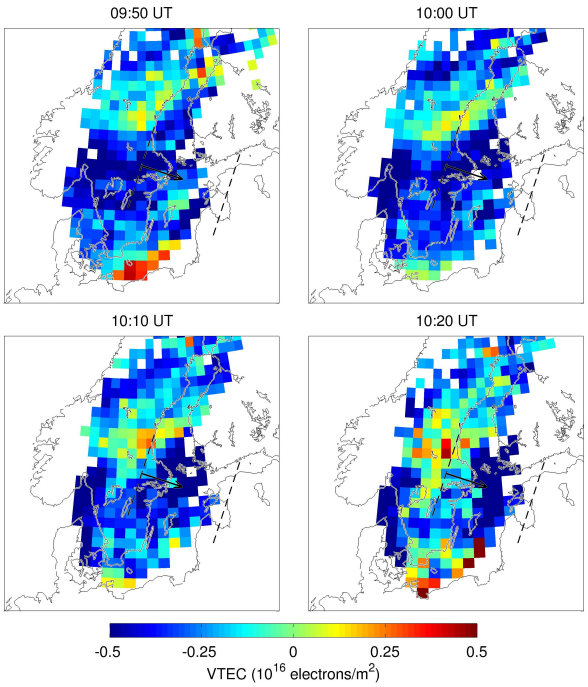


Figure 25: The TEC derived from the GPS data in a 2-D horizontal grid, and the wave properties of the detected TIDs superimposed on the plots, at four times on 20 January 2010.

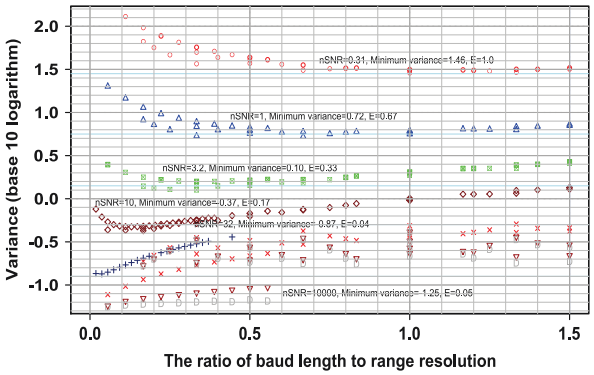


Figure 26: Posteriori variance of the lag profile as a function of the ratio of the baud length to desired range resolution for the case of measurement with different nSNR scenarios. The different symbols represent different combinations of discretisation accuracy and model lengths so that numerical calculations have been possible with the computers we use (R run on a PC with 8 GB RAM). Up to target strength $\mathrm{nSNR} = 32$ it is evident that a rather clear relationship between pulse length and posteriori variance can be interpreted, but for stronger targets we have not been able to produce enough results to be able to display a clear relationship.

boxcar with a given fixed energy and the baud length is the only design parameter, the results extend to many traditional ways of pulse compression coding through arguments derived from recent results on rigorous experiment comparison and perfect coding.

M. S. Lehtinen, and B. Damtie, "Radar baud length optimisation of spatially incoherent time-independent targets", Journal of Atmospheric and Solar-Terrestrial Physics, 105, 281–286, doi:10.1016/j.jastp.2012.10.010, 2013.

## Radar interferometer calibration of the EISCAT Svalbard Radar and a additional receiver station

The EISCAT Svalbard Radar has two parabolic dishes. In order to attempt to implement radar aperture synthesis imaging methods three smaller, passive receive array antennas were built. Several science goals for this new receiver system exist, the primary of which is to study so called naturally enhanced ion acoustic lines. In order to compare radar aperture synthesis imaging results with measurements from optical imagers, calibration of the radar interferometer system is necessary. Schlatter et al. (2013) present the phase calibration of the EISCAT Svalbard interferometer including one array antenna. The calibration was done using the coherent scatter from satellites passing through the radar beam. Optical signatures of the satellite transits provide accurate position for the satellites. Using transits of a number of satellites sufficient for mapping the radar beam, the interferometric cross-phase was fitted within the radar beam. This calibration technique will be applied to all antenna pairs of the antenna configuration for future interferometry studies.

N. M. Schlatter, et al., "Radar interferometer calibration of the EISCAT Svalbard Radar and a additional receiver station", Journal of Atmospheric and Solar-Terrestrial Physics, 105, 287-292, doi:10.1016/j.jastp.2012.11.017, 2013.

## Ionospheric electron density profiles inverted from a spectral riometer measurement

The first implementation of the so-called spectral riometer technique for the ionospheric electron density profile estimation is presented. In contrast to the traditional riometer operating at a single frequency, this experiment monitors the cosmic radio noise at 244 frequencies, ranging from 10 MHz to

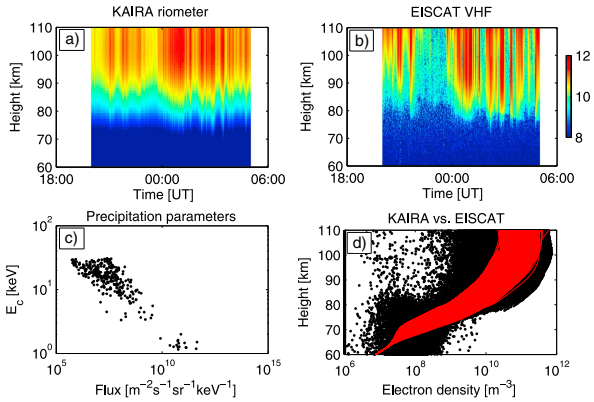


Figure 27: Inversion results. (a) Electron density (base-10 logarithm, $m^{?3}$) inverted from the absorption data. (b) EISCAT VHF electron density profiles retrieved from an experiment optimised for the D and E layers. Both (a) and (b) have the same colour scale. (c) Maximum a posteriori values of the precipitation parameters used in the fitting, i.e. characteristic energy versus electron flux. (d) Riometer electron density estimates (red) plotted on top of all the EISCAT electron density measurements (black).

80 MHz, by using the new Kilpisjärvi Atmospheric Imaging Receiver Array (KAIRA) radio telescope. The received power at each time and frequency is compared to the corresponding quiet-day value, resulting in the cosmic radio noise absorption spectrum as a measurement of ionisation in the ionosphere. In this study, the observed absorption spectrum is used to invert the corresponding electron density profile by applying a simple parameterised electron precipitation model. By comparing the inverted electron density profiles to a simultaneous and nearly co-located EISCAT VHF radar measurement on 13–14 November 2012, Kero et al. (2014) show that the spectral riometry approach is capable of producing realistic electron density profiles under conditions of substorm-related electron precipitation (Figure 27).

A. Kero, et al., "Ionospheric electron density profiles inverted from a spectral riometer measurement", Geophysical Research Letters 41 (15), 5370–5375, doi:10.1002/2014GL060986, 2014

## Medium-scale 4-D ionospheric tomography using a dense GPS network

The ionosphere above Scandinavia in December 2006 has been successfully imaged by 4-dimensional tomography using the software package MIDAS from the University of Bath (Figure 28). The method concentrates on medium-scale structures: 100 km to 2000 km in horizontal size. The input consists of TEC measurements from the dense GPS network Geotrim in Finland. In order to ensure sufficient vertical resolution, EISCAT radar data from Tromsø are used to provide the vertical profile information.

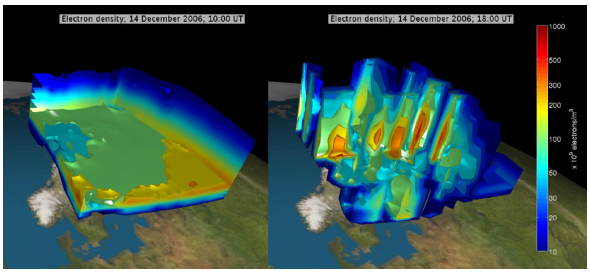


Figure 28: Two snapshots of the 3-dimensional inversion results for 14 December.

The TEC offset of the measurements is unknown, but the inversion procedure is able to determine this automatically. This auto-calibration is shown to work well.

Comparisons with EISCAT radar results and with occultation results show that the inversion using EISCAT data for profile information is much better able to resolve vertical profiles of irregular structures than the inversion using built-in profiles. Still, with either method the intensities of irregular structures of sizes near the resolution (about 100 km horizontal size) can be underestimated. Also, the accuracy of the inversion worsens above areas where no receivers are available.

M. Van de Kamp M, "Medium-scale 4-D ionospheric tomography using a dense GPS network", Annales Geophysicae, 31, 75–89, 2013.

## First observation of the anomalous electric field in the topside ionosphere by ionospheric modification

A technique was developed to estimate the steady state, field-aligned anomalous electric field in the topside ionosphere. If the ionosphere is pumped with high-power high-frequency radio waves, the F region electron temperature is raised, increasing the plasma pressure gradient in the topside ionosphere (Figure 29). This results in ion upflow along the magnetic field line. The electric field is estimated from a modified ion momentum equation and the MSIS model.

M. J. Kosch, et al., "First observation of the anomalous electric field in the topside ionosphere by ionospheric

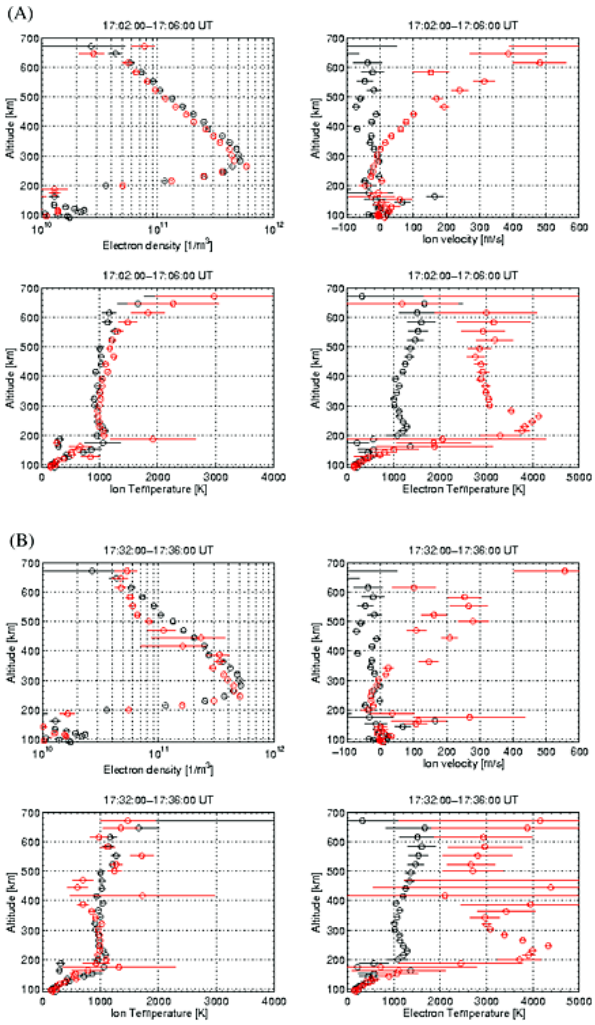


Figure 29: EISCAT field-aligned radar observations for 23 October 2013 for the selected intervals of (a) 17:02 UT – 17:06 UT and (b) 17:32 UT – 17:36 UT. Pump-on data are in red. Pump-off data (17:21 UT – 17:24 UT) are in black. Shown as a function of altitude are electron density (Figures a and b, top left), ion velocity (Figures a and b, top right), ion temperature (Figures a and b, bottom left), and electron temperature (Figures a and b, bottom right). The data uncertainty is also indicated.

modification over EISCAT", Geophysical Research Letters, 41, doi:10.1002/2014GL061679, 2014.

## Kilpisjärvi Atmospheric Imaging Receiver Array — First Results

The Kilpisjärvi Atmospheric Imaging Receiver Array (KAIRA) is a dual antenna array radio receiver based on LOFAR technology. The main purpose of the system is to function as a bi-static phased-array receiver for the EISCAT Tromsø VHF radar,

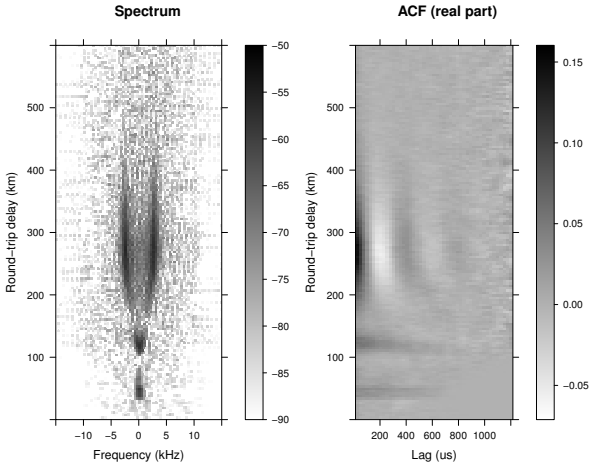


Figure 30: First multi-beam bi-static incoherent scatter radar measurement demonstrating the measurement of a full ionospheric incoherent scatter spectrum profile. Different altitude regions measured with the different beams are summed together to form a single profile. The spectrum is shown on the left and power is reported in dB units in arbitrary scale. The real part of the autocorrelation function estimates are shown on the right.

as well as to function as a wide band imaging riometer. Due to the wide frequency coverage, the system can also be used as a bi-static radar receiver for various nearby meteor- and MST-radars. Other examples of possible uses for the system include broad-band observations of solar radio emissions and ionospheric scintillation. In addition to a technical overview, Vierinen et al. (2014) present the first results from this recently completed system. These include the first multi-beam bi-static incoherent scatter radar observation (Figure 30), as well as a broad-band riometer absorption measurement.

J. Vierinen, et al., "Kilpisjärvi Atmospheric Imaging Receiver Array: First Results", IEEE International Symposium on Phased Array Systems & Technology, 15–18 October 2013, Waltham, MA, IEEE.

## Plasma parameter estimation from multi-static, multi-beam incoherent scatter data

Multi-static incoherent scatter radars are superior to mono-static facilities in the sense that multi-static systems can measure plasma parameters from multiple directions in volumes limited by beam dimensions and measurement range resolution. Virtanen et al. (2014) propose a new in-

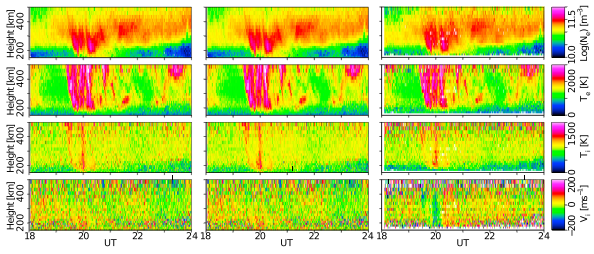


Figure 31: Analysis results for an EISCAT VHF Bella experiment. Plasma parameter estimates (left) from analysis of mono-static EISCAT Tromsø VHF data alone, (middle) from bistatic analysis with data from the Tromsø VHF and KAIRA, projected to the mono-static Tromsø VHF line of sight, and (right) from KAIRA data alone. From top to bottom, the plasma parameters are electron density, electron temperature, line-of-sight ion temperature, and line-of-sight ion velocity.

coherent scatter analysis technique that uses data from all receiver beams of a multi-static, multi-beam radar system and produces, in addition to the plasma parameters typically measured with mono-static radars, estimates of ion velocity vectors and ion temperature anisotropies. Because the total scattered energy collected with remote receivers of a modern multi-static, multi-beam radar system may even exceed the energy collected with the core transmit-and-receive site, the remote data improve the accuracy of all plasma parameter estimates, including those that could be measured with the core site alone. The new multi-static analysis method is applied for data measured by the tri-static European Incoherent Scatter VHF radar and the Kilpisjärvi Atmospheric Imaging Receiver Array (KAIRA) multi-beam receiver and show that a significant improvement in accuracy is obtained by adding KAIRA data in the multi-static analysis (Figure 31). The development of a pronounced ion temperature anisotropy during high-speed ionospheric plasma flows in substorm conditions is also demonstrated.

I. Virtanen, et al., "Plasma parameter estimation from multistatic, multibeam incoherent scatter data", Journal of Geophysical Research Space Physics, 119, 10 528–10 543, doi:10.1002/2014JA020540.2014, 2014.

# List of publications

## Publications 2013


Aikio, A. T., T. Pitkänen, I. Honkonen, M. Palmroth, and O. Amm, IMF effect on the polar cap contraction and expansion during a period of substorms, Ann. Geophys., 31, 1021-1034, doi:10.5194/angeo-31-1021-2013, 2013.

Argese, Chiara, Type-I ion outflow from the high latitude ionosphere, Master's Thesis in Space Physics, University of Tromsø, Norway, 2013.

Bauer, P., A. Giraud, W. Kofman, M. Petit, and P. Waldteufel, How the Saint Santin incoherent scatter system paved the way for a French involvement in EISCAT, Hist. Geo Space Sci., 4, 97-103, doi:10.5194/hgss-4-97-2013, 2013.

Belova, E., S. Kirkwood, and T. Sergienko, EISCAT and ESRAD radars observations of polar mesosphere winter echoes during solar proton events on 11-12 November 2004, Ann. Geophys., 31, 1177-1190, doi:10.5194/angeo-31-1177-2013, 2013.

Borisova, T. D., N. F. Blagoveshchenskaya, I. M. Ivanova, and M. T. Rietveld, Dependence of the Pc4 Magnetic Pulsation Parameters on the Radiated Power of the EISCAT HF Heating Facility, Geomagnetism and Aeronomy, 53, 1, 32-42, 2013.

Birch, M. J., J. K. Hargreaves, B.J.I. Bromage, Properties of auroral radio absorption patches observed in the morning sector using imaging riometer and incoherent-scatter radar, Journal of Atmospheric and Solar-Terrestrial Physics, 105-106, 262-272, 2013.

Blagoveshchenskaya, N. F., T.D. Borisova, T. K. Yeoman, M. T. Rietveld, I. Häggström, I. M. Ivanova, Plasma modifications induced by an X-mode HF heater wave in the high latitude F region of the ionosphere, Journal of Atmospheric and Solar-Terrestrial Physics, 105-106, 231-244, 2013.

Bryers, C., M. Kosch, A. Senior, T. Yeoman amd M. Rietveld, DIY Northern Lights, Astronomy and Geophysics, 54, 6, 43-44, 2013.

Cai, L., A. T. Aikio and T. Nygén, Height-dependent energy exchange rates in the high-latitude E region ionosphere, J. Geophys. Res., 118, 11, , 7369-7383, DOI: 10.1002/2013JA019195, 2013.

Carlson, H. C., K. Oksavik, J. I. Moen, Thermally Excited 630.0 nm O(1D) Emission in the Cusp: A Frequent High-Altitude Transient Signature, J. Geophys. Res., 118, 9, DOI: 10.1002/jgra.50516, 2013.

Cheng, M., B. Xu, Z. Wu, H. Li, Z. Wang, Z. Wu, J. Wu, J. Wu, Observation of VHF incoherent scatter spectra disturbed by HF heating, Journal of Atmospheric and Solar-Terrestrial Physics, 105-106, 245-252, 2013.

Cresswell-Moorcock, K., C. J. Rodger, A. Kero, A. B. Collier, M. A. Clilverd, I. Häggström, T. Pitkänen, A reexamination of latitudinal limits of substorm-produced energetic electron precipitation, J. Geophys. Res., DOI: 10.1002/jgra.50598, 2013.

Di Loreto, Massimo, On the relation between type-II ion outflow and naturally enhanced ion acoustic lines in the polar ionosphere, Master's Thesis in Space Physics, University of Tromsø, Norway, 2013.

Forte, B., N. D. Smith, C. N. Mitchell, F. Da Dalt, T. Panicciari, A. T. Chartier, D. Stevanovic, M. Vuckovic, J. Kinrade, J. R. Tong, I. Häggström, and E. Turunen, Comparison of temporal fluctuations in the total electron content estimates from EISCAT and GPS along the same line of sight, Ann. Geophys., 31, 745-753, doi:10.5194/angeo-31-745-2013, 2013.

Galushko, V. G., V. G. Bezrodny, A. V. Koloskov, V. V. Paznukhov, B. W. Reinisch, HF wave scattering by field-aligned plasma irregularities considering refraction in the ionosphere, Radio Sci., 48, 2, 180–189, DOI: 10.1029/2012RS005072, 2013.

van de Kamp, M. M. J. L., Medium-scale 4-D ionospheric tomography using a dense GPS network, Ann. Geophys., 31, 75-89, doi:10.5194/angeo-31-75-2013, 2013.

Li, Q. and M. Rapp, PMSE-observations with the EISCAT VHF and UHF-Radars: Ice particles and their effect on ambient electron densities, J. Atmos. Sol. Terr. Phys., 104, 270-276, 2013.

Luehr, H., and S. Marker, High-latitude thermospheric density and wind dependence on solar and magnetic activity, in "Climate and Weather of the Sun-Earth system (CAWSES). Highlights from a Priority Program", Ed. F.-J. Luebken, Springer, 189-205, 2013.

Mahmoudian, A., W.A. Scales, On the signature of positively charged dust particles on plasma irregularities in the mesosphere, J. Atmos. Sol. Terr. Phys., 104, 260-269, http://dx.doi.org/10.1016/j.jastp.2012.12.002, 2013.

Markkanen, J., T. Nygrén, M. Markkanen, M. Voiculescu, and A. Aikio, High-precision measurement of satellite range and velocity using the EISCAT radar, Ann. Geophys., 31, 859-870, doi:10.5194/angeo-31-859-2013, 2013.

Matuura, N., T. Tsuda and S. Nozawa, Field-Aligned Current Loop Model on Formation of Sporadic Metal Layers, J. Geophys. Res., 118, 7, 4628–4639, DOI: 10.1002/jgra.50414, 2013.

Moen, J., K. Oksavik, L. Alfonsi, Y. Daabakk, V. Romano, and L. Spogli,Space weather challenges of the polar cap ionosphere, J. Space Weather Space Clim., 3, A02, DOI: 10.1051/swsc/2013025, 2013.

Nozawa, S., T. D. Kawahara, N. Saito, C. M. Hall, T. T. Tsuda, T. Kawabata, S. Wada, A. Brekke, T. Takahashi, H. Fujiwara, Y. Ogawa, R. Fujii, Variations of the neutral temperature and sodium density between 80 and 107?km above Tromsø during the winter of 2010-2011 by a new solid state sodium LIDAR, J. Geophys. Res., DOI: 10.1002/2013JA019520, 2013.

Ogawa, Y., M. Sawatsubashi, S. C. Buchert, K. Hosokawa, S. Taguchi, S. Nozawa, S. Oyama, T. T. Tsuda, and R. Fujii, Relationship between auroral substorm and ion upflow in the nightside polar ionosphere, J. Geophys. Res., 118, 11,7426–7437, DOI: 10.1002/2013JA018965, 2013.

Pitkänen, T., A. T. Aikio, L. Juusola, Observations of polar cap channel and plasma sheet bursts during substorm expansion, J. Geophys. Res., 118, 2, 774–784, DOI: 10.1002/jgra.50119, 2013.

Pitout, F., P.-L. Blelly, D. Alcaydé, High-latitude ionospheric response to the solar eclipse of 1 August 2008: EISCAT observations and TRANSCAR simulation, J. Atmos. Sol. Terr. Phys., 105-106, 336-349, 2013.

Rapp, M., I. Strelnikova, Q. Li, N. Engler, G. Teiser, Charged aerosol effects on the scattering of radar waves from the D-region, in "Climate and Weather of the Sun-Earth system (CAWSES). Highlights from a Priority Program", Ed. F.-J. Luebken, Springer, 339-363, 2013.

Roettger, J. and N. Engler, EISCAT's contributions to high latitude ionosphere and atmospheric science within CAWSES in Germany, in "Climate and Weather of the Sun-Earth system (CAWSES). Highlights from a Priority Program", Ed. F.-J. Luebken, Springer, 235-246, 2013.

Sakai, J., S. Taguchi, K. Hosokawa, Y. Ogawa, Steep plasma depletion in dayside polar cap during a CME-driven magnetic storm, J. Geophys. Res., 118, 1, 462-471, doi:10.1029/2012JA018138, 2013.

Schlatter, N. M.,Enhanced Radar Backscatter from the Ionosphere, Licentiate Thesis, Royal Institute of Technology, School of Electrical Engineering, Stockholm, Sweden, 2013.

Schlatter, N. M., T. Grydeland, N. Ivchenko, V. Belyey, J. Sullivan, C. La Hoz, M. Blixt, Radar interferometer calibration of the EISCAT Svalbard Radar and a additional receiver station, Journal of Atmospheric and Solar-Terrestrial Physics, 105-106, 287-292, 2013.

Schlatter, N. M., N. Ivchenko, B. Gustavsson, T. Leyser, and M. Rietveld, Observations of HF induced instability in the auroral E region, Ann. Geophys., 31, 1103-1108, doi:10.5194/angeo-31-1103-2013, 2013.

Schlatter, N. M., N. Ivchenko, T. Sergienko, B. Gustavsson, and B. U. E. Brändström, Enhanced EISCAT UHF backscatter during high-energy auroral electron precipitation, Ann. Geophys., 31, 1681-1687, doi:10.5194/angeo-31-1681-2013, 2013.

Senior, A., M. T. Rietveld, I. Haggstrom, and M. J. Kosch, Radio-Induced Incoherent Scatter Ion Line Enhancements with Wide Altitude Extents in the High-Latitude Ionosphere, Geophys. Res. Lett., 40, 9, 1669-1674, DOI: 10.1002/grl.50272, 2013.

Simon Wedlund, C., H. Lamy, B. Gustavsson, T. Sergienko, U. Brändström, Estimating energy spectra of electron precipitation above auroral arcs from ground-based observations with radar and optics, J. Geophys. Res., DOI: 10.1002/jgra.50347, 2013.

Strelnikova, I., and M. Rapp, Statistical characteristics of PMWE observations by the EISCAT VHF radar, Ann. Geophys., 31, 359-375, doi:10.5194/angeo-31-359-2013, 2013.

Tanaka, Y., A. Shinbori, T. Hori, Y. Koyama, S. Abe, N. Umemura, Y. Sato, M. Yagi, S. UeNo, Satoru, A. Yatagai, Y. Ogawa, and Y. Miyoshi, Analysis software for upper atmospheric data developed by the IUGONET project and its application to polar science, Advances in Polar Science, 24, 4, 231-240, 2013.

Tecsor, Irina, Mutual coupling effects and optimum architecture of a sparse antenna array, Master of Science Thesis, KTH, Stockholm, TRITA-ICT-EX-2013:X, Sweden, June 2013.

Tsuda, T. T., S. Nozawa, T. D. Kawahara, T. Kawabata, N. Saito, S. Wada, Y. Ogawa, S. Oyama, C. M. Hall, M.

Tsutsumi, M. K. Ejiri, S. Suzuki, T. Takahashi, and T. Nakamura, Decrease in sodium density observed during auroral particle precipitation over Tromsø, Norway, Geophys. Res. Lett., 40, 17, 4486–4490, DOI: 10.1002/grl.50897, 2013.

Vickers, H., M. J. Kosch, E. Sutton, Y. Ogawa, C. La Hoz, Thermospheric atomic oxygen density estimates using the EISCAT Svalbard Radar, J. Geophys. Res., 118, 3, 1319–1330, DOI: 10.1002/jgra.50169, 2013.

J. Vierinen, A. Kero, M. T. Rietveld, High latitude artificial periodic irregularity observations with the upgraded EISCAT heating facility, Journal of Atmospheric and Solar-Terrestrial Physics, 105-106, 253-261, 2013.

Wissing, J. M., J. P. Bornebusch and M.-B. Kallenrode, Atmospheric ionization due to precipitating charged particles, in "Climate and Weather of the Sun-Earth system (CAWSES). Highlights from a Priority Program", Ed. F.-J. Luebken, Springer, , 223-234, 2013.

Wu, Y., R. Liu, B. Zhang, Z. Wu, H. Hu, S. Zhang, Q. Zhang, J. Liu, F. Honary, Multi-instrument observations of plasma features in the Arctic ionosphere during the main phase of a geomagnetic storm in December 2006, Journal of Atmospheric and Solar-Terrestrial Physics, 105-106, 358-366 , 2013.

# Publications 2014

Blagoveshchenskaya, N. F., T. D. Borisova, M. Kosch, T. Sergienko, U. Brändström, T. K. Yeoman, I. Häggström, Optical and Ionospheric Phenomena at EISCAT under Continuous X-mode HF Pumping, J. Geophys. Res., 119, DOI: 10.1002/2014JA020658, 2014.

Borisova, T. D., N. F. Blagoveshchenskaya, A. S. Kalishin, M. Kosch, A. Senior, M. T. Rietveld, T. K. Yeoman, and I. Hagstrom, Phenomena in the High Latitude F-Region of the Ionosphere Induced by a HF Heater Wave at Frequencies near the Fourth Electron Gyroharmonic, Radiophysics and Quantum Electronics, 62, 1, 1-22, 2014.

Bryers, Carl, Quantitative modelling of ionospheric modification experiments at EISCAT, Ph.D thesis, University of Lancaster, UK, 2014.

Cai, H., F. Li, G. Shen W. Zhan, K. Zhou I. W. McCrea, and S. Ma, E layer dominated ionosphere observed by EISCAT/ESR radars during solar minimum, Ann. Geophys., 32, 1223-1231, doi:10.5194/angeo-32-1223-2014, 2014.

Chau, J. L., J. Röttger, M. Rapp, PMSE strength during enhanced D region electron densities: Faraday rotation and absorption effects at VHF frequencies, J. Atmos. Sol. Terr. Phys., 118, A, 113-118, DOI:10.1016/j.jastp.2013.06.015, 2014.

Falck, S., Snickars, F., EISCAT in Space: Spatial aspects of the economic and societal importance of the European incoherent scatter radar system and an ionospheric heater in Fenno-Scandinavia and on Svalbard, in "The Region and Trade: New Analytical Directions" Batayal, A. and Nijkamp, P., (eds), World Scientific Publishing, Singapore, 2014

Falck, S., Snickars, F., EISCAT in Space: Spatial aspects of the economic and societal importance of the European incoherent scatter radar system and an ionospheric heater in Fenno-Scandinavia and on Svalbard, report, KTH Royal Institute of Technology, Sweden, 2014.

Fedorenko, Yu., E. Tereshchenko, S. Pilgaev, V. Grigoryev, N. Blagoveshchenskaya, Polarization of ELF waves generated during ”beat-wave” heating experiment near cut-off frequency of the Earth-ionosphere waveguide, Rad. Sci., 49, DOI: 10.1002/2013RS005336, 2014.

Fujiwara, H., S. Nozawa, Y. Ogawa, R. Kataoka, Y. Miyoshi, H. Jin, and H. Shinagawa, Extreme ion heating in the dayside ionosphere in response to the arrival of a coronal mass ejection on 12 March 2012, Ann. Geophys., 32, 831-839, doi:10.5194/angeo-32-831-2014, 2014.

Goodbody, B. C., Radar and Optical Studies of Small Scale Features in the Aurora: the Association of Optical Signatures with Naturally Enhanced Ion Acoustic Lines (NEIALS), PhD thesis, University of Southampton, UK, 2014.

Ieda, A., S. Oyama, H. Vanhamäki, R. Fujii, A. Nakamizo, O. Amm, T. Hori,M. Takeda, G. Ueno, A. Yoshikawa, R. J. Redmon,W. F. Denig, Y. Kamide, and N. Nishitani, Approximate forms of daytime ionospheric conductance, J. Geophys. Res. Space Physics, 119, 10,397-10,415, doi:10.1002/2014JA020665, 2014.

Ishida, T., Y. Ogawa, A. Kadokura, Y. Hiraki and I. Häggström, Seasonal variation and solar activity dependence of the quiet-time ionospheric trough, J. Geophys. Res., 119, 8, 6774–6783, DOI: 10.1002/2014JA019996, 2014.

Kero, A., Vierinen, D. McKay-Bukowski, C.-F. Enell, M. Sinor, L. Roininen and Y. Ogawa, Ionospheric electron density profiles inverted from a spectral riometer measurement, Geophys. Res. Lett., 41, 15, 5370–575, DOI: 10.1002/2014GL060986, 2014.

Koloskov, A. V., Y. M. Yampolski , A. V. Zalizovsky, V. G. Galushko , A. S. Kashcheev, C. La Hoz, A. Brekke, V. Belyey, M. T. Rietveld, Network of Internet-controlled HF receivers for ionospheric researches, Radiophysics and Radio Astronomy (in Russian), in press, 2014.

Kosch, M. J., H. Vickers, Y. Ogawa, A. Senior, N. Blagoveshchenskaya, First observation of the anomalous electric field in the topside ionosphere by ionospheric modification over EISCAT, Geophys. Res. Lett., 41, 21, 7427-7435, DOI: 10.1002/2014GL061679, 2014.

Kosch, M. J., C. Bryers, M. T. Rietveld, T. K. Yeoman and Y. Ogawa, Aspect angle sensitivity of pump-induced optical emissions at EISCAT, Earth, Planets and Space, 66:159, DOI: 10.1186/s40623-014-0159-x, 2014.

Mogilevsky, M. M., D. V. Chugunin, I. L. Moiseenko, and T. V. Romantsova, Suppression of Auroral Kilometric Radiation by an HF Heating Facility, Cosmic Research, 52, 1, 68-71, 2014.

Nicolls, M. J., H. Bahcivan, I. Häggström, M. Rietveld, Direct Measurement of Lower-Thermospheric Neutral Density using Multi-Frequency Incoherent Scattering, Geophys. Res. Lett., 41, DOI: 10.1002/2014GL062204, 2014.

Ogawa, Y., T. Motoba, S. C. Buchert, I. Häggström and S. Nozawa, Upper atmosphere cooling over the past 33 years, Geophys. Res. Lett., 41, 15, 5629–5635, DOI: 10.1002/2014GL060591, 2014.

Panasenko, S. V., M. T. Rietveld, C. La Hoz, I. F. Domnin, Travelling Ionospheric Disturbances over Kharkiv, Ukraine, Accompanying the Operation of the EISCAT Heater Facility, Bulletin of the National Technical University "Kharkiv Polytechnic Institute". Series: Radiophysics and Ionosphere, Kharkiv, 47, 92-98, 2014.

Pellinen-Wannberg, A. K., I. Häggström, J. D. C. Sánchez, J. M. C. Plane, A. Westman, Strong E region ionization caused by the 1767 trail during the 2002 Leonids, J. Geophys.Res., 119, 9, 7880–7888, DOI: 10.1002/2014JA020290, 2014.

Pilipenko, V., V. Belakhovsky, A. Kozlovsky, E. Fedorov, K. Kauristie, ULF wave modulation of the ionospheric parameters: Radar and magnetometer observations, Journal of Atmospheric and Solar-Terrestrial Physics, 108, 68-76, 2014.

Pinedo, H., C. La Hoz, O. Havnes, M. Rietveld, Electron-ion temperature ratio estimations in the summer polar mesosphere when subject to HF radio wave heating, Journal of Atmospheric and Solar-Terrestrial Physics, 118, A, 106-112, http://dx.doi.org/10.1016/j.jastp.2013.12.016, 2014.

Sakai, J., S. Taguchi , K. Hosokawa, Y. Ogawa, Storm-time enhancements of 630.0-nm airglow associated with polar cap patches, J. Geophys. Res., 119, 3, 2214–2228, doi:10.1029/2013JA019197, 2014.

Schlatter, N. M., N. Ivchenko,I. Häggström, On the relation of Langmuir turbulence radar signatures to auroral conditions, J. Geophys. Res., 119, 10, 8499–8511, DOI: 10.1002/2013JA019457, 2014.

Senior, A., A. Mahmoudian, H. Pinedo, C. La Hoz, M. T. Rietveld, W. A. Scales, and M. J. Kosch, First modulation of high-frequency polar mesospheric summer echoes by radio heating of the ionosphere, Geophys. Res. Lett., 41, 15, 5347-5353, DOI: 10.1002/2014GL060703, 2014.

Skjæveland, Å., J. Moen, H. C. Carlson, Which cusp upflow events can possibly turn into outflows?, J. Geophys. Res., 119, 8, 6876–6890, DOI: 10.1002/2013JA019495, 2014.

Tereshchenko, E. D., O. I. Shumilov, E. A. Kasatkina and A. D. Gomonov, Features of amplitude and Doppler frequency variation of ELF/VLF waves generated by "beat-wave" HF heating at high latitudes, Geophys. Res. Lett., 41, doi:10.1002/2014GL060376, 2014.

Tuttle, S., Calculating the auroral electron energy, Astronomy and Geophysics, 55, 4, 17-19, 2014.

Tuttle, S., B. Gustavsson, and B. Lanchester, Temporal and spatial evolution of auroral electron energy spectra in a region surrounding the magnetic zenith, J. Geophys. Res., doi:10.1002/2013JA019627, 2014.

van de Kamp, M., D. Pokhotelov, and K. Kauristie, TID characterised using joint effort of incoherent scatter radar and GPS, Ann. Geophys., 32, 1511-1532, doi:10.5194/angeo-32-1511-2014, 2014.

van der Meeren, C., K. Oksavik, D. Lorentzen, J. I. Moen, and V. Romano, GPS scintillation and irregularities at the front of an ionization tongue in the nightside polar ionosphere, J. Geophys. Res. Space Physics, 119, 8624-8636, doi:10.1002/2014JA020114, 2014.

Vickers, H., M. J. Kosch, E. Sutton, L. Bjoland, Y. Ogawa and C. LaHoz, A solar cycle of upper thermosphere density observations from the EISCAT Svalbard Radar, J. Geophys. Res., 119, 8, 6833–6845, DOI: 10.1002/2014JA019885, 2014.

Wendel, J., Upper atmosphere has cooled steadily for three decades, EOS, 95, 47, 444, DOI: 10.1002/2014EO470008, 2014.

Zabotin, N. A., V. U. Zavorotny, M. T. Rietveld, Physical mechanisms associated with long range propagation of the signals from ionospheric heating experiments, Radio Sci., 49, 10, 987–995, DOI: 10.1002/2014RS005573, 2014.

Zhivolup, T. G., The F2-layer Parameter Variations during Spring Equinox 2013, according to the Kharkiv and EISCAT Incoherent Scatter Radars Data, Bulletin of the National Technical University "Kharkiv Polytechnic Institute". Series: Radiophysics and Ionosphere, Kharkiv, 47, 50-56, 2014.

# EISCAT Operations 2013 – 2014

The EISCAT radars operate in two basic modes, using approximately half the available observing time for each. In the Special Programme mode, users conduct individual experiments dedicated to specific experiments and objectives. The resulting data are reserved for the exclusive use of the experimenters for one year from the date of collection. Special programmes often make use of the well developed pulse schemes and observing modes of the Common Programme. EISCAT Common Programmes are conducted for the benefit of the entire user community and the resulting data are immediately available to all. The Common Programme modes are developed and maintained by EISCAT staff, and the overall programme is monitored by the Scientific Oversight Committee (SOC). Common Programme operations are often conducted as part of the coordinated World Day programme organised by the International Union of Radio Scientists (URSI) Incoherent Scatter Working Group (ISWG).

Common Programme One, CP-1, uses a fixed transmitting antenna, pointing along the geomagnetic field direction. The three-dimensional velocity and anisotropy in other parameters are measured by means of the receiving stations at Kiruna and Sodankylä (see map, inside front cover). CP-1 is capable of providing results with very good time resolution and is suitable for the study of substorm phenomena, particularly auroral processes where conditions might change rapidly. The basic time resolution is 5 s. Continuous electric field measurements are derived from the tri-static F-region data. On longer time scales, CP-1 measurements support studies of diurnal changes, such as atmospheric tides, as well as seasonal and solar-cycle variations. The observation scheme uses alternating codes for spectral measurements.

Common Programme Two, CP-2, is designed to make measurements from a small, rapid transmitter antenna scan. One aim is to identify wave-like phenomena with length and time scales comparable with, or larger than, the scan (a few tens of kilometers and about ten minutes). The present version consists of a four-position scan which is completed in six minutes. The first three positions form a triangle with vertical, south, and south-east positions, while the fourth is aligned with the geomagnetic field. The remote site antennas provide three-dimensional velocity measurements in the F-region. The pulse scheme is identical with that of CP-1.

Common Programme Three, CP-3, covers a 10° latitudinal range in the F-region with a 17-position scan up to 74°N in a 30 min cycle. The observations are made in a plane defined by the magnetic meridian through Tromsø, with the remote site antennas making continuous measurements at 275 km altitude. The coding scheme uses alternating codes. The principle aim of CP-3 is the mapping of ionospheric and electrodynamic parameters over a broad latitude range.

Common Programmes One, Two, and Three are run on the UHF radar. Three further programmes are designed for use with the VHF system. The UHF and VHF radars are often operated simultaneously during the CP experiments. Such observations offer comprehensive data sets for atmospheric, ionospheric, and magnetospheric studies.

Common Programme Four, CP-4, covers geographic latitudes up to almost 80°N (77°N invariant latitude) using a low elevation, split-beam configuration. CP-4 is particularly suitable for studies of high latitude plasma convection and polar cap phenomena. However, with the present one-beam configuration of the VHF radar, CP-4 is run with either both UHF and VHF radars or with UHF only in a two position scan.

Common Programme Six, CP-6, is designed for low altitude studies, providing spectral measurements at mesospheric heights. Velocity and electron density are derived from the measurements and the spectra contain information on the aeronomy of the mesosphere. Vertical antenna pointing is used.

Common Programme Seven, CP-7, probes high altitudes and is particularly aimed at polar wind studies. The present version, with only one of the VHF klystrons running, is designed to cover

altitudes up to 1500 km vertically above Ramfjordmoen.

Equivalent Common Programme modes are available for the EISCAT Svalbard Radar. CP-1 is directed along the geomagnetic field (81.6° inclination). CP-2 uses a four position scan. CP-3 is a 15 position elevation scan with southerly beam swinging positions. CP-4 combines observations in the F-region viewing area with field-aligned and vertical measurements. Alternating code pulse schemes have been used extensively for each mode to cover ranges of approximately 80 km to 1200 km with integral clutter removal below 150 km. CP-6 is similar to the mainland radar CP-6.

The tables on the next pages summarise the accounted hours on the various facilities for each month and for each Common Programme mode (CP) or Associate (SP).

*Dr. Ingemar Häggström*
*Senior Scientist, EISCAT Scientific Association*

**KST COMMON PROGRAMMES**

| 2013 | Jan | Feb | Mar | Apr | May | Jun | Jul | Aug | Sept | Oct | Nov | Dec | Total | % | Target% |
|---|---|---|---|---|---|---|---|---|---|---|---|---|---|---|---|
| **CP1** | | 1 | 2 | 86 | 2.5 | | | | | 0.5 | | | 92 | 19 | 16 |
| **CP2** | 125 | | | | | | | | | | | | 125 | 26 | 16 |
| **CP3** | | | | | | | | | | | 85 | | 85 | 18 | 12 |
| **CP4** | | | | | | | | | | | | | 0 | 0 | 10 |
| **CP6** | | | | | | 1 | 166.5 | | | | 0.5 | | 168 | 35 | 20 |
| **CP7** | | | | | 4.5 | | | | | | | | 4.5 | 1 | 18 |
| **UP** | | | | | | | | | | | | | 0 | 0 | |
| **Total** | 125 | 1 | 2 | 86 | 7 | 1 | 166.5 | 0 | 0 | 0.5 | 85.5 | 0 | **474.5** | 100 | |
| % | 26 | 0 | 0 | 18 | 1 | 0 | 35 | 0 | 0 | 0 | 18 | 0 | 100 | | |

**KST SPECIAL PROGRAMMES**

| 2013 | Jan | Feb | Mar | Apr | May | Jun | Jul | Aug | Sept | Oct | Nov | Dec | Total | Incl AA | Target |
|---|---|---|---|---|---|---|---|---|---|---|---|---|---|---|---|
| **CN** | | | | | | 22.5 | 5 | 2.5 | | | | | 30 | 30 | 64 |
| **FI** | | | 60.5 | | | | | | | | 36.5 | | 97 | 97 | 88 |
| **NI** | 10 | | 38.5 | | | | | | | | | 54.5 | 103 | 103 | 103 |
| **NO** | | | 7 | 3 | 55.5 | 97 | 69.5 | | | 11.5 | 13.5 | 28 | 285 | 285 | 198 |
| **SW** | | | 10 | 3 | 3.5 | 50.5 | | | | | 31.5 | 14 | 112.5 | 113 | 149 |
| **UK** | | | 5 | 4.5 | 16 | 27.5 | 11.5 | | | 31.5 | | | 96 | 96 | 91 |
| **AA** | | | | | | | | | | | | | 0 | | |
| **Total** | 10 | 0 | 121 | 10.5 | 75 | 197.5 | 86 | 2.5 | 0 | 43 | 81.5 | 96.5 | **723.5** | **724** | **694** |
| **%** | 1 | 0 | 17 | 1 | 10 | 27 | 12 | 0 | 0 | 6 | 11 | 13 | 100 | | |

| | EI | CN | FI | NI | NO | SW | UK | |
|---|---|---|---|---|---|---|---|---|
| **Target** | | 9.27 | 12.73 | 14.88 | 28.55 | 21.49 | 13.08 | % |

**KST OTHER PROGRAMMES**

| 2013 | Jan | Feb | Mar | Apr | May | Jun | Jul | Aug | Sept | Oct | Nov | Dec | Total | Target |
|---|---|---|---|---|---|---|---|---|---|---|---|---|---|---|
| **PP** | 21 | 15 | | 16 | | 18 | 14 | 14 | | 27 | 1.5 | 12 | 138.5 | 108 |
| **EI** | | | | | 2 | | | | | | 13.5 | 23 | 38.5 | 30 |
| **RU** | | 134 | | | | | | | | 129.5 | 28 | | 291.5 | 170 |
| **TB** | | | | | | | | | | 12 | | | 12 | 12 |
| **Total** | 21 | 149 | 0 | 16 | 2 | 18 | 14 | 14 | 0 | 168.5 | 43 | 35 | **480.5** | **320** |

**KST TOTALS**

| 2013 | Jan | Feb | Mar | Apr | May | Jun | Jul | Aug | Sept | Oct | Nov | Dec | Total | Target |
|---|---|---|---|---|---|---|---|---|---|---|---|---|---|---|
| **CP** | 125 | 1 | 2 | 86 | 7 | 1 | 166.5 | 0 | 0 | 0.5 | 85.5 | 0 | 474.5 | 450 |
| **SP** | 10 | 0 | 121 | 10.5 | 75 | 197.5 | 86 | 2.5 | 0 | 43 | 81.5 | 96.5 | 723.5 | 694 |
| **OP** | 0 | 149 | 0 | 16 | 2 | 18 | 14 | 14 | 0 | 168.5 | 43 | 35 | 459.5 | 320 |
| **Total** | 135 | 150 | 123 | 112.5 | 84 | 216.5 | 266.5 | 16.5 | 0 | 212 | 210 | 131.5 | **1657.5** | **1464** |

**USAGE BREAKDOWN**

| 2013 | Jan | Feb | Mar | Apr | May | Jun | Jul | Aug | Sept | Oct | Nov | Dec | Total | Target |
|---|---|---|---|---|---|---|---|---|---|---|---|---|---|---|
| **UHF** | 147 | 77.5 | 78 | 93.5 | 26.5 | 55.5 | 32.5 | 6.5 | | 125.5 | 145 | 92.5 | 880 | 591 |
| **VHF** | 9 | | 25 | 13.5 | 31.5 | 96 | 145 | 6 | | 9 | | 23 | 358 | 517 |
| **Heating** | | 72 | 16.5 | 4 | 17 | 34 | 23 | 2 | | 79 | 41.5 | 9.5 | 298.5 | 206 |
| **Passive KST** | | | 12.5 | 6.5 | 36 | 120 | 263.5 | 7 | | | 11.5 | 25 | 482 | 600 |
| **Bolt array** | | | | | | | | | | | | | 0 | |
| **ESR** | 132 | 56 | 49 | 94.5 | 7 | 8 | 64.5 | 0 | 0 | 10 | 176 | 102.5 | 699.5 | 926 |
| **Passive ESR** | | | | | | | | | | | | | 0 | |

**ESR COMMON PROGRAMMES**

| 2013 | Jan | Feb | Mar | Apr | May | Jun | Jul | Aug | Sept | Oct | Nov | Dec | Total | % | Target% |
|---|---|---|---|---|---|---|---|---|---|---|---|---|---|---|---|
| **CP1** | | | 0.5 | 77 | 1 | | 2.5 | | | | | | 81 | 26 | 54 |
| **CP2** | 85 | | | | | | | | | | | | 85 | 27 | 16 |
| **CP3** | | | | | | | | | | | 88 | | 88 | 28 | 12 |
| **CP4** | | | | | | | | | | | | | 0 | 0 | 10 |
| **CP6** | | | | | | | 62 | | | | | | 62 | 20 | |
| **CP7** | | | | | | | | | | | | | 0 | 0 | |
| **UP** | | | | | | | | | | | | | 0 | 0 | |
| **Total** | 85 | 0 | 0.5 | 77 | 1 | 0 | 64.5 | 0 | 0 | 0 | 88 | 0 | **316** | 100 | |
| % | 27 | 0 | 0 | 24 | 0 | 0 | 20 | 0 | 0 | 0 | 28 | 0 | 100 | | |

**ESR SPECIAL PROGRAMMES**

| 2013 | Jan | Feb | Mar | Apr | May | Jun | Jul | Aug | Sept | Oct | Nov | Dec | Total | Incl AA | Target |
|---|---|---|---|---|---|---|---|---|---|---|---|---|---|---|---|
| **CN** | | | | | | | | | | | | | 0 | 0 | 32 |
| **FI** | | | 6 | | | | | | | 2 | 16 | | 24 | 24 | 43 |
| **NI** | 15.5 | | 28 | | | | | | | | | 11.5 | 55 | 55 | 51 |
| **NO** | 14.5 | 18.5 | 3.5 | 15 | 0.5 | 1.5 | | | | | 42 | 18.5 | 114 | 114 | 97 |
| **SW** | 2.5 | 18.5 | | 0.5 | 0.5 | 1.5 | | | | | 1.5 | 50 | 75 | 75 | 73 |
| **UK** | 14.5 | 19 | | 2 | 2 | 5 | | | | 8 | 0.5 | 22.5 | 73.5 | 74 | 45 |
| **AA** | | | | | | | | | | | | | 0 | | |
| **Total** | 47 | 56 | 37.5 | 17.5 | 3 | 8 | 0 | 0 | 0 | 10 | 60 | 102.5 | **341.5** | **342** | **341** |
| **%** | 14 | 16 | 11 | 5 | 1 | 2 | 0 | 0 | 0 | 3 | 18 | 30 | 100 | | |

**ESR OTHER PROGRAMMES**

| 2013 | Jan | Feb | Mar | Apr | May | Jun | Jul | Aug | Sept | Oct | Nov | Dec | Total | Target |
|---|---|---|---|---|---|---|---|---|---|---|---|---|---|---|
| **PP** | | | 11 | | | | | | | | 18 | | 29 | 92 |
| **EI** | | | | | | | | | | | | | 0 | 20 |
| **RU** | | | | | | | | | | | 10 | | 10 | 20 |
| **TB** | | | | | 3 | | | | | | | | 3 | 3 |
| **Total** | 0 | 0 | 11 | 0 | 3 | 0 | 0 | 0 | 0 | 0 | 28 | 0 | **42** | **135** |

**ESR TOTALS**

| 2013 | Jan | Feb | Mar | Apr | May | Jun | Jul | Aug | Sept | Oct | Nov | Dec | Total | Target |
|---|---|---|---|---|---|---|---|---|---|---|---|---|---|---|
| **CP** | 85 | 0 | 0.5 | 77 | 1 | 0 | 64.5 | 0 | 0 | 0 | 88 | 0 | 316 | 450 |
| **SP** | 47 | 56 | 37.5 | 17.5 | 3 | 8 | 0 | 0 | 0 | 10 | 60 | 102.5 | 341.5 | 341 |
| **OP** | 0 | 0 | 11 | 0 | 3 | 0 | 0 | 0 | 0 | 0 | 28 | 0 | 42 | 135 |
| **Total** | 132 | 56 | 49 | 94.5 | 7 | 8 | 64.5 | 0 | 0 | 10 | 176 | 102.5 | **699.5** | **926** |

**KST COMMON PROGRAMMES**

| 2014 | Jan | Feb | Mar | Apr | May | Jun | Jul | Aug | Sept | Oct | Nov | Dec | Total | % | Target% |
|---|---|---|---|---|---|---|---|---|---|---|---|---|---|---|---|
| **CP1** | 30.5 | | 1 | 88 | | | 13 | | 2 | 1.5 | | | 136 | 15 | 16 |
| **CP2** | | | | | | | | | | | | | 0 | 0 | 16 |
| **CP3** | | | | | | | | | | | | | 0 | 0 | 12 |
| **CP4** | | | | | | | | | | | | 269.5 | 269.5 | 30 | 10 |
| **CP6** | 462.5 | | | | | | 16 | | 1.5 | | | | 480 | 54 | 20 |
| **CP7** | | | | | | | | | | | | | 0 | 0 | 18 |
| **UP** | | | | | | | | | | | | | 0 | 0 | |
| **Total** | 493 | 0 | 1 | 88 | 0 | 0 | 29 | 0 | 3.5 | 1.5 | 0 | 269.5 | **885.5** | 100 | |
| % | 56 | 0 | 0 | 10 | 0 | 0 | 3 | 0 | 0 | 0 | 0 | 30 | 100 | | |

**KST SPECIAL PROGRAMMES**

| 2014 | Jan | Feb | Mar | Apr | May | Jun | Jul | Aug | Sept | Oct | Nov | Dec | Total | Incl AA | Target |
|---|---|---|---|---|---|---|---|---|---|---|---|---|---|---|---|
| **CN** | | | 54 | | | 10.5 | 17.5 | | | 29 | | | 111 | 112 | 113 |
| **FI** | | 7.5 | 2.5 | | 4 | 20 | | | | | 69.5 | | 103.5 | 105 | 130 |
| **NI** | 12 | 28 | 36.5 | | | | | | 0.5 | | | 27 | 104 | 105 | 136 |
| **NO** | 9 | 34 | 35.5 | | 12.5 | 25 | 41.5 | | | | 60.5 | 25 | 243 | 246 | 289 |
| **SW** | | 66.5 | 46 | | 4.5 | | 3.5 | | | | 2.5 | 6.5 | 129.5 | 132 | 226 |
| **UK** | | | 28 | 3 | 9 | 14 | 23 | | | | 32.5 | 4 | 113.5 | 115 | 133 |
| **AA** | | | | | | 2 | | | 5.5 | 2.5 | | | 10 | | |
| **Total** | 21 | 136 | 202.5 | 3 | 30 | 71.5 | 85.5 | 0 | 6 | 31.5 | 165 | 62.5 | **814.5** | **815** | **1026** |
| **%** | 3 | 17 | 25 | 0 | 4 | 9 | 10 | 0 | 1 | 4 | 20 | 8 | 100 | | |

| | EI | CN | FI | NI | NO | SW | UK | |
|---|---|---|---|---|---|---|---|---|
| **Target** | | 10.99 | 12.69 | 13.26 | 28.16 | 21.99 | 12.92 | % |

**KST OTHER PROGRAMMES**

| 2014 | Jan | Feb | Mar | Apr | May | Jun | Jul | Aug | Sept | Oct | Nov | Dec | Total | Target |
|---|---|---|---|---|---|---|---|---|---|---|---|---|---|---|
| **PP** | 31.5 | 8.5 | 1 | | | | | | | | 27.5 | 14 | 82.5 | 70 |
| **EI** | | | 13 | | 2.5 | 1 | | | | | | | 16.5 | 30 |
| **RU** | | | | | | | | | | 20 | | | 20 | 55 |
| **TB** | | | | | | | | | | | | | 0 | 0 |
| **Total** | 31.5 | 8.5 | 14 | 0 | 2.5 | 1 | 0 | 0 | 0 | 20 | 27.5 | 14 | **119** | **155** |

**KST TOTALS**

| 2014 | Jan | Feb | Mar | Apr | May | Jun | Jul | Aug | Sept | Oct | Nov | Dec | Total | Target |
|---|---|---|---|---|---|---|---|---|---|---|---|---|---|---|
| **CP** | 493 | 0 | 1 | 88 | 0 | 0 | 29 | 0 | 3.5 | 1.5 | 0 | 269.5 | 885.5 | 540 |
| **SP** | 21 | 136 | 202.5 | 3 | 30 | 71.5 | 85.5 | 0 | 6 | 31.5 | 165 | 62.5 | 814.5 | 1026 |
| **OP** | 0 | 8.5 | 14 | 0 | 2.5 | 1 | 0 | 0 | 0 | 20 | 27.5 | 14 | 87.5 | 155 |
| **Total** | 514 | 144.5 | 217.5 | 91 | 32.5 | 72.5 | 114.5 | 0 | 9.5 | 53 | 192.5 | 346 | **1787.5** | **1721** |

**USAGE BREAKDOWN**

| 2014 | Jan | Feb | Mar | Apr | May | Jun | Jul | Aug | Sept | Oct | Nov | Dec | Total | Target |
|---|---|---|---|---|---|---|---|---|---|---|---|---|---|---|
| **UHF** | 60.5 | 71 | 95 | 6 | 15.5 | 21.5 | 38.5 | | 7.5 | 51 | 116.5 | 56.5 | 539.5 | 547 |
| **VHF** | 323 | 40 | 72 | 62 | 16 | 23 | 32.5 | | 2 | 1.5 | 68 | 199.5 | 839.5 | 822 |
| **Heating** | | 24 | 49.5 | | | 19 | 27.5 | | | | | | 120 | 202 |
| **Passive KST** | 645 | 43 | | 115.5 | | 37 | 60 | | | | 34 | 359.5 | 1294 | 600 |
| **Bolt array** | | | | | | | | | | | | | 0 | |
| **ESR** | 336 | 26 | 33 | 66.5 | 10.5 | 2 | 0 | 13.5 | 38 | 0 | 142 | 142 | 809.5 | 898 |
| **Passive ESR** | | | | | | 4 | | | | | | | 4 | |

**ESR COMMON PROGRAMMES**

| 2014 | Jan | Feb | Mar | Apr | May | Jun | Jul | Aug | Sept | Oct | Nov | Dec | Total | % | Target% |
|---|---|---|---|---|---|---|---|---|---|---|---|---|---|---|---|
| **CP1** | 50.5 | 0.5 | | 61.5 | | | | 0.5 | | | | | 113 | 25 | 54 |
| **CP2** | 217.5 | | | | | | | | | | | | 217.5 | 48 | 16 |
| **CP3** | | 1 | | | | | | | | | | | 1 | 0 | 12 |
| **CP4** | | | | | | | | | | | | 100.5 | 100.5 | 22 | 10 |
| **CP6** | 8.5 | | | 0.5 | 0.5 | | | | 15 | | | | 24.5 | 5 | |
| **CP7** | | | | | | | | | | | | | 0 | 0 | |
| **UP** | | | | | | | | | | | | | 0 | 0 | |
| **Total** | 276.5 | 1.5 | 0 | 62 | 0.5 | 0 | 0 | 0.5 | 15 | 0 | 0 | 100.5 | **456.5** | 100 | |
| % | 61 | 0 | 0 | 14 | 0 | 0 | 0 | 0 | 3 | 0 | 0 | 22 | 100 | | |

**ESR SPECIAL PROGRAMMES**

| 2014 | Jan | Feb | Mar | Apr | May | Jun | Jul | Aug | Sept | Oct | Nov | Dec | Total | Incl AA | Target |
|---|---|---|---|---|---|---|---|---|---|---|---|---|---|---|---|
| **CN** | | | | | | | | | | | | | 0 | 1 | 42 |
| **FI** | | | | | | | | | | | 38 | | 38 | 40 | 49 |
| **NI** | 16 | 5 | 20 | | | | | 13 | 12.5 | | | | 66.5 | 68 | 51 |
| **NO** | 8 | 19.5 | 13 | | 4 | | | | | | 41.5 | 10.5 | 96.5 | 100 | 108 |
| **SW** | 9 | | | | 2 | | | | | | 31.5 | 9 | 51.5 | 54 | 84 |
| **UK** | 8 | | | | 4 | 1 | | | | | 17.5 | 13.5 | 44 | 46 | 49 |
| **AA** | | | | | | 2 | | | 10.5 | | | | 12.5 | | |
| **Total** | 41 | 24.5 | 33 | 0 | 10 | 3 | 0 | 13 | 23 | 0 | 128.5 | 33 | **309** | **309** | **383** |
| **%** | 13 | 8 | 11 | 0 | 3 | 1 | 0 | 4 | 7 | 0 | 42 | 11 | 100 | | |

**ESR OTHER PROGRAMMES**

| 2014 | Jan | Feb | Mar | Apr | May | Jun | Jul | Aug | Sept | Oct | Nov | Dec | Total | Target |
|---|---|---|---|---|---|---|---|---|---|---|---|---|---|---|
| **PP** | 18.5 | | | | | | | | | | 13.5 | 8.5 | 40.5 | 130 |
| **EI** | | | | | | | | | | | | | 0 | 20 |
| **RU** | | | | | | | | | | | | | 0 | 0 |
| **TB** | | | | 4.5 | | | | | | | | | 4.5 | 5 |
| **Total** | 18.5 | 0 | 0 | 4.5 | 0 | 0 | 0 | 0 | 0 | 0 | 13.5 | 8.5 | **45** | **155** |

**ESR TOTALS**

| 2014 | Jan | Feb | Mar | Apr | May | Jun | Jul | Aug | Sept | Oct | Nov | Dec | Total | Target |
|---|---|---|---|---|---|---|---|---|---|---|---|---|---|---|
| **CP** | 276.5 | 1.5 | 0 | 62 | 0.5 | 0 | 0 | 0.5 | 15 | 0 | 0 | 100.5 | 456.5 | 360 |
| **SP** | 41 | 24.5 | 33 | 0 | 10 | 3 | 0 | 13 | 23 | 0 | 128.5 | 33 | 309 | 383 |
| **OP** | 18.5 | 0 | 0 | 4.5 | 0 | 0 | 0 | 0 | 0 | 0 | 13.5 | 8.5 | 45 | 155 |
| **Total** | 336 | 26 | 33 | 66.5 | 10.5 | 3 | 0 | 13.5 | 38 | 0 | 142 | 142 | **810.5** | **898** |

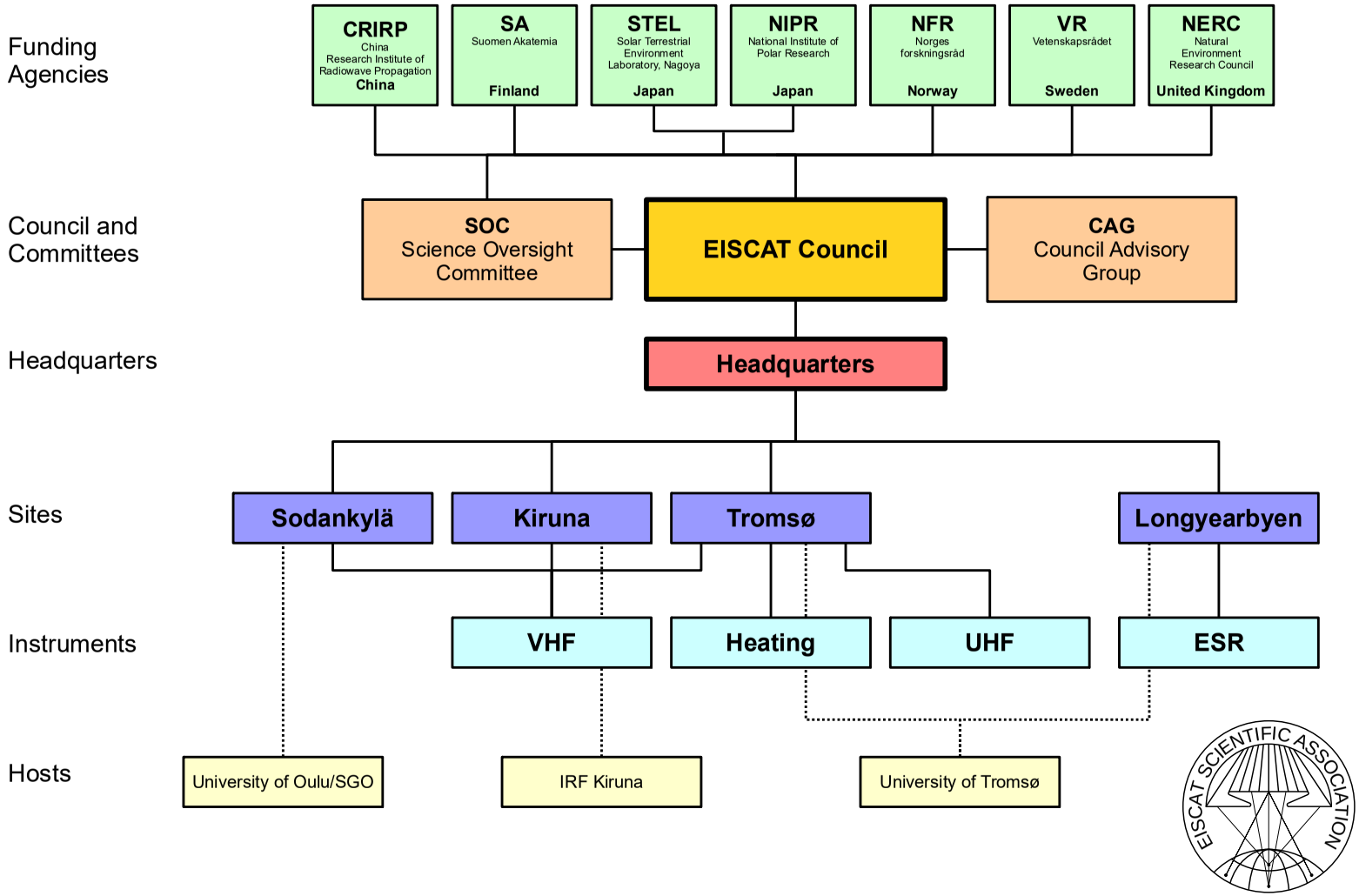


EISCAT organisational diagram, December 2014.

# EISCAT Scientific Association

## December 2014

## Council

The Council consists of a Delegation with a maximum of three persons from each Associate.

| | |
|---|---|
| **Finland** | |
| Dr. A. Aikio | |
| Prof. T. Pulkkinen | |
| Dr. K. Sulonen | Delegate |
| **Japan** | |
| Dr. H. Miyaoka | Delegate |
| Dr. S. Nozawa | |
| **Norway** | |
| Prof. A. Brekke | |
| Dr. B. Jacobsen | Delegate |
| Dr. L. Lønnum | |
| **P. R. of China** | |
| Dr. Z. Ding | |
| Prof. Q. Dong | |
| Prof. J. Wu | *Chairperson*, Delegate |
| **Sweden** | |
| Dr. T. Andersson | Delegate |
| Prof. J. Gumbel | |
| **United Kingdom** | |
| Dr. M. Freeman | Delegate |
| Dr. I. McCrea | *Vice-Chairperson* |

## Scientific Oversight Committee

The EISCAT scientific community organises the Scientific Oversight Committee (SOC), under the guidance of the Council.

| | |
|---|---|
| Dr. S. Buchert | Sweden |
| Dr. D. Hysell | External member |
| Prof. W. Jun | P. R. of China |
| Dr. A. Kavanagh | United Kingdom |
| Dr. D. Knudsen | External member |
| Prof. C. La Hoz | Norway |
| Dr. Y. Ogawa | *Chairperson*, Japan |
| Dr. T. Ulich | Finland |

## Director

Dr. C. Heinselman

## Council Advisory Group

The Council Advisory Group (CAG) prepares matters to be brought to the Council.

| | |
|---|---|
| Dr. A. Aikio | Council Member |
| Mr. H. Andersson | Head of Administration |
| Dr. T. Andersson | Council Chairperson |
| Prof. A. Brekke | Council Member |
| Dr. C. Heinselman | Director |
| Dr. I. McCrea | Council Member |
| Dr. H. Miyaoka | Council Member |

## Executives

Senior Management

| | |
|---|---|
| Mr. H. Andersson | Head of Adm., Deputy Dir. |
| Dr. C. Heinselman | Director |
| Prof. I. Mann | Head of Projects |

## Site Leaders

Station Managers

| | |
|---|---|
| Mr. R. Jacobsen | Tromsø Radar |
| Mr. L. Lövqvist | Kiruna Site |
| Mr. J. Markkanen | Sodankylä Site |
| Dr. M. Rietveld | Tromsø Heating |
| Dr. A. Westman | EISCAT Svalbard Radar |

Photo from the Annual Review Meeting, 14–16 October 2013, at the Rica Narvik Hotel in Norway. *Back row from left:* Craig Heinselman, Jussi Markkanen, Ingemar Häggström, Lars-Göran Vanhainen, Ola Hjelløkken, Elisabet Goth, Henrik Andersson, Ingrid Mann, Espen Helgesen. *Middle row from left:* Halvard Boholm, Assar Westman. *Front row from left:* Anders Tjulin, Stian Grande, Arild Stenberg, Guttorm Mikalsen, Erlend Danielsen, Michael Rietveld, Roger Jacobsen.


Photo from the Annual Review Meeting, 1–3 October 2014, at Abisko Turiststation in Sweden. From left: Assar Westman, Lennart Lövqvist, Peter Bergqvist, Elisabet Goth, Gunnar Isberg, Jussi Markkanen, Ingrid Mann, Mike Rietveld, Halvard Boholm, Roger Jacobsen, Erlend Danielsen, Stian Grande, Espen Helgesen, Guttorm Mikalsen, Carl-Fredrik Enell, Knut Hellvig, Arild Stenberg, Anders Tjulin, Henrik Andersson, Craig Heinselman

EISCAT Scientific Association
Registered as a Swedish non-profit organisation
Organisation number: 897300-2549

Annual report for the financial year 2013-01-01 – 2013-12-31

The EISCAT Council and the Director for the Association submits herewith the annual report for 2013.

# ADMINISTRATION REPORT

**Ownership, organisation and objective**

The EISCAT Scientific Association was established in 1975 through an agreement between six European organisations. Japan joined in 1996 and the Peoples Republic of China in 2007.

The EISCAT Associates at 2013-12-31 are: China Research Institute of Radiowave Propagation (Peoples Republic of China), National Institute of Polar Research (Japan), Natural Environment Research Council (United Kingdom of Great Britain and Northern Ireland), Norges forskningsråd (Norway), Solar-Terrestrial Environment Laboratory, Nagoya University (Japan), Suomen Akatemia (Finland), and Vetenskapsrådet (Sweden).

The now running EISCAT Agreement came into force 2007-01-01, with all Associates making long term funding commitments to the Association. The Association has its formal seat in Kiruna, Sweden, and is registered as a non-profit organisation.

The aim of the Association is to make significant progress in the understanding of physical processes in the high latitude atmosphere by means of experimental programmes generally conducted using the incoherent scatter radar technique, which may be carried out as part of wider international projects. For this purpose, the Association has developed, constructed, and now operates, a number of radar facilities at high latitudes. At present, these comprise a system of stations at Tromsö (Norway), Kiruna (Sweden), Sodankylä (Finland), and Longyearbyen (Svalbard).

The Association is fully funded by the Associates but additional operations may also be funded by short term additional contributions from both Associate and non-Associate bodies. Depending on the available funding, scientific priorities and operational targets are adjusted on an annual basis.

The EISCAT Council is charged with the overall administration and supervision of the Association's activities. The Council appoints a Director, who is responsible for the daily management and operation of the facilities of the Association.

**Operation and scientific development**

The EISCAT Radars delivered a full programme of operations for the user community and operated reliably throughout the year with only some interruptions due to equipment or operational problems.

The various EISCAT radars operated for a total of 2 378 accounted hours (2 596 hours in 2012).

Common Programmes amounted to 33% (42%) of the operations. Special Programmes amounted to 45% (42%) and other operations amounted to 22% (16%) of the total hours.

Scientists from Ukraine and Russia paid for the use of the facilities. Totally 316 hours (300 hours) were accounted on behalf of these countries. Both Ukraine and Russia have Affiliate agreements. The introduced Peer-Review Programme attracted several

applications and user groups from Chile, Finland, Germany, Japan, Russia, USA and United Kingdom were granted time, at no cost, on the systems. Peer-Review time amounted to 168 accounted hours (100 hours).

Four EU Framework Programme 7 projects were ongoing at the end of the year: EISCAT_3D_2 "EISCAT_3D: A European three-dimensional imaging radar for atmospheric and geospace research (Preparatory Phase)", ENVRI "Common Operations of Environmental Research Infrastructures", ESPAS "Near-Earth Space Data Infrastructure for e-Science" and COOPEUS "Strengthening the cooperation between the US and the EC in the field of environmental research infrastructures". EISCAT Headquarters is the coordinator of EISCAT_3D_2 and partner in the other projects. The bid for a further FP7 project, MISW: "Mitigation of space weather threats to GNSS services", got acceptance and this project will start 2014-02-01. MISW is funded under FP7-SPACE-2013-1 and will run for 30 months. The EISCAT involvement amounts to 10 staff months.

The "third antenna system on Svalbard with dual mode capabilities" development continued also during 2013. All local permits are now in place but a final approval from the Norwegian government is needed before the EISCAT Council can make a decision how to proceed with the project.

The project: planning of EISCAT_3D, "planering av EISCAT_3D", are now well underway. Specific staff are tied to this project which is funded by a Vetenskapsrådet (Sweden) grant. The planning work during 2013 was much focused on expanding the international consortium that will fund the new infrastructure.

**Future operation and scientific development**

All systems are ready for users. These comprise of the EISCAT Svalbard Radar, Heating and the UHF and VHF radars with the possibility to run the VHF in tristatic mode by using the antennas in Kiruna and Sodankylä for reception. The small receive-only array in Kiruna will be used for field-tests in the EISCAT_3D preparatory phase project. The array will be dismantled after these tests.

**The work of the Council and its committees**

The Council had four meetings during the year. The postponed 2012 autumn meeting was held 5 – 6 February 2013 in Beijing, P. R. of China, and an extraordinary follow-on meeting was held 17 April 2013 in Copenhagen, Denmark. The first ordinary 2013 meeting was held at the Research Council in Norway, 27 – 28 May, 2013, under the leadership of the new Chairperson, Prof. Jian Wu. The autumn meeting was held in Leeds, UK, 30 – 31 October, 2013. The Scientific Oversight Committee had two meetings during the year. The spring meeting was held at the National Institute of Polar Research, Tokyo, Japan, under the leadership of Prof. Cesar La Hoz. The autumn meeting was held in Lancaster, UK under the leadership of the new Chairperson, Dr. Yasunobu Ogawa. The Council Advisory Group did not have any meetings this year.

The work at Council and its committees were much related to regular activities, including financial aspects. The extraordinary Council meeting focused primarily on matters relating to the 3rd antenna system on Svalbard project. Council decided in the autumn meeting to have the Associates increase the annual financial contribution with 5%.

**Budget development during the year**
The 2013 operations ended under the operating target set for the year. The mainland systems were in total on target but the Svalbard radar was used only for 700 hours, 24% less than budgeted. The fault in the Svalbard 32 meter antenna was only resolved in October and this problem contributed to the lack of interest in using the system during 2013.

The overall spend followed well the forecast for the year and the regular income was well on target. Income from project work became better than anticipated.

Council decided to make a large investment by buying a new partial set of klystrons for the Svalbard radar. The basis for the decision came from information that the type of klystron will no longer be produced and that a final last-time order would be honoured only during a short time. Since the Association has financial constraints, an upper monetary limit was set and the Executives were tasked to order either 8 or 10 klystrons depending on the per unit price. After negotiations with the manufacturer, a total of 10 klystrons was ordered with an order total of about 5 MSEK. The delivery is expected summer 2014 and 2.8 MSEK was put in the Capital Operating reserve to cover a part of the total cost. The remainder, 2.2 MSEK, will be drawn from the 2014 operating funds, if possible. If not, the sum will need to come from own reserves. The 10 klystrons will mean that there are enough spares to push the expected lifetime of the Svalbard transmitter system with another 10 to 15 years.

**The long-term budget plan**
The long-term budget plan is difficult. The 5% increase of the annual contribution will improve the situation. The highest priority is to maintain a reasonable level of operations and to avoid staff complement reductions in the near future. Carrying forward staff and skills is particularly important since the EISCAT_3D implementation is expected to start within the coming 1-2 years.

**The result for 2013 and profit/loss handling**
The transfer of funds needed to part-pay the ordered klystrons to Svalbard meant that the year ended in balance.

## PROFIT AND LOSS ACCOUNTS

in thousands of Swedish Crowns

| | | 2013 | 2012 |
|---|---|---|---|
| | Note 1 | | |
| Associate contributions | Note 2 | 20 631 | 22 325 |
| Other operating income | | 12 194 | 10 572 |
| | | 32 825 | 32 897 |
| Operation costs | | -8 692 | -7 998 |
| Administration costs | | -4 349 | -4 716 |
| Personnel costs | Note 3 | -18 605 | -17 170 |
| Depreciation of fixed assets | | -1 079 | -1 061 |
| | | -32 724 | -30 946 |
| *Operating profit/loss* | | *100* | *1 952* |
| Interest income | | 115 | 195 |
| Other financial income and cost | | 366 | 1 337 |
| Own reserves and funds | Note 4 | -1 660 | -2 188 |
| | | -1 179 | -656 |
| *Profit/loss after financial items* | | *-1 079* | *1 295* |
| Appropriations | Note 5 | 0 | -2 356 |
| Transfer from funds invested | Note 6 | 1 079 | 1 061 |
| | | 1 079 | -1 295 |
| *Net profit/loss for the year* | | *0* | *0* |

## BALANCE SHEET

in thousands of Swedish Crowns

| | | 2013 | 2012 |
|---|---|---|---|
| ASSETS | | | |
| Fixed assets | | | |
| *Tangible fixed assets* | Note 7 | | |
| Buildings | | 2 662 | 2 895 |
| Radar systems | | 651 | 742 |
| Equipment and tools | | 1 827 | 1 759 |
| | | 5 140 | 5 396 |
| Current assets | | | |
| Receivables | | 8 865 | 3 392 |
| Prepayments and accrued income | Note 8 | 5 296 | 5 578 |
| Cash at bank and in hand | Note 9 | 30 631 | 33 148 |
| | | 44 792 | 42 117 |
| *Total assets* | | *49 932* | *47 513* |
| CAPITAL AND LIABILITIES | | | |
| Capital | | | |
| Funds invested | Note 10 | 5 140 | 5 396 |
| Funds held on reserve | Note 11 | 21 862 | 21 024 |
| | | 27 002 | 26 420 |
| Current liabilities | | | |
| Liabilities, trade | Note 12 | 22 530 | 20 326 |
| Provisions | Note 13 | 0 | 429 |
| Other liabilities | | 400 | 339 |
| | | 22 930 | 21 093 |
| *Total capital and liabilities* | | *49 932* | *47 513* |
| *Pledged assets* | | *none* | *none* |
| *Contingent liabilities* | | *none* | *none* |

## STATEMENT OF CASH FLOWS

in thousands of Swedish Crowns

| | ***2013*** | ***2012*** |
|---|---|---|
| Operating activities | | |
| Operating result before financial items | 100 | 1 952 |
| Transfer from funds invested | 1 079 | 1 061 |
| | | |
| Interest received | 115 | 195 |
| Currency exchange rate changes | 341 | 1 283 |
| Extra ordinary income and cost | 26 | 54 |
| | | |
| Increase/decrease of receivables | -5 473 | -957 |
| Increase/decrease of prepayments and accrued income | 282 | -3 376 |
| Increase/decrease of creditors and liabilities | 1 837 | 9 580 |
| | | |
| *Cash flow from operations* | *-1 694* | *9 791* |
| | | |
| Investment activities | | |
| Investments in tangible assets | -823 | -810 |
| | | |
| *Cash flow from investment activities* | *-823* | *-810* |
| | | |
| *Cash flow for the year* | *-2 517* | *8 982* |
| | | |
| *Liquid assets at the beginning of the year* | *33 148* | *24 166* |
| | | |
| *Liquid assets at the end of the year* | *30 631* | *33 148* |

**NOTES**

**Note 1** *Accounting principles*

The accounting and valuation principles applied are consistent with the provisions of the Swedish Annual Accounts Act and generally accepted accounting principles (bokföringsnämnden allmänna råd och vägledningar).

All amounts are in thousands of Swedish kronor (SEK) unless otherwise stated.

*Receivables*
Receivables are stated at the amounts estimated to be received, based on individual assessment.

*Receivables and payables in foreign currencies*
Receivables and payables in foreign currencies are valued at the closing day rate. Where hedging measures have been used, such as forwarding contracts, the agreed exchange rate is applied. Gains and losses relating to operations are accounted for under other financial income and cost.

*Bank accounts in foreign currencies*
Bank balances in foreign currencies are valued at the closing day rate.

*Fixed assets*
Tangible fixed assets are stated at their original acquisition values after deduction of depreciation according to plan. Assets are depreciated systematically over their estimated useful lives. The following periods of depreciation are applied: Buildings 5 - 50 years, Radar systems 3 - 20 years and Equipment and tools 1 - 5 years.

**Note 2** *Associate contributions*

The Associates contributed to the operation during the year in accordance with the agreement. The commitments are in local currencies. The received contributions have been accounted in SEK.

| | 2013 |
|---|---|
| CRIRP (P. R. of China) | 3 053 |
| NIPR (Japan) | 1 385 |
| RCN (Norway) | 5 435 |
| SA (Finland) | 3 060 |
| NERC (United Kingdom) | 2 027 |
| VR (Sweden) | 5 670 |
| | 20 631 |

Accumulated contributions status as of 2013-12-31

| | 1976 - 2013 |
|---|---|
| Previous Associates | 382 168 |
| CRIRP (P. R. of China) | 22 374 |
| NIPR (Japan) | 73 537 |
| RCN (Norway) | 156 554 |
| SA (Finland) | 71 504 |
| NERC (United Kingdom) | 226 280 |
| VR (Sweden) | 129 899 |
| | 1 062 316 |

**Note 3** *Personnel costs and average number of employees*

The Association employs directly the Headquarters staff, currently about eight positions, including the Director. The Headquarters is located in Kiruna, Sweden. The personnel working at the Kiruna (Sweden), Sodankylä (Finland), Svalbard and Tromsö (Norway) sites are not employed by the Association. Instead, the personnel are provided via site contracts by the Swedish Institute of Space Physics (Kiruna site staff), Oulu University (Sodankylä staff) and Tromsö University (Tromsö and Svalbard staff). The Association refunds all expenses related to the provided staff, as well as an additional overhead.

| | ***2013*** | ***2012*** |
|---|---|---|
| *Personnel costs in total* | | |
| Salaries and emoluments paid to the Director | 1 552 | 1 385 |
| Other personnel, employed and provided via site contracts | 11 619 | 11 067 |
| Social security contributions amounted to | 4 826 | 4 192 |
| of which for pension costs | 2 349 | 2 026 |

The new Director, Dr. Craig Heinselman, started his time-limited employment 2013-01-01. His employment contract with Council is for up to three years.

Of the pension costs, 270 kSEK (354 kSEK) relates to the Director. He and all other directly employed staff are included in ITP like occupational pension plans. For the personnel provided via site contracts, the pension plans are handled by their respective employer.

The members of the board (EISCAT Council) and members of committees, who represents Associates, do not receive remunerations from the Association. Travel expenses in connection with Council and committee meetings are normally covered by the Associates. For the Council Advisory Group, the Association cover meeting and travel costs.

*Salaries and emoluments and average number of staff per country*

| | | |
|---|---|---|
| Finland | | |
| Salaries and emoluments | 585 | 592 |
| Average number of staff - men and women | 1 + 0 | 1 + 0 |
| Norway (including Svalbard) | | |
| Salaries and emoluments | 5 173 | 5 971 |
| Average number of staff - men and women | 8 + 0 | 9 + 0 |
| Sweden | | |
| Salaries and emoluments | 7 414 | 5 890 |
| Average number of staff - men and women | 8 + 2 | 7 + 2 |

*Members of the board and Directors at year-end - men and women*
The board consist of delegations from every Associate country each having a Delegate (formal member) and up to two Representatives.

| | | |
|---|---|---|
| Board members (EISCAT Council) | 11 + 3 | 11 + 3 |
| Directors | 1 + 0 | 1 + 0 |

**Note 4** *Own reserves and funds*

The funds for the purchase of ten new klystrons to the Svalbard radar (totally 462 kGBP or about 5 MSEK), to be delivered in 2014, will be drawn from operating funds in 2013 and 2014. For this year, 2 833 kSEK was set aside in the Capital Operating reserve for this funding.

| | | |
|---|---|---|
| Capital Operating reserve | | |
| Transfer to the reserve | -826 | -941 |
| Transfer to the reserve (additional) | -2 833 | 0 |
| Transfer from the reserve | 792 | 790 |
| Investments made | -823 | -810 |
| Spare parts reserve | | |
| Transfer to the reserve | -10 | -19 |
| Transfer from the reserve | 0 | 29 |

| | 2013 | 2012 |
|---|---|---|
| Surplus fund | | |
| Transfer from the fund | 2 040 | 0 |
| Transfer to the fund | 0 | -1 237 |
| *Sum own reserves and funds* | *-1 660* | *-2 188* |

**Note 5** *Appropriations*

The outcome for this year was balanced. The 2012 outcome resulted in a surplus (2 356 kSEK), which was transferred to the surplus fund.

**Note 6** *Transfer from funds invested*

The depreciation cost is covered by funds from Capital - funds invested

**Note 7** *Tangible fixed assets*

Changes in tangible fixed assets during 2013.

| | | |
|---|---|---|
| Buildings | | |
| Opening acquisition value | 42 428 | 42 428 |
| Acquisitions during the year | 0 | 0 |
| Disposals during the year | -5 | 0 |
| Closing acquisition value | 42 424 | 42 428 |
| | | |
| Opening accumulated depreciation | -39 533 | -39 234 |
| Depreciations during the year | -234 | -299 |
| Disposals during the year | 5 | 0 |
| Closing accumulated depreciation | -39 762 | -39 533 |
| | | |
| Closing residual value | 2 662 | 2 895 |
| | | |
| Radar systems | | |
| Opening acquisition value | 244 693 | 244 693 |
| Acquisitions during the year | 0 | 0 |
| Disposals during the year | 0 | 0 |
| Closing acquisition value | 244 693 | 244 693 |
| | | |
| Opening accumulated depreciation | -243 952 | -243 861 |
| Depreciations during the year | -90 | -90 |
| Disposals during the year | 0 | 0 |
| Closing accumulated depreciation | -244 042 | -243 952 |
| | | |
| Closing residual value | 651 | 742 |
| | | |
| Equipment and tools | | |
| Opening acquisition value | 31 354 | 33 459 |
| Acquisitions during the year | 823 | 810 |
| Disposals during the year | 450 | 2 915 |
| Closing acquisition value | 31 726 | 31 354 |
| | | |
| Opening accumulated depreciation | -29 595 | -31 838 |
| Depreciations during the year | -755 | -672 |
| Disposals during the year | 450 | 2 915 |
| Closing accumulated depreciation | -29 899 | -29 595 |
| | | |
| Closing residual value | 1 827 | 1 759 |
| | | |
| *Sum tangible fixed assets* | *5 140* | *5 396* |

**Note 8** *Prepayments and accrued income*

Resources in staff and direct costs spent in the now four plus one (EU and VR funded) ongoing projects are covered by accrued income until settled by periodic report claims. Periodic reports are due at various times. For 2013, both EISCAT_3D_2 and ESPAS had second period reporting and ENVRI had its first periodic report.

| | 2013 | 2012 |
|---|---|---|
| Prepaid rents | 105 | 104 |
| Prepaid insurances | 531 | 533 |
| Accrued income, COOPEUS project | 341 | 63 |
| Accrued income, EISCAT_3D_2 project | 706 | 2 777 |
| Accrued income, ENVRI project | 156 | 58 |
| Accrued income, ESPAS project | 167 | 215 |
| Accrued income, VR-PG project | 3 185 | 110 |
| Other items | 106 | 1 717 |
| | 5 296 | 5 578 |

**Note 9** *Bank balances status*

| | | |
|---|---|---|
| Nordea | 30 631 | 33 147 |
| Cash in hand | 0 | 1 |
| | 30 631 | 33 148 |

**Note 10** *Funds invested status*

| | | |
|---|---|---|
| Buildings | 2 662 | 2 895 |
| Radar Systems | 651 | 742 |
| Equipment and Tools | 1 827 | 1 759 |
| | 5 140 | 5 396 |

**Note 11** *Funds held on reserve*

Both investments and spare parts purchases were less than budgeted. Both actions were budget neutral since the differences were covered by reserve transfers. Funds for part-paying the delivery of ten klystrons for Svalbard were added to the Capital Operating reserve.

| | | |
|---|---|---|
| Capital operating reserve | 5 070 | 2 203 |
| Equipment repair fund | 754 | 754 |
| Investment fund | 7 971 | 7 971 |
| Restructuring reserve | 4 101 | 4 101 |
| Spare parts reserve | 149 | 139 |
| Surplus fund | 3 815 | 5 856 |
| | 21 862 | 21 024 |

**Note 12** *Liabilities, trade*

Four projects financed by EU's European Commission through the Framework Programme 7 scheme and one project financed through Vetenskapsrådet are ongoing. All projects work with prefinancing. The prefinancing is kept as liability until the project has ended and been financially concluded. The guarantee fund is kept as contingency by the Commission for the EISCAT_3D_2 project, which EISCAT is the Co-ordinator of. The guarantee fund will be released after the end of the project, 2014-09-30.

| | | |
|---|---|---|
| COOPEUS prefinancing | 1 632 | 1 581 |
| EISCAT_3D_2 guarantee fund, whole project | 1 991 | 1 929 |
| EISCAT_3D_2 prefinancing | 5 282 | 4 881 |
| ENVRI prefinancing | 536 | 519 |
| ESPAS prefinancing | 2 513 | 2 408 |
| VR-PG prefinancing | 7 000 | 3 500 |
| Other prefinancing | 0 | 2 134 |
| Liabilities, trade | 3 577 | 3 374 |
| | 22 530 | 20 326 |

**Note 13** *Provisions*

| | | |
|---|---|---|
| Provisions | 0 | 429 |
| | 0 | 429 |

Nagoya 2014-06-10

Dr. Tomas Andersson

Prof. Qing-sheng Dong

Dr. Mervyn Freeman

Dr. Bjørn Jacobsen

Dr. Hiroshi Miyaoka

Dr. Kati Sulonen

Dr. Craig Heinselman
Director

Our audit report was issued on 2014-06-18

Mrs. Annika Wedin
Authorised Public Accountant

pwc

# Audit report

## To the council of EISCAT Scientific Association, Corporate Identity Number 897300-2549

### Report on the annual accounts

I have audited the annual accounts of EISCAT Scientific Association for the year 2013.

#### *Responsibilities of the council and the director for the annual accounts*

The council and the director are responsible for the preparation and fair presentation of the annual accounts in accordance with the Annual Accounts Act, and for such internal control as the council and the director determine is necessary to enable the preparation of annual accounts that are free from material misstatement, whether due to fraud or error.

#### *Auditor's responsibility*

My responsibility is to express an opinion on the annual accounts based on my audit. I conducted my audit in accordance with International Standards on Auditing and generally accepted auditing standards in Sweden. Those standards require that I comply with ethical requirements and plan and perform the audit to obtain reasonable assurance about whether the annual accounts are free from material misstatement.

An audit involves performing procedures to obtain audit evidence about the amounts and disclosures in the annual accounts. The procedures selected depend on the auditor's judgment, including the assessment of the risks of material misstatement of the annual accounts, whether due to fraud or error. In making those risk assessments, the auditor considers internal control relevant to the association's preparation and fair presentation of the annual accounts, in order to design audit procedures that are appropriate in the circumstances, but not for the purpose of expressing an opinion on the effectiveness of the association's internal control. An audit also includes evaluating the appropriateness of accounting policies used and the reasonableness of accounting estimates made by the council and the director, as well as evaluating the overall presentation of the annual accounts.

I believe that the audit evidence I have obtained is sufficient and appropriate to provide a basis for my audit opinion.

#### *Opinion*

In my opinion, the annual accounts have been prepared in accordance with the Annual Accounts Act and present fairly, in all material respects, the financial position of the association as of 31 December 2013 and its financial performance and its cash flows for the year then ended in accordance with the Annual Accounts Act. The statutory administration report is consistent with the other parts of the annual accounts.

### Report on other legal and regulatory requirements

In addition to my audit of the annual accounts, I have also audited the administration of the council and the director of EISCAT Scientific Association for the year 2013.

#### *Responsibilities of the council and the director*

The council and the director are responsible for the administration.

#### *Auditor's responsibility*

My responsibility is to express an opinion with reasonable assurance on the administration based on my audit. I conducted the audit in accordance with generally accepted auditing standards in Sweden.

As a basis for my opinion on the council and the director´s administration, in addition to my audit of the annual accounts, I examined significant decisions, actions taken and circumstances of the association in order to determine whether any member of the council or the director have undertaken any action or is guilty of negligence which may entail a liability for damages. I also examined whether any council member or the director has, in any other way, acted in contravention of the Annual Accounts Act or the statutes.

I believe that the audit evidence I have obtained is sufficient and appropriate to provide a basis for my opinion.

#### *Opinion*

The council and the director have not acted in contravention of the statutes.

Gävle, 18 June 2014

Annika Wedin
Authorized Public Accountant

EISCAT Scientific Association
Registered as a Swedish non-profit organisation
Organisation number: 897300-2549

Annual report for the financial year 2014-01-01 – 2014-12-31

The EISCAT Council and the Director for the Association submits herewith the annual report for 2014.

# ADMINISTRATION REPORT

**Ownership, organisation and objective**

The EISCAT Scientific Association was established in 1975 through an agreement between six European organisations. Japan joined in 1996 and the Peoples Republic of China in 2007.

The EISCAT Associates at 2014-12-31 are: China Research Institute of Radiowave Propagation (Peoples Republic of China), National Institute of Polar Research (Japan), Natural Environment Research Council (United Kingdom of Great Britain and Northern Ireland), Norges forskningsråd (Norway), Solar-Terrestrial Environment Laboratory, Nagoya University (Japan), Suomen Akatemia (Finland), and Vetenskapsrådet (Sweden).

The now running EISCAT Agreement came into force 2007-01-01, with all Associates making long term funding commitments to the Association. The Association has its formal seat in Kiruna, Sweden, and is registered as a non-profit organisation.

The aim of the Association is to make significant progress in the understanding of physical processes in the high latitude atmosphere by means of experimental programmes generally conducted using the incoherent scatter radar technique, which may be carried out as part of wider international projects. For this purpose, the Association has developed, constructed, and now operates, a number of radar facilities at high latitudes. At present, these comprise a system of stations at Tromsö (Norway), Kiruna (Sweden), Sodankylä (Finland), and Longyearbyen (Svalbard).

The Association is fully funded by the Associates but additional operations may also be funded by short term additional contributions from both Associate and non-Associate bodies. Depending on the available funding, scientific priorities and operational targets are adjusted on an annual basis.

The EISCAT Council is charged with the overall administration and supervision of the Association's activities. The Council appoints a Director, who is responsible for the daily management and operation of the facilities of the Association.

**Operation and scientific development**

The EISCAT Radars delivered a full programme of operations for the user community and operated reliably throughout the year.

The various EISCAT radars operated for a total of 2 757 accounted hours (2 378 hours in 2013).

Common Programmes amounted to 49% (33%) of the operations. Special Programmes amounted to 43% (45%) and other operations amounted to 8% (22%) of the total hours.

France, Ukraine and Russia have Affiliate agreements and totally 60 hours (316 hours) were accounted on behalf of these countries. The Peer-Review Programme made it possible for users from Belgium, France, Netherlands, Norway, South Korea, Sweden UK and USA to run

experiments, at no cost, on the systems. Peer-Review time amounted to 128 accounted hours (168 hours).

Three EU Framework Programme 7 projects were ongoing at the end of the year: COOPEUS "Strengthening the cooperation between the US and the EC in the field of environmental research infrastructures", ESPAS "Near-Earth Space Data Infrastructure for e-Science" and MISW: "Mitigation of space weather threats to GNSS services". The EISCAT_3D_2 "EISCAT_3D: A European three-dimensional imaging radar for atmospheric and geospace research (Preparatory Phase)" and ENVRI "Common Operations of Environmental Research Infrastructures" both ended in autumn. In autumn EISCAT joined as partner five application consortia's bidding for H2020 project funding. Two bids were successful and a third passed the evaluation threshold but all funding had then already been distributed to bids achieving higher ranks. The two new projects, EGI-Engage "Engaging the EGI Community towards an Open Science Commons" and ENVRI PLUS "Environmental Research Infrastructures Providing Shared Solutions for Science and Society" will both start in the first half of 2015. The latter project means a large commitment for EISCAT with 46 staff-months of funding over four years.

The project: planning of EISCAT_3D, "planering av EISCAT_3D", continued throughout the year. A request to extend the length of the project to autumn 2015 was submitted in December. A 4 MSEK follow-on project "EISCAT_3D: nästa generations internationella radarsystem för utforskning av atmosfären och den jordnära rymden" started 1 January 2014. These two projects, both funded by Vetenskapsrådet (Sweden), runs partially in parallel but will be managed in sequence. Both projects support the EISCAT_3D project office and consortium building work.

**Future operation and scientific development**

All systems are ready for users. These comprise now of the EISCAT Svalbard Radar, Heating and the UHF and VHF radars with the possibility to run the VHF in tristatic mode by using the antennas in Kiruna and Sodankylä for reception.

**The work of the Council and its committees**

The Council had two ordinary meetings under the leadership of the Chairperson, Prof. Jian Wu. The spring meeting was held 10 – 11 June at the Nagoya University in Japan. The autumn meeting was held in Helsinki 6 – 7 November at the Academy of Finland. The Scientific Oversight Committee, under the leadership of the Chairperson, Dr. Yasunobu Ogawa, had two meetings during the year. The spring meeting was held 3 - 4 April at the DLR institute in Weßling, Germany. The autumn meeting was held in Beijing, 24 -25 August. The Council Advisory Group did not have any meetings this year.

The work at Council and its committees were much related to regular activities, including financial aspects. Council decided also to replace the advisory group with an Administrative and Finance Committee. This committee, initially formed as an adHoc structure, will have its first meeting in the beginning of 2015. The Administrative and Finance Committee will formally come into existence when the revised Agreement is activated. The 3rd antenna system on Svalbard project was effectively terminated when Council was informed that Norwegian authorities considered the antenna to be undesirable.

**Budget development during the year**
The 2014 operations ended on the operating target set for the year. The mainland systems were used more than budgeted and the Svalbard radar was used less. The mainland interest was much driven by the continued possibility to perform UHF radar measurements, which at the time of budgeting in 2013, seemed to be impossible due the loss of the frequency spectrum. The Svalbard radar operating hours budget had therefore been increased to compensate for the loss of the UHF hours.

The overall spend followed well the forecast for the year and the regular income was higher than expected since Ukraine managed to continue their Affiliation. Value changes in short-term deposits added further income.

The purchase of 10 new klystrons was completed in September. The final cost, including GBP-SEK exchange rate variation, finally became 5.3 MSEK. Part of the funding, 2.8 MSEK, was set aside already in 2013. The remainder was drawn from the annual operating funds.

**The long-term budget plan**
The long-term budget plan continues to be challenging. The highest priority is to maintain a reasonable level of operations and to avoid staff complement reductions in the near future since staff and skills will be needed for the EISCAT_3D implementation phase.

**The result for 2014 and profit/loss handling**
The year was balanced by covering the deficit, 218 kSEK, from the Investment fund.

## PROFIT AND LOSS ACCOUNTS

in thousands of Swedish Crowns

| | | | |
|---|---|---|---|
| | Note 1 | ***2014*** | ***2013*** |
| Associate contributions | Note 2 | 21 837 | 20 631 |
| Other operating income | | 6 640 | 12 194 |
| | | 28 476 | 32 825 |
| Operation costs | | -5 730 | -8 692 |
| Administration costs | | -4 139 | -4 349 |
| Personnel costs | Note 3 | -19 102 | -18 605 |
| Depreciation of fixed assets | | -1 384 | -1 079 |
| | | -30 355 | -32 724 |
| *Operating profit/loss* | | *-1 878* | *100* |
| Interest income | | 61 | 115 |
| Other financial income and cost | | 1 183 | 366 |
| Own reserves and funds | Note 4 | -968 | -1 660 |
| | | 276 | -1 179 |
| *Profit/loss after financial items* | | *-1 602* | *-1 079* |
| Appropriations | Note 5 | 218 | 0 |
| Transfer from funds invested | Note 6 | 1 384 | 1 079 |
| | | 1 602 | 1 079 |
| *Net profit/loss for the year* | | *0* | *0* |

## BALANCE SHEET

in thousands of Swedish Crowns

| | | 2014 | 2013 |
|---|---|---|---|
| ASSETS | | | |
| Fixed assets | | | |
| *Tangible fixed assets* | Note 7 | | |
| Buildings | | 2 437 | 2 662 |
| Radar systems | | 5 765 | 651 |
| Equipment and tools | | 2 354 | 1 827 |
| | | 10 556 | 5 140 |
| Current assets | | | |
| Receivables | | 5 477 | 8 865 |
| Prepayments and accrued income | Note 8 | 8 039 | 5 296 |
| Cash at bank and in hand | Note 9 | 22 959 | 30 631 |
| | | 36 476 | 44 792 |
| *Total assets* | | *47 032* | *49 932* |
| CAPITAL AND LIABILITIES | | | |
| Capital | | | |
| Funds invested | Note 10 | 10 556 | 5 140 |
| Funds held on reserve | Note 11 | 15 811 | 21 862 |
| | | 26 367 | 27 002 |
| Current liabilities | | | |
| Liabilities, trade | Note 12 | 20 291 | 22 530 |
| Provisions | | 0 | 0 |
| Other liabilities | | 373 | 400 |
| | | 20 664 | 22 930 |
| *Total capital and liabilities* | | *47 032* | *49 932* |
| *Pledged assets* | | *none* | *none* |
| *Contingent liabilities* | | *none* | *none* |

## STATEMENT OF CASH FLOWS

in thousands of Swedish Crowns

| | ***2014*** | ***2013*** |
|---|---|---|
| Operating activities | | |
| Operating result before financial items | -1 878 | 100 |
| Transfer from funds invested | 1 384 | 1 079 |
| | | |
| Interest received | 61 | 115 |
| Currency exchange rate changes | 973 | 341 |
| Extra ordinary income and cost | 210 | 26 |
| | | |
| Increase/decrease of receivables | 3 388 | -5 473 |
| Increase/decrease of prepayments and accrued income | -2 743 | 282 |
| Increase/decrease of creditors and liabilities | -2 266 | 1 837 |
| | | |
| *Cash flow from operations* | *-872* | *-1 694* |
| | | |
| Investment activities | | |
| Investments in tangible assets | -6 800 | -823 |
| | | |
| *Cash flow from investment activities* | *-6 800* | *-823* |
| | | |
| *Cash flow for the year* | *-7 672* | *-2 517* |
| | | |
| *Liquid assets at the beginning of the year* | *30 631* | *33 148* |
| | | |
| *Liquid assets at the end of the year* | *22 959* | *30 631* |

**NOTES**

**Note 1** *Accounting principles*

The accounting and valuation principles applied are consistent with the provisions of the Swedish Annual Accounts Act and generally accepted accounting principles (bokföringsnämnden allmänna råd och vägledningar).

All amounts are in thousands of Swedish kronor (SEK) unless otherwise stated.

*Receivables*
Receivables are stated at the amounts estimated to be received, based on individual assessment.

*Receivables and payables in foreign currencies*
Receivables and payables in foreign currencies are valued at the closing day rate. Where hedging measures have been used, such as forwarding contracts, the agreed exchange rate is applied. Gains and losses relating to operations are accounted for under other financial income and cost.

*Bank accounts in foreign currencies*
Bank balances in foreign currencies are valued at the closing day rate.

*Fixed assets*
Tangible fixed assets are stated at their original acquisition values after deduction of depreciation according to plan. Assets are depreciated systematically over their estimated useful lives. The following periods of depreciation are applied: Buildings 5 - 50 years, Radar systems 3 - 20 years and Equipment and tools 1 - 5 years.

**Note 2** *Associate contributions*

The Associates contributed to the operation during the year in accordance with the agreement. The commitments are in local currencies. The received contributions have been accounted in SEK.

| | 2014 |
|---|---|
| CRIRP (P. R. of China) | 3 246 |
| NIPR (Japan) | 1 417 |
| RCN (Norway) | 5 594 |
| SA (Finland) | 3 401 |
| NERC (United Kingdom) | 2 508 |
| VR (Sweden) | 5 670 |
| | 21 837 |

Accumulated contributions status as of 2014-12-31

| | 1976 - 2014 |
|---|---|
| Previous Associates | 382 168 |
| CRIRP (P. R. of China) | 25 620 |
| NIPR (Japan) | 74 955 |
| RCN (Norway) | 162 148 |
| SA (Finland) | 74 905 |
| NERC (United Kingdom) | 228 788 |
| VR (Sweden) | 135 569 |
| | 1 084 153 |

**Note 3** *Personnel costs and average number of employees*

The Association employs directly the Headquarters staff, currently about nine positions, including the Director. The Headquarters is located in Kiruna, Sweden. The personnel working at the Kiruna (Sweden), Sodankylä (Finland), Svalbard and Tromsö (Norway) sites are not employed by the Association. Instead, the personnel are provided via site contracts by the Swedish Institute of Space Physics (Kiruna site staff), Oulu University (Sodankylä staff) and Tromsö University (Tromsö and Svalbard staff). The Association refunds all expenses related to the provided staff, as well as an additional overhead.

| | ***2014*** | ***2013*** |
|---|---|---|
| *Personnel costs in total* | | |
| Salaries and emoluments paid to the Director | 1 475 | 1 552 |
| Other personnel, employed and provided via site contracts | 12 084 | 11 619 |
| Social security contributions amounted to | 5 025 | 4 826 |
| of which for pension costs | 2 474 | 2 349 |

The Director, Dr. Craig Heinselman, started his employment 2013-01-01. His employment contract with Council is for up to three years. It can thereafter be extended with another term.

Of the pension costs, 283 kSEK (270 kSEK) relates to the Director. He and all other directly employed staff are included in ITP like occupational pension plans. For the personnel provided via site contracts, the pension plans are handled by their respective employer.

The members of the board (EISCAT Council) and members of committees, who represents Associates, do not receive remunerations from the Association. Travel expenses in connection with Council and committee meetings are normally covered by the Associates. For the Council Advisory Group, the Association cover meeting and travel costs.

*Salaries and emoluments and average number of staff per country*

| | | |
|---|---|---|
| Finland | | |
| Salaries and emoluments | 626 | 585 |
| Average number of staff - men and women | 1 + 0 | 1 + 0 |
| Norway (including Svalbard) | | |
| Salaries and emoluments | 5 491 | 5 173 |
| Average number of staff - men and women | 8 + 0 | 8 + 0 |
| Sweden | | |
| Salaries and emoluments | 7 442 | 7 414 |
| Average number of staff - men and women | 8 + 2 | 8 + 2 |

*Members of the board and Directors at year-end - men and women*
The board consist of delegations from every Associate country each having a Delegate (formal member) and up to two Representatives.

| | | |
|---|---|---|
| Board members (EISCAT Council) | 11 + 3 | 11 + 3 |
| Directors | 1 + 0 | 1 + 0 |

**Note 4** *Own reserves and funds*
A large investment was done during the year when ten new klystrons to the Svalbard radar was bought. The total purchase amounted to 5 322 kSEK. It was partially funded by the 2 833 kSEK that was set aside in 2013. The remaining part was covered by 2014 operating funds.

| | | |
|---|---|---|
| Capital Operating reserve | | |
| Transfer to the reserve | -1 235 | -3 659 |
| Transfer from the reserve | 4 239 | 792 |
| Investments made | -6 800 | -823 |
| Spare parts reserve | | |
| Transfer to the reserve | -10 | -10 |
| Transfer from the reserve | 37 | 0 |

| | 2014 | 2013 |
|---|---|---|
| Surplus fund | | |
| Transfer from the fund | 2 800 | 2 040 |
| Transfer to the fund | 0 | 0 |
| *Sum own reserves and funds* | *-968* | *-1 660* |

**Note 5** *Appropriations*

The outcome for this year became a deficit relative to the budget amounting to -218 kSEK. The deficit was covered by a transfer from the Investment fund. The 2013 outcome was balanced.

**Note 6** *Transfer from funds invested*

The depreciation cost is covered by funds from Capital - funds invested

**Note 7** *Tangible fixed assets*

Changes in tangible fixed assets during 2014.

| | | |
|---|---|---|
| Buildings | | |
| Opening acquisition value | 42 424 | 42 428 |
| Acquisitions during the year | 4 | 0 |
| Disposals during the year | -14 | -5 |
| Closing acquisition value | 42 413 | 42 424 |
| | | |
| Opening accumulated depreciation | -39 762 | -39 533 |
| Depreciations during the year | -228 | -234 |
| Disposals during the year | 14 | 5 |
| Closing accumulated depreciation | -39 976 | -39 762 |
| | | |
| Closing residual value | 2 437 | 2 662 |
| | | |
| Radar systems | | |
| Opening acquisition value | 244 693 | 244 693 |
| Acquisitions during the year | 5 394 | 0 |
| Disposals during the year | 0 | 0 |
| Closing acquisition value | 250 087 | 244 693 |
| | | |
| Opening accumulated depreciation | -244 042 | -243 952 |
| Depreciations during the year | -280 | -90 |
| Disposals during the year | 0 | 0 |
| Closing accumulated depreciation | -244 322 | -244 042 |
| | | |
| Closing residual value | 5 765 | 651 |
| | | |
| Equipment and tools | | |
| Opening acquisition value | 31 726 | 31 354 |
| Acquisitions during the year | 1 402 | 823 |
| Disposals during the year | 480 | 450 |
| Closing acquisition value | 32 649 | 31 726 |
| | | |
| Opening accumulated depreciation | -29 899 | -29 595 |
| Depreciations during the year | -876 | -755 |
| Disposals during the year | 480 | 450 |
| Closing accumulated depreciation | -30 295 | -29 899 |
| | | |
| Closing residual value | 2 354 | 1 827 |
| | | |
| *Sum tangible fixed assets* | *10 556* | *5 140* |

**Note 8** *Prepayments and accrued income*

Resources in staff and direct costs spent in ongoing externally funded projects are covered by accrued income until settled by periodic report claims. The EISCAT_3D_2 and ENVRI projects ended and two new, MISW and VR-OG, started during the year.

| | 2014 | 2013 |
|---|---|---|
| Prepaid rents | 109 | 105 |
| Prepaid insurances | 594 | 531 |
| Accrued income, COOPEUS project | 458 | 341 |
| Accrued income, EISCAT_3D_2 project | 0 | 706 |
| Accrued income, ENVRI project | 0 | 156 |
| Accrued income, ESPAS project | 1 312 | 167 |
| Accrued income, MISW project | 173 | 0 |
| Accrued income, VR-OG project | 0 | 0 |
| Accrued income, VR-PG project | 5 312 | 3 185 |
| Other items | 81 | 106 |
| | 8 039 | 5 296 |

**Note 9** *Bank balances status*

| | | |
|---|---|---|
| Nordea | 22 957 | 30 631 |
| Cash in hand | 2 | 0 |
| | 22 959 | 30 631 |

**Note 10** *Funds invested status*

| | | |
|---|---|---|
| Buildings | 2 437 | 2 662 |
| Radar Systems | 5 765 | 651 |
| Equipment and Tools | 2 354 | 1 827 |
| | 10 556 | 5 140 |

**Note 11** *Funds held on reserve*

Regular investments and spare parts purchases were both more than budgeted. The funds set aside in the Capital operating reserve for part-paying the purchase of the ten klystrons for Svalbard were used. The outcome deficit, -218 kSEK, was covered by funds from the Investment fund.

| | | |
|---|---|---|
| Capital operating reserve | 2 065 | 5 070 |
| Equipment repair fund | 754 | 754 |
| Investment fund | 7 753 | 7 971 |
| Restructuring reserve | 4 101 | 4 101 |
| Spare parts reserve | 122 | 149 |
| Surplus fund | 1 015 | 3 815 |
| | 15 811 | 21 862 |

**Note 12** *Liabilities, trade*

All externally funded projects work with prefinancing. For European Commission projects, these are in EUR's. The prefinancing is used to cover reported and approved costs. The ENVRI and EISCAT_3D_2 projects ended late in the year such that the approval of costs did not occur within 2014. The EISCAT_3D_2 guarantee fund is kept as contingency by the Commission for the EISCAT_3D_2 project, which EISCAT is the Co-ordinator of. The guarantee fund will be released when the final reporting has been approved by the Commission.

| | | |
|---|---|---|
| COOPEUS prefinancing | 1 522 | 1 632 |
| EISCAT_3D_2 guarantee fund, whole project | 2 111 | 1 991 |
| EISCAT_3D_2 prefinancing | 1 826 | 5 282 |
| ENVRI prefinancing | 484 | 536 |
| ESPAS prefinancing | 2 291 | 2 513 |
| MISW prefinancing | 519 | 0 |
| VR-OG prefinancing | 2 000 | 0 |
| VR-PG prefinancing | 7 000 | 7 000 |
| Liabilities, trade | 2 537 | 3 577 |
| | 20 291 | 22 530 |

Kiruna 2015-06-10

Dr. Tomas Andersson

Prof. Qing-sheng Dong

Dr. Mervyn Freeman

Dr. Bjørn Jacobsen

Dr. Hiroshi Miyaoka

Dr. Kati Sulonen

Dr. Craig Heinselman
Director

Our audit report was issued on 2015-06-17.

Mrs. Annika Wedin
Authorised Public Accountant

pwc

# Auditor's report

## To the council of EISCAT Scientific Association, Corporate Identity Number 897300-2549

### Report on the annual accounts

I have audited the annual accounts of EISCAT Scientific Association for the year 2014.

#### *Responsibilities of the council and the director for the annual accounts*

The council and the director are responsible for the preparation and fair presentation of the annual accounts in accordance with the Annual Accounts Act, and for such internal control as the council and the director determine is necessary to enable the preparation of annual accounts that are free from material misstatement, whether due to fraud or error.

#### *Auditor's responsibility*

My responsibility is to express an opinion on the annual accounts based on my audit. I conducted my audit in accordance with International Standards on Auditing and generally accepted auditing standards in Sweden. Those standards require that I comply with ethical requirements and plan and perform the audit to obtain reasonable assurance about whether the annual accounts are free from material misstatement.

An audit involves performing procedures to obtain audit evidence about the amounts and disclosures in the annual accounts. The procedures selected depend on the auditor's judgment, including the assessment of the risks of material misstatement of the annual accounts, whether due to fraud or error. In making those risk assessments, the auditor considers internal control relevant to the association's preparation and fair presentation of the annual accounts, in order to design audit procedures that are appropriate in the circumstances, but not for the purpose of expressing an opinion on the effectiveness of the association's internal control. An audit also includes evaluating the appropriateness of accounting policies used and the reasonableness of accounting estimates made by the council and the director, as well as evaluating the overall presentation of the annual accounts.

I believe that the audit evidence I have obtained is sufficient and appropriate to provide a basis for my audit opinion.

#### *Opinion*

In my opinion, the annual accounts have been prepared in accordance with the Annual Accounts Act and present fairly, in all material respects, the financial position of the association as of 31 December 2014 and its financial performance and its cash flows for the year then ended in accordance with the Annual Accounts Act. The statutory administration report is consistent with the other parts of the annual accounts.

### Report on other legal and regulatory requirements

In addition to my audit of the annual accounts, I have also audited the administration of the council and the director of EISCAT Scientific Association for the year 2014.

#### *Responsibilities of the council and the director*

The council and the director are responsible for the administration.

#### *Auditor's responsibility*

My responsibility is to express an opinion with reasonable assurance on the administration based on my audit. I conducted the audit in accordance with generally accepted auditing standards in Sweden.

As a basis for my opinion on the council and the director´s administration, in addition to my audit of the annual accounts, I examined significant decisions, actions taken and circumstances of the association in order to determine whether any member of the council or the director have undertaken any action or is guilty of negligence which may entail a liability for damages. I also examined whether any council member or the director has, in any other way, acted in contravention of the Annual Accounts Act or the statutes.

I believe that the audit evidence I have obtained is sufficient and appropriate to provide a basis for my opinion.

#### *Opinion*

The council and the director have not acted in contravention of the statutes.

Gävle, 17 June 2015

Annika Wedin
Authorized Public Accountant

Report 2013 – 2014 of the EISCAT Scientific Association


EISCAT Headquarters
Box 812, SE-981 28 Kiruna, Sweden

Scientific contributions: EISCAT Associates and staff

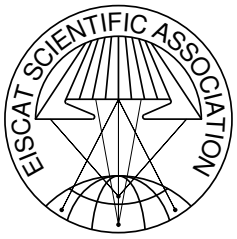


# The EISCAT Associates

December 2014

## CRIRP

China Research Institute of Radiowave Propagation
China
*www.crirp.ac.cn*

## NERC

Natural Environment Research Council
United Kingdom
*www.nerc.ac.uk*

## NFR

Norges forskningsråd
Norway
*www.forskningsradet.no*

## NIPR

National Institute of Polar Research
Japan
*www.nipr.ac.jp*

## SA

Suomen Akatemia
Finland
*www.aka.fi*

## STEL

Solar Terrestrial Environment Laboratory, Nagoya
Japan
*www.stelab.nagoya-u.ac.jp*

## VR

Vetenskapsrådet
Sweden
*www.vr.se*

# EISCAT Scientific Association

## Headquarters

EISCAT Scientific Association
Box 812
SE-981 28 Kiruna, Sweden
Phone: +46 980 79150
Fax: +46 980 79159
*www.eiscat.se*

## Sites

### Kiruna

EISCAT Kiruna Site
Box 812
SE-981 28 Kiruna, Sweden
Phone: +46 980 79136
Fax: +46 980 29276

### Longyearbyen

EISCAT Svalbard Radar
Postboks 432
N-9171 Longyearbyen, Svalbard
Phone: +47 790 21236
Fax: +47 790 21751

### Sodankylä

EISCAT Sodankylä Site
Tähteläntie 54B
FIN-99600 Sodankylä, Finland

### Tromsø

EISCAT Tromsø Site
Ramfjordmoen
N-9027 Ramfjordbotn, Norway
Phone: +47 776 20730
Fax: +47 776 20740